NOISE PATH IDENTIFICATION FOR VIBRO-ACOUSTICALLY COUPLED STRUCTURES

A THESIS SUBMITTED TO
THE GRADUATE SCHOOL OF NATURAL AND APPLIED SCIENCES
OF
THE MIDDLE EAST TECHNICAL UNIVERSITY

BY

A. HAKAN SERAFETTINOGLU

IN PARTIAL FULFILLMENT OF THE REQUIREMENTS FOR THE DEGREE OF

DOCTOR OF PHILOSOPHY

IN

THE DEPARTMENT OF MECHANICAL ENGINEERING

MARCH 2004

Approval of the Graduate School of Natural and Applied Sciences

_____
Prof. Dr. Canan ÖZGEN
Director

I certify that this thesis satisfies all the requirements as a thesis for the degree of Doctor of Philosophy.

_____
Prof. Dr. S. Kemal IDER
Head of Department

This is to certify that we have read this thesis and that in our opinion it is fully adequate, in scope and quality, as a thesis for the degree of Doctor of Philosophy.

_____
Prof. Dr. Mehmet ÇALISKAN
Supervisor

Examining Committee Members

Prof. Dr. Y. Samim ÜNLÜSOY (Chairman) _____

Prof. Dr. Mehmet ÇALISKAN _____

Prof. Dr. Yücel ERCAN _____

Prof. Dr. Bülent E. PLATIN _____

Assoc. Prof. Dr. Yusuf ÖZYÖRÜK _____

ABSTRACT

NOISE PATH IDENTIFICATION FOR

VIBRO-ACOUSTICALLY COUPLED STRUCTURES

A. Hakan Serafettinoglu

Ph. D., Mechanical Engineering Department

Supervisor : Prof. Dr. Mehmet Çaliskan

March 2004, 211 pages

Structures of machinery with practical importance, such as home appliances or transportation vehicles, can be considered as acoustically coupled spaces surrounded by elastic enclosures. When the structures of machinery are excited mechanically by means of prime movers incorporated into these structures through some elastic connections, generation of noise becomes an inevitable by-product. For noise control engineering purposes, a thorough understanding of

emission, transmission and radiation of sound from structure is required prior to a possible and practical modeling of noise transfer mechanisms. Finally, development of a model for complete noise generation and transfer mechanisms is needed which is essential for the abatement of annoying sound generation.

In this study, an experimental and analytical (finite element) methodology for the modal analysis of acoustical cavities is developed, and successfully applied to a case study. The acoustical transmission problem of the structure is investigated via vector intensity analysis. Results of this investigation are used for a noise path qualification, whereas the transfer functions between sources of noise and some relevant receiving points are obtained by use of vibro-acoustic reciprocity principle. The concept of transfer path analysis is investigated by using the multi input, multi output linear system theory for vibro-acoustic modeling of machinery structures. Finally, resolution and ranking of noise sources and transfer paths are accomplished via spectral correlation methodologies developed.

The methodology can be extended to any system with linear, time invariant parameters, where principles of superposition and reciprocity are applicable.

Key Words: Noise Control, Linear Systems, Transfer Path Analysis, Spectral Correlation Analysis

ÖZ

AKUSTIK YAPISAL BAGLASIK SISTEMLERDE GÜRÜLTÜ PATIKALARININ TANILANMASI

A. Hakan Serafettinoglu

Doktora, Makina Mühendisligi Bölümü

Tez Yöneticisi : Prof. Dr. Mehmet Çaliskan

Mart 2004, 211 sayfa

Gündelik hayatimizda önemli yer tutan elektrikli ev aletleri, ulasim araçlari gibi makinalar elastik bir gövde tarafindan çevrelenmis akustik olarak baglantili kabinler olarak tanimlanabilirler. Bu makinalar, elastik yataklar üzerine yerlestirilmis güç/tahrik üniteleri tarafindan uyarildiklarinda gürültü yayilimi kaçinilmaz bir yan ürün olarak ortaya çikmaktadir. Gürültü denetimi mühendisligi uygulamalari için gerekli modellemelerin olusturulmasindaki ilk adim, bu kosullar

altinda ortaya çikacak ses yayinimi, tasinimi ve yalitimi mekanizmalarinin anlasilmasidir.

Bu arastirmada, iletim patikalari çözümlemesi kavrami, çok girdili, çok çiktili dogrusal dizgeler kuraminin titresim-akustik davranisi modellemesine uygulanmasi ile tartisilmistir. Deneysel ve sonlu elemanlar yöntemleri kullanilarak akustik bosluklarin biçimsel çözümlemesine yönelik bir yöntem gelistirilmis ve yöntem bir örnek çalisma ile sinanmistir. Yapi üzerinden ses iletimi problemi ses yeginligi ölçümleri ile incelenmistir. Sonuçlar dogrultusunda gürültü iletim yollarinin modellenmesine gidilmis, iletim yollarini temsil eden iletim fonksiyonlarinin belirlenmesi ise titresim-akustik karsiliklilik ilkesi kullanilarak gerçeklestirilmistir. Gürültü kaynaklarinin ve patikalarinin çözümlemesi ve siralanmasi gelistirilen yöntemlerle gerçeklestirilmistir. Bu çalismada gelistirilen yöntemler, üst üste bindirme ve karsiliklilik ilkesinin saglandigi zaman bagimsiz parametreli, tüm dogrusal dizgeler için geçerlidir.

Anahtar Sözcükler: Gürültü Denetimi, Dogrusal Dizgeler, Iletim Patikalari Çözümlemesi, Spektral Ilinti Çözümlemesi

ACKNOWLEDGEMENTS

The author is grateful to his parents for their never ending moral support; to Dr. Mehmet Çaliskan for his patience and faith to the outcome of this research, and finally to the colleagues at Arçelik A.S. Research & Technology Development Center, Vibration and Acoustics Laboratory for their technical assistance. Finally, he would like to thank to Arçelik A.S. R.&T.D. Center for use of technical infrastructure and, above all the necessary time they allowed for the completion of this research.

… to my father

A. Ünal Serafettinoglu

and to the memory of my beloved mother

Seyhan Serafettinoglu
(13.03.38-02.04.04)

TABLE OF CONTENTS

LIST OF TABLES

Table **Page**

LIST OF FIGURES

Figure **Page**

LIST OF SYMBOLS

A	Surface area
B	Bending stiffness
c	Speed of sound
c_B	Bending wavelength
C	Acoustical compliance
d	Distance between two nodes
$E[\ ]$	Expected value of [ ]
E	Young's modulus
f	Cyclical frequency
f_c	Critical frequency
Df	Bandwidth resolution

$G(x,y)$	Green's function
$G_{xx}(f)$	Autospectral density function (one-sided)
$G_{xy}(f)$	Cross-spectral density function (one-sided)
$H(f)$	Frequency response function
$H_{xy}(f)$	Transfer function
I	Second moment of area per unit width, about panel neutral axis
$\vec{I}(x,t)$	Acoustical intensity
$Im\{\}$	Imaginary part of a complex quantity
j	$\sqrt{-1}$
k	Wave number
K_n	Gain of n^{th} eigen-function
L_W	Acoustical power level in dB's
m	Surface density a material.
M_A	Acoustical mass, (inertance)

$p(x,t)$	Acoustic sound pressure
Q_{vol}	Volume velocity forcing function
$Re\{\}$	Real part of a complex quantity
$S_{xx}(f)$	Autospectral density function (two-sided)
$S_{xy}(f)$	Cross-spectral density function (two-sided)
t	Time variable
Dt	Sampling interval
T	Record length, period
$\bar{u}(x,t)$	Vector acoustic particle velocity
V	Volume
W	Acoustical power
$x(t)$	Time history records
$X(f)$	Fourier transform of $x(t)$
$z(y)$	Acoustic impedance
$b(y)$	Normalized specific acoustic admittance

g	Ratio of specific heats
$g^{2}_{xy}(f)$	Ordinary coherence function
$d(x-y)$	Dirac's delta function
h_{n}	Mechanical dissipation of n^{th} eigen-function
$q_{xx}(f)$	Phase angle of $G_{xx}(f)$
l	Wavelength
m	Mean value
$?$	Poisson's ratio
r_{0}	Density of the medium
s	Standart deviation
s^{2}	Variance
s_{rad}	Radiation efficiency
t	Time variable
Y_{n}	n^{th} eigen-function
w	Angular frequency

$[^{*}]$ Complex conjugate of [ ]

$[\hat{\ }]$ Estimate of [ ]

$\langle\ \rangle$ Space-time average

CHAPTER 1

INTRODUCTION

1.1 General

Acoustical radiation in terms of sound waves into the surrounding media from machinery assumes an ever-increasing objection due to the annoyance given to the exposed community. Structurally, any machinery can be considered as being composed of acoustically coupled spaces surrounded by some structural elements acting as acoustical enclosures, equipped with sources of noise incorporated into this structure through some elastic connections. In such machinery, sources of noise are present either due to the operation of prime movers, such as electrical motors, internal combustion engines or, due to physical excitation related to the functions of the machinery, such as fluid flow or impact of solid materials.

Propagation of sound waves is the result of mechanical disturbances of an elastic media, which causes pressure oscillations about an equilibrium state. The elastic media of propagation may be of fluid or solid origin. Human ear is capable

to sense small pressure fluctuations in air about the atmospheric pressure. Sound perceived as objectionable information through air by a human ear is named as acoustical noise, or simply noise.

Sound waves, as a time-dependent, longitudinal pressure wave propagation in elastic media have two fundamental properties related to their perception by ear: the frequency of oscillations, and their amplitude. An average healthy human with normal hearing capacity can perceive sound, roughly, in the frequency range of 15 – 16,000 Hz, which is named as the normal audible frequency range. Similar averaged values related to perceivable amplitudes are observed to be around 20 μPa, which defines the threshold of hearing as the lower bound and 200 Pa as the upper bound, termed as threshold of pain above which permanent loss of hearing is inevitable.

The characteristics of the stimulating sound energy as a source, and the physical response of the media of propagation as a path determines what can be perceived by the receiver. Annoyance, which describes the subjective reaction to noise as a psycho-acoustical phenomenon, is related to the physiology and psychology of the receiving person. The common practice in any noise control strategy on the abatement of annoyance for a receiving person is to formulate the problem by relating to the concepts of source, path and receiver as; control at the source, control at the transmission path and, finally, control at the receiver.

Noise control strategy at the source aims at, primarily, the elimination or reduction of the noise generating mechanisms, which is named as the low noise

machinery design. Obviously, if achieved, this is the most valuable strategy to be fulfilled. However, in most cases, these noise generation mechanisms are effective due to required functions of the machinery, and consequently, they can not be altered with ease. Moreover, they assume a high cost sensitivity, which is an important asset in the production and purchase of most machines of practical use. The second possible approach is the isolation of sources from rest of the propagation media, which can also be considered as a special version of control at the transmission path. Noise control at the receiver, on the other hand, is the isolation of the receiver from the propagation media and by a similar reasoning; this strategy can be considered as another special version of control at the transmission path.

Finally, the noise control at the transmission path is the practice of noise abatement, which includes every possible way of reducing the noise energy transmitted to a receiving point by modifying the media of propagation. The physical realization of this local energy attenuation is achieved in practice in two ways, namely, the direct and the indirect methods. The direct method is the absorption of sound energy by some means of heat dissipation due to mechanical friction on the media of propagation. Usually, a physical implementation of absorptive materials is not possible due to economical, geometrical and technical constraints. The indirect method is changing the path of propagation in such a way that the excess acoustical energy can be moved and confined in some region of the media, which is away from the target region of receiver and where the mechanical energy loss mechanisms can be effectively implemented.

Most of the machinery of practical importance can be reduced to a system equivalent to the one depicted in Figure 1.1, where a source of acoustical noise and a receiver as a human ear or a pressure pick-up are enclosed in two separate volumes by some structural constructions, and placed in an environment where the sound energy is propagating. In the noise control terminology, these structures can be named as acoustical enclosures and the volumes enclosed by these structures as acoustical cavities.

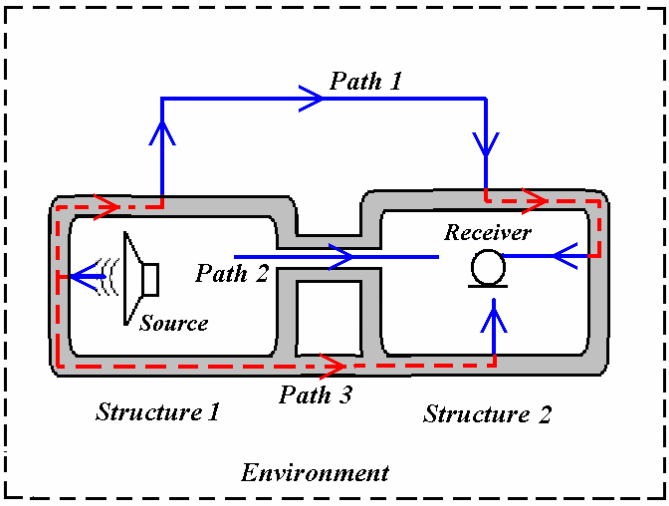

Figure 1.1 Depiction of a Generalized Noise Control Problem

There are direct structural (Path 3) and acoustical (Path 2) connections in between the enclosures and an indirect connection via the surrounding environment (Path 1), which has both structural and acoustical parts. Some physical examples for such systems can be found in transportation vehicle bodies, such as an automobile or an airplane, with engine compartment acting as the enclosure one, and the passenger compartment as the enclosure 2.

In Figure 1.2, another configuration is depicted as a structure of machine

structures composed of two main sub-structures enclosing two distinct sources of noise, coupled to each other acoustically and structurally, and a receiver located somewhere in the surrounding environment. The generalized transmission paths can be arbitrarily chosen with respect to the structural configuration and their possible dominance on the noise transmission characteristics. In this figure, Path 1 and Path 2 represents the paths dominated by the structural behavior of sub-structures 1 and 2, respectively, whereas, Path 3 represents the noise path due to their coupled structural behavior.

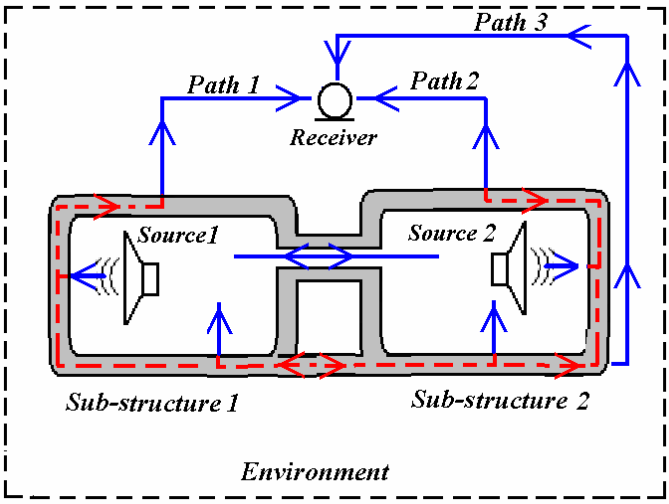

Figure 1.2 Depiction of a Simplified Noise Control Problem

Typical examples of these kinds of generalized problems can be given as prime movers, such as electrical generator or electrical appliances of every sort operating in rooms of buildings with receivers located in some others rooms. A more interesting example from the machinery design point of view will be all sorts of machinery operating at domestic environments, such as home appliances, or at occupational areas, such as air conditioning units and their transmission

ducts, or at production areas such as punch presses.

The physical phenomena undergone by a structure when acting as an acoustical enclosure by the effect of some acoustical excitations are illustrated schematically in Figure 1.3. Classification of noise propagation mechanisms as airborne or structure borne, related to the media of generation or transmission is a common and versatile practice, where, the terms coined for acoustics related to the elastic media when it is only air or solid structures, respectively. Another common terminology, although conceptually incorrect, is the use of the word sound for airborne propagation, and vibration for the structure-borne counter part. With these premises in hand, one can classify a noise source as well as its transmission paths as airborne or structure-borne.

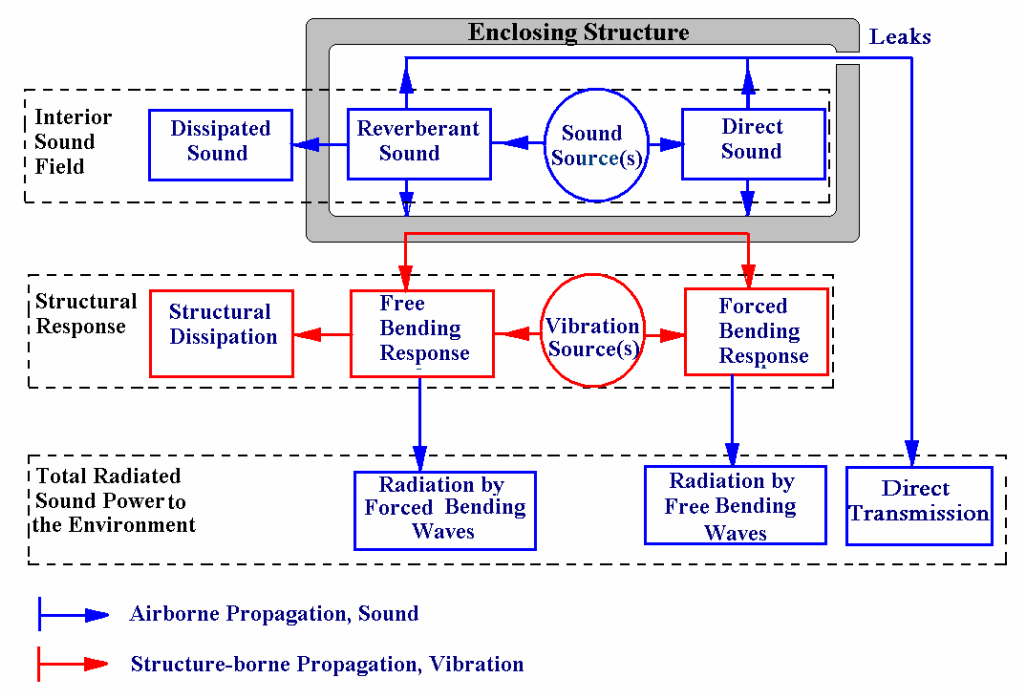

Figure 1.3 Underlying Physical Phenomena for an Acoustical Enclosure

In Figure 1.3, the internal cavity enclosed by the structure is acoustically excited by some air-borne sources, which gives rise to a so-called direct sound field due to the forcing sound waves by the exciter and a reverberant field which is the result of free response of the acoustical cavity. The last component of the acoustical field will be the dissipated part of the reverberant acoustical energy due to the acoustically absorptive elements that may be present in the cavity.

The structure of the enclosure, on the other hand, will be excited at the boundary walls by direct and reverberant sound fields, together with some possible vibration sources attached to the structure. The response of the system, which is acoustically relevant due to the frequency range of interest, will be the generation of mechanical bending waves throughout the elastic medium of the structure.

Similar to the air-borne propagation, these bending waves will assume two main components related to the free and force response of the structure, and a dissipation mechanism. Finally, on the outer boundary of the structure where the elastic media of the surrounding environment is in touch, these bending waves will be radiated as air-borne sound to the environment. The last contribution to the environmental noise will be the direct transmission of airborne sound field in the cavity through the structural leaks.

The physical description of the noise transmission problem, therefore, requires the solutions of the cavity acoustics problem for the reverberant sound field in the enclosure, and the response of the structure coupled with the inside

acoustical field. In many practical cases, the closed form solutions for the coupled vibro-acoustical problem are too complicated for practical engineering applications. The non-homogenous and non-isotropic behavior of the multi-layered materials used in the construction of the machinery structures is one of the most severe difficulties in such analysis. Related to this difficulty, the coupling of this multi-layered elements with different material properties present an analytically intangible problem of wave mechanics.

Most uncoupled problems can be solved for simpler cases such as infinitely extended walls with isotropic and homogenous wall properties. Although dimensionally reduced solutions are quite helpful for gaining some physical insight into the problem, they fall short for design and identification purposes. When the internal cavities can be expressed in geometries where, a well-defined fundamental solution as a Green's Function is possible (i.e. prismatic, cylindrical, spherical, etc. shapes), analytical solutions are achievable to a certain extent. However, this is hardly the case for almost all of the acoustical cavities enclosed by practical machine structures.

To be able to overcome these shortages, computer aided engineering tools, such as finite element and/or boundary element methods (FEM/BEM) have assumed a great importance in structural analysis in the last couple of decades. Although, the state of the art in vibro-acoustic FEM/BEM research is at the transmission of sound phenomena, versatile software that can handle full and practical modeling of real life structures is still far away in the engineering horizon as robust, commercially available design tools. As a result, a correct and

feasible methodology for the identification of noise transmission paths requires a hybrid approach of analytical, numerical and experimental modeling.

1.2 Aims of the Study

The first task of this research is the development and implementation of some hybrid methodologies for determining the response of acoustically and structurally coupled enclosed volumes. For this purpose, the cavity acoustics is investigated by means of experimental acoustical modal analysis techniques, which help to verify and qualify solutions obtained from FEM applications.

The transmission of sound through the structure, on the other hand, is investigated by means of near field sound intensity mapping techniques. As energy based methodology, the practical engineering metrics of sound transmission, such as radiation efficiency and Insertion Loss, can be obtained directly from these implementations.

The final aim of any research on the modeling of the noise transmission path identification problems must handle excitation due to an arbitrary distribution of noise source with practical and possible media of propagation media and many receiver points of practical interest. The physical insight and guidance earned at the first step of the modeling is used to evaluate the validity of such a generalized model.

The experimental noise path identification problem can be modeled in this

case as a multi input, multi output (MIMO) system, where the transfer functions between inputs and outputs represent the complex mechanism of propagation, transmission and radiation of sound over some particular transfer paths. This methodology has recently been named as transfer path analysis (TPA) and found some important applications especially in transportation problems, such as automotive interior or passenger train cabinet design or noise path identification of buildings with heavy machinery installations.

In this study, the method is implemented to acoustically and structurally coupled machinery structures excited by multi noise sources, with multi receiving points with acoustical pick-ups. The possible transmission paths are defined in accordance with the design engineering requirements aimed to reduce the annoyance of the machinery.

CHAPTER 2

LITERATURE REVIEW

2.1 Analytical and Numerical Methodologies

As a result of rapid advancements in related applications, rigorous methodologies have been developed on the vibro-acoustical behavior of structurally, acoustically coupled cavities [**1,2,3,4,5**]. The common practice in noise control engineering is to analyze the problem with respect to the frequency range of interest.

The modal decomposition of boundary value problems, as in the case of acoustical wave propagation, is at the fundamentals of most of the analytical solutions up to some frequencies where modal overlapping starts. The upper bound of the frequency range of interest is manifested by the corresponding wavelengths, which stay large compared to some characteristic dimensions of the structures of interest. For many machine structures, which have direct contact with human bodies, the upper bound for this low frequency range can go up to 1 kHz, but hardly any higher. For higher frequency emission problems where modal

densities become higher, the use of statistical energy analysis (SEA) assumes a common practice for engineering analysis, whereas for lower frequency range, experimental modal analysis and finite element methods (FEM) constitute fundamental methodologies [**1**,**2**,**5**].

The recent and rapid advancement in computational technologies has helped developing powerful numerical tools for acoustical engineers based mainly on finite element and/or boundary element methods (FEM/BEM) [**6**]. Although there are no theoretical limitations, FEM is more useful for solution of interior acoustics fields, whereas BEM finds rigorous applications for exterior radiation problems. Theoretically, these methods can also be considered as modal decomposition problems, therefore, they are bounded by an upper frequency range as well. For the upper frequency range where wavelength of propagation is much smaller compared to the characteristic dimensions of the structures, ray tracing is the preferred numerical methodology [**4**].

Other than the frequency limitations, the main drawback of numerical methods is due to the shortcomings related to physical properties of the materials when the materials do not bear isotropic, homogenous properties. For bodies with different as well as large characteristic impedances, as in the case of sound transmission problems for machinery structures, the generalized versions of these methods becomes completely useless [**1**,**4**].

2.2 Experimental Methodologies

The determination of the modal behavior of acoustical cavities by frequency response measurements lies at the foundation of experimental modal analysis. One of the main drawbacks of the numerical methods for the solution of cavity acoustics is in modeling the material properties of the system, usually the acoustical properties of the surface lining. Experimental methods are useful to help eliminate these kinds of problems. However, they have limitations in precision of spatial resolutions due to the instrumentation problems. The main drawback is the implementation of a constant volume velocity source as for acoustical excitation.

Singh and Schary [**7**], Kung and Singh [**8**], Nieter and Singh [**9**] have applied the technique to simple geometries with one dimension such as rectangular and cylindrical cavities with volume sources capable of producing one-dimensional flow at some boundary points. Byrne [**10**] has developed an approximating methodology for determining the modal shape functions and applied it to a rectangular cavity. Byrne has used the cavity pressure measured for volume source calibration and noted the limitation for the low order acoustic modes with modal indices less than 3.

Wyckaert and Augusztinovicz [**5**] have developed a method for structurally and acoustically coupled cavities due to a flexible wall, with the motivation of analyzing automobile passenger compartments. The analysis is

again reported for low orders of frequencies below 250 Hz.

The construction of three dimensional volume sources has been investigated by many researchers for various reasons, such as by Salava [**11**], for acoustical impedance measurements, by Anthony and Elliott [**12**], for the construction of secondary sources in active noise control applications. The latter researchers have investigated several methods for the calibration of volume sources in a comparative approach. Lee and Ih [**13**], Kim and Ih [**14**] have successfully applied these methods for the source strength determination of volume sources under *in-situ* conditions.

The use and measurement of intensity techniques in noise source identification, and energy based vibro-acoustic analysis has covered a long way from theoretical possibility to commercial availability. An excellent treatise by Fahy [**15**] on the subject discusses the fundamental concepts of sound intensity measurement in a broad engineering perspective, regarding instrumentation and some basic applications. The use of this method for analyzing acoustical fields due to vibrating structures for the investigation of their radiation and transmission characteristics has been the interest of structural engineers in the last couple of decades.

Mann et al [**16**] have investigated the character of the near field energy related quantities, and shown that active intensity alone is not enough to describe the related energy field. They have emphasized the importance of reactive intensity as well as the curl of active intensity in the identification of a noise

source in such energetic fields. Li and Pascal [**17**] have introduced the coherence matrix method based on particle velocity, pressure and the curl of active intensity and used the rank of it to determine the behavior of multi source distributions. Bolton et al [**18**] have investigated the theory and measurements of sound transmission through multi-panel structures lined with elastic porous materials, and use the intensity technique in a double room environment with a reverberation room and an anechoic enclosure serving source and receiving rooms respectively. However, they have not extended the investigation with finite panel sizes, which might form an enclosure.

2.3 Transfer Path Analysis and the Principle of Reciprocity

The determination of frequency response functions (FRF), or transfer functions between the excitation sources and receiver locations is an invaluable tool for noise control engineering problems. Regarding the versatility and broad usage of the technique as an engineering application in the area of interest, a common term has been coined for this sort of experimental methodology as TPA. There is also an effort of research on the analytical foundations of methodology in terms of source modeling.

Applications of TPA are concentrated in mainly two areas of interest in noise path identification problems, namely, building acoustics and transportation noise. The research on building and room acoustics with TPA formulation is related mainly to the noise transmission problems at multi flat structures excited

especially by large machinery located on resilient mounts. Investigations related to the transportation engineering are focused on automobile and truck cabinets, train passenger cars and on ship structures. In the former group of problems, the transmission paths are usually of structure borne type, whereas, in the latter case of transportation cars, path identification involves air-borne type paths as well.

For structures where excitation sources are mounted by means of some resilient vibration pads, where all the excitation energy flows through the machinery, the problems can be reduced to an analysis of a one dimensional structure borne sound transmission problems. As a matter of fact, for structures where the prime movers are not an integral part of the structure, this simplification is quite valid, as in the cases of electric generators, fans of heating, ventilating systems mounted on building structures, or diesel motors of cruiser ships. In such cases, a one-dimensional analytical model for the transmission path is also possible.

Moorhouse and Gibbs [**19**] have investigated the structure borne noise emission characteristics of vibrating machinery through resilient mounts. They have modeled the excitation mechanism as free velocity of the machine at the machine mount points, and determined the responses by means of a mobility analysis. The motivation behind the analysis is the prediction of the vibration at given locations of the structure by simple free velocity measurements of the machinery before they are mounted. Later, the same authors [**20**] have applied the methodology to the structure borne power estimation of resiliently mounted fans and compared their results with the measured values. Furthermore, they have

proposed a generalized standard methodology for the estimation of structure borne sound power of machinery from similar type of analytical transmission path analysis [**21**].

Mondot and Petersson [**22**] have worked on an introductory, theoretical study on the description of structure borne sources, and later Petersson and Gibbs [**23**] have worked on the generalized problem of source descriptor concept where all translational and rotational degrees of freedoms are considered as again in a mobility type formulation. Although most of the problems are very well handled by one dimensional translational (or rotational) formulation, when the frequency range of interest increases other degrees of freedoms become effective as well. They have reported no practical cases of application for their formulation.

Fullford and Gibbs [**24,25**] have studied on the formulation of multi-point-connected systems for structure borne sound power estimations. The source models are again of mobility type with excitations mechanisms modeled as free velocities. The main contribution of the study is the consideration of coupling effects between different excitation mechanisms via the structure, which assumes great practical values when source mechanisms are mutually correlated.

Another way of describing a structure borne type source is expression of the excitation mechanism as a distribution of forces, which is named in the literature as pseudo-forces method. The forces are qualified as pseudo because these are not actual, physical forces acting on the system. Obviously, the measurement of the physical forces at the contact points is rather difficult, if not

impossible, due to the obvious fact that mechanical forces are through variables, hence can only be measured by breaking the structure. Therefore, an indirect method is applied, by considering fictitious, hence, pseudo-forces at some arbitrary locations on the machinery, where the force magnitudes are determined in such a way that they approximate the response generated by the actual running forces. Note that the formulation for the structure is of impedance type in case of modeling the excitation as applied free forces.

Janssens, Termeer and de Jong [**26**] have compared the mobility matrix method and pseudo-forces method for practical applications. They have concluded that the accuracy of pseudo-force approach is suitable for source ranking and transfer path analysis, whereas, the mobility method gives more insight into the physics of the problem at the application points of sources.

Jansenns, Verheij and Thompson [**27**] have applied this concept to structural sound transmission problems in ships. They have started with a multi-dimensional formulation and investigated possible reductions on these dimensions by comparing the response from the modeling forces and from the actual operating forces. They have concluded that a one-dimensional model would have been imprecise where they have reduced the dimension of the sources down to two at least.

Bettella, Harrison and Sharp [**28**] have investigated the creep groan noise of automotives with the similar pseudo-forces methodology. In this analysis, the transmission path is, of course, is a hybrid one, which connects structure borne

excitation mechanism with air-borne receivers. However, they have neglected the structure borne excitation mechanism and replaced the excitation with an equivalent volume velocity source distribution. They have investigated the transmission path via reciprocal measurements. Creep groan is high intensity, low-frequency sound and vibration problem. Consequently, they have found that the cavity acoustic resonance of the automobile cabinet is very effective on the transmission path determination. The research is limited with its model as a single input single, output system and no major results have been reported in the study.

Beer and Verheij [**29**] have investigated the pass-by noise from freight trains due to the rolling noise. The transmission paths are again hybrid type with structure borne excitation from the vibration of wheels due to the roughness of the rails, and receivers in the neighborhood of the railroad, with the entire train superstructure as multi dimensional transmission paths. The problem therefore involves the cavity resonance of the whole superstructure. The concept of vibro-acoustic reciprocity has been widely exploited in the investigation, with volume velocity excitation at the outer receiving points and measurement of sound pressure and/or vibration velocity at particular on the paths of transmission. The cavity resonance and the transmission characteristics of the train superstructure are discussed but no specific analysis or measurement has been carried out for a through identification.

The principle of vibro-acoustic reciprocity is widely exploited in TPA methodology for the experimental determination of acoustical transfer functions. The foundations of the principle had been given by Rayleigh in his acclaimed

treatise on the theory of sound [**30**]. The principle of reciprocity holds for linear, time invariant parameter systems, and in plain words, it manifests that excitation and response points can be changed respectively for this type of systems.

Extensions of the principle of reciprocity to a wide range of vibro-acoustical excitation and response mechanisms have been given by Verheij [**31**], which can be used in different, practical vibro-acoustic transmission path ranking and identification problems. A useful set of equal point-to-point frequency response functions in reciprocal systems has also been tabulated with relevant system descriptions

Ver and Oliphant [**32**] have summarized the use of vibro-acoustic reciprocity in source-path-receiver analysis by exploiting applied research on automobile and aircraft noise with practical considerations on instrumentation.

Mason and Fahy [**33**] have studied a noise prediction technique for the propeller noise transmission through aircraft fuselages. The technique depends on reciprocal measurements made by an omni-directional sound source calibrated in an impedance tube with an anechoic termination. They have evaluated the validity of the measurements by means of an enclosure out of flat panel structures. However, no in-situ measurements related to the aircraft fuselages have been reported.

MacMartin, Basso, and Slingerland [**34**] have attacked the same aircraft fuselage transmission problem, and used reciprocal measurements for the determination of fuselage to inside cavity frequency response functions. The

fuselage noise transmission problem is then combined with computer predictions of the propeller sound pressure field to predict the interior noise field.

Zheng, Fahy and Anderton [**35**] have applied the reciprocity principle to the case of sound radiation from an internal combustion engine casing. The main advantage of the method is that the surface vibrational velocity of the structure is obtained from near-field intensity probe measurements where the equality of acoustical particle velocity via no-slip condition at the boundaries has been exploited. The free field transfer functions from machine surface to the receiving points in the field have been obtained as a result and contribution of different parts of the structure have been investigated.

Stratman [**36**] on the other hand, have determined acoustical transfer functions via reciprocal measurements for low frequency (<200Hz) response of woofers in audio systems. However, Stratman has not actually constructed a real volume velocity source, but approximated the volume velocity of the source by measuring near the loudspeakers placed at around the listener positions. Although not discussed in the article, this can have validity only if the transmission paths are purely air-borne type. This is normally the case for audio systems, but hardly the case for structurally coupled machinery enclosure problems.

Beguet and Chauray [**37**] have applied the concept of coherence analysis and artificial excitation method, which can be considered as MIMO and TPA formulation, respectively, for the identification of transmission path in interior acoustical problems, related mainly to automobile passenger compartments. They

mention the importance of experimental methods for the analysis of the cavity acoustics in these problems, such as, acoustical intensity and modal analysis techniques, but no further information has been presented.

Gilbert, Moller, and Ryu [**38**] have developed a commercial software based on multi-channel system produced by Brüel&Kjaer under MATLAB environment. The software handles transmission path analysis problems excited by resiliently mounted prime movers, mainly electrical motors, under run-up, run-down conditions.

Li, Ball, and Leung [**39**] have exploited the coherence analysis under the name of independent component analysis (ICA) applied to the identification of diesel engine sources. The ICA assumes the measured data from m sensors is a linear mixture of n dimensional unobserved independent sources, where for $m \geq n$. The analysis have been carried out in time domain in order to separate transient type noise events such as piston slap, inlet valve open etc.

Finally, estimation of Frequency Response Functions (FRF), which is at the core of all experimental noise transmission path identification techniques, depends on the theory of correlation (coherence) and spectral analysis. Two excellent treatises by Bendat and Piersol [**40**, **41**] are extensively used by the interested researchers in the area. For multi input multi output system formulations, their terminology and methodology has become the standard of such analyses.

2.4 Discussion

The purpose of this research is the application of the concept of TPA as a noise path identification methodology, to structurally and acoustically coupled structures. Physical phenomena are examined on the prospective propagation paths; FEM and experimental modal analysis, together with methods of acoustical intensity are applied for the enhancement of path modeling. The paths are defined as a combination of transmission of airborne and structure borne sound problems. Vibro-acoustic transfer functions are estimated experimentally from operational measurements by means of a coherence analysis, and directly from reciprocal measurements.

CHAPTER 3

FORMULATION OF THE PROBLEM

3.1 Description of the Problem

The physical description of the noise transmission problem from machinery structures as acoustical enclosures requires the solutions of the cavity acoustics problem for the reverberant sound field in the enclosure, and the response of the structure coupled with the inside acoustical field. Limitations of the analytical and numerical methods related to the acoustical and structural coupling of the multi-layered machinery structures with different material properties require a hybrid approach of analytical, numerical and experimental modeling for the identification of noise transmission paths.

However, the primary aim of a noise transmission path identification problem is the estimation of the responses at some receiver points of practical interest, due to excitations by some arbitrary distribution of noise sources relate to the functions of the machinery. This problem can modeled as a multi input, multi output (MIMO) system, named in practice as transfer path analysis (TPA) where

the transfer functions between inputs and outputs represent the complex mechanism of propagation, transmission and radiation of sound over some particular transfer paths. The physical insight and guidance earned at the first step of the modeling is used to evaluate the validity of such a generalized model.

3.2 Limitations on the Problem

The methodologies applied and developed in this study is valid for linear, time invariant parameter systems, where principles of superposition and reciprocity are valid. These are fundamental assumptions of linear acoustics theory, which is exploited, in practice, for most of the practical noise emission problems with success.

Fundamental frequencies related to the operational conditions of the prime movers of machinery are usually present at the low audible frequency range. This fundamental frequency assumes some integer multiples, or the so-called harmonics, due to the existing mechanical power transmission, or conversion characteristics. Number of blades of propellers or number of tooth of gears can be named as examples for these. Typical fundamental frequencies can be given as 50 Hz for electrical machinery due to the line frequency of the alternating power supply, or from 1000 to 6000 rpm for automobiles with internal combustion engines corresponding to a range of 20-100 Hz.

On the other hand, commercially available acoustical absorption materials, which have heat dissipation characteristics in accordance with either porous or

fibrous type heat dissipation mechanism, are very little effective at the low frequency ranges. It is not uncommon to find cut-off frequencies for such materials where their absorption fall below 10% in energy base, in a range 500 to 1000 Hz. It can be concluded that, in the low frequency range, most of the machinery structures are mechanically excited and the resulting vibro acoustical energy is difficult to be absorbed. Hence, identification and possible retrofitting of transmission paths are most valuable at the low frequency range.

The present investigation is dedicated to a frequency range below 1000 Hz for the identification vibro-acoustical characteristics of the structures. By this way, the study is limited to a region where modal decomposition is possible and statistical methods related to higher modal densities are not considered.

Theoretically, there is no limitation on the upper frequency range for the method of Transfer Path Analysis as far as correct instrumentation is used. However, at lower frequencies, determination of frequency response function (FRF) measurements involve difficulties due to two main physical constraints; the low mobility characteristics of the structure and the low efficiency of the acoustical transducers, that is loudspeakers, used as exciters. Hence, this study exploits the modal decomposition theory and related experimentation together with the TPA methodology as two complemental and confirmative approaches for each other.

3.3 Scope and Procedure of the Study

The formulation of the problem is depicted in Figure 3.1 schematically for an acoustically, structurally coupled enclosure. The structure is assumed to be placed in an environment, where fluid loading is negligible. In this study, fully anechoic and semi-anechoic chambers are used, where fluid loading as a result of reflections is almost negligible. Measurements in anechoic environments can be applied to any room of practical importance by considering experimentally or analytically obtained room transfer functions.

The cavities of the enclosure are excited by sources of air-borne type, whereas, the enclosure walls are excited by structural borne type sources acting either inside or outside of the structure. Air-borne acoustical sources placed out of the internal cavities, but propagating through the enclosed space are also included in the generalized approach. Needless to mention, the dimension of the problem is determined by the number of sources and receivers involved in the physical system, and the methodology of this study set no theoretical limitations on the dimension.

The cavity acoustics is investigated by modal decomposition techniques using FEM. Modal shapes and frequencies are cross-examined by analytical results obtained from separation of variables techniques related to some approximated rectangular cavities. Furthermore, a lumped parameter model of the acoustical system in terms of some acoustical masses and compliances is also

used for the examination of low frequency bulk system behavior. Finally, the results are confirmed with an experimental acoustical modal analysis technique.

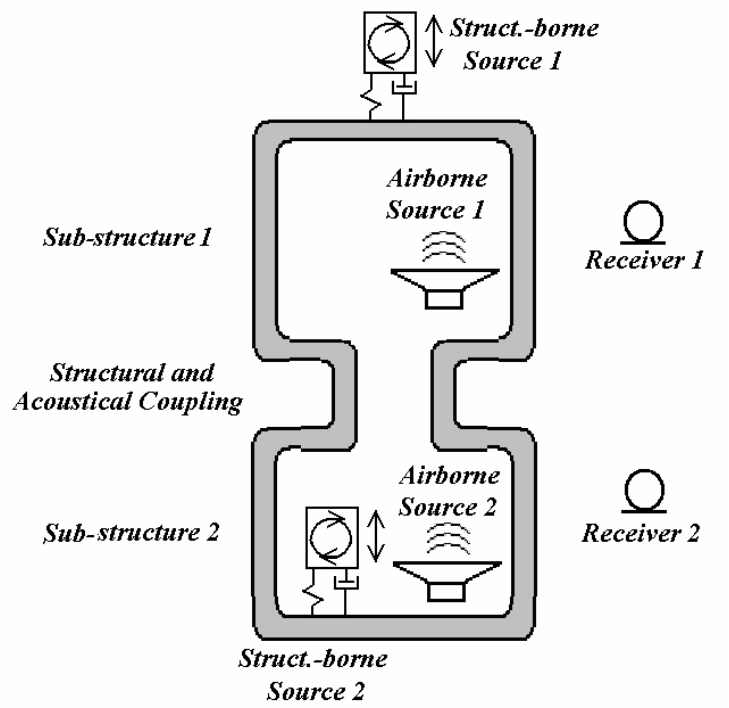

Figure 3.1 Enclosure with Multi Source Multi Receiver

The system parameters are essentially subject to change due to the temperature gradients present in the system, which is actually the main function of the system in hand. Modal parameters of the system is also checked for this case by conducting the experimental analysis during the cooling down of the system after maintaining nominal compartment temperatures with maximum loading at ambient room temperatures.

The acoustical transmission problem of the structure is investigated via vector intensity measurements conducted all over the surface, in a fully-anechoic chamber, with acoustical excitation inside the enclosure cavities by means of

calibrated sound sources. Therefore, a transfer function approach is applied in terms of energetic behavior of the system.

Source modeling is accomplished by considering pressure sources as air-borne type excitation and velocity sources, hence suitable for mobility formulation, as structure-borne type excitation. The transfer path analysis is conducted in a hemi-anechoic room, with microphones at several receiving positions.

The principle of vibro-acoustic reciprocity is exploited for experimental determination of FRF between the source and receiver points. For this purpose, an omni-directional volume source with dodecahedral geometry is designed, manufactured, certified through free field measurements and used.

Frequency domain signal processing is carried out by a multi-channel analyzer, whereas, data processing is carried out by means MATLAB m-file routines.

Due to experimental nature of the research as an identification problem, a refrigerator cabinet is chosen as a case study. The cabinet as an enclosure is constructed with 1mm thick polypropylene origin inside walls, external walls out of stainless steel metal sheets of 0.5 mm thickness, and polyurethane foam of 10-30 mm thickness in between these walls, functioning as thermal insulator. Under normal working conditions, the external and internal temperatures of such walls assume a gradient changing at the average from $-23^{o}C$ to $4^{o}C$ at the inside, and $20^{o}C$ to $60^{o}C$ at the outside. Therefore, the structure can be considered as an

enclosure with a various thickness, inhomogeneous, multi-layered wall structure with unevenly distributed temperature gradients.

The inside cavities, serving as a cold and fresh food compartments of the structure, are coupled acoustically to each other via two small complex rooms that envelope the evaporator and the air handling canals. Finally, a tubular section connecting the lower to the upper compartment for forcing the cold air from the evaporator region to the lower fresh food section. In normal operating conditions, the structure is equipped by two air moving devices, and a hermetic compressor, mounted on different locations, therefore, serving as an excellent case study in the scope of this research.

3.4 Flow of the Research

1. **Investigation of the structure for vibro-acoustic behavior**

    a. Study of the transmission of air-borne noise through the multi-layered enclosure walls via surface vector sound intensity methodology.

    b. Numerical modal analysis of the cavities

    c. Experimental modal analysis of the cavities

    d. Bulk parameter modal of the acoustical system

    e. Interpretation and comparison of the results

2. **Transfer Path Measurements on the Structure**

    a. Definition of noise sources and noise transfer paths, MIMO modeling of the system

    b. Operational measurements of the enclosure

        i. Source strength identification

        ii. Transfer function determination from the MIMO model

    c. Reciprocity measurement of the transfer functions at specified source, receiver and path configurations by means of an omni-

directional volume source as a reciprocal transducer.

d. Noise Transmission Path Identification

i. Comparison of the Noise Transfer Functions from the MIMO model and direct reciprocal measurements.

ii. Source strength ranking

iii. Noise path ranking

3. Post-processing and interpretation of results

CHAPTER 4

IDENTIFICATION OF ACOUSTICALLY COUPLED CAVITIES

4.1 Introduction

In this chapter, experimental methods are examined on the noise transmission path identification of acoustically coupled spaces, with structurally coupled boundaries. The experimental works are applied to a structure, which encloses acoustically coupled cavities, with multi layered material walls, namely a domestic type refrigerator cabinet. The frequency range of the problem is 1000 Hz and this frequency range is extended in the upper bound to 2000 Hz, when possible, in order to get an insight for the quality of measurements on the one hand, and for getting further insight of the problem in the mid to high frequency behavior of the enclosure.

At the first section of this chapter, the acoustical transmission problem of the structure is investigated via vector intensity measurements. Following this section, cavity acoustics problem is attacked by means of modal decomposition and lumped parameter acoustical system modeling techniques. The theory behind

the modal decomposition techniques is examined at the beginning of the section, which is followed by finite element analysis and experimental acoustical modal analysis studies. A very low frequency, lumped parameter model of the structure in hand is also developed.

At the end of the chapter, results of all the experimental investigations are summarized and incorporated with each other so that a complete description of low frequency behavior of the enclosure is obtained.

4.2 Transmission of Sound from Acoustical Enclosures

A structure that isolates the propagation of sound energy from one spatial domain of interest to another serves as an acoustical enclosure. The primary acoustical function of an enclosure is to isolate either the sources from the environment where it is build into or, the receivers form the environment where the sources of sound are operating. Figure 4.1 depicts these two cases schematically.

In the former case (CASE I) the so-called receiver is located in the isolated region and some practical examples of these kinds of structures are interior cabinets of transportation machinery, recording studios, acoustical measurement chamber. On the other hand, in the latter case (CASE II), the isolated region is located outside the structure where the aim is to obtain a noise free environment for the receiver(s). This latter case, obviously, encompasses the type of structures investigated in this study such as electrical appliances, engine casings of

transportation equipment, power generation units, etc.

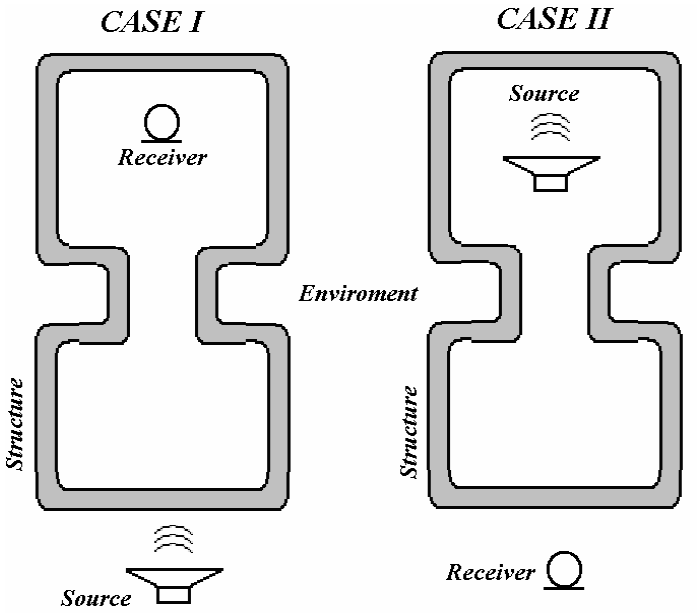

Figure 4.1 Two Primary Cases for a Structure Acting as an Enclosure

4.2.1 Sound Transmission from an Acoustical Enclosure

The energetic behavior of an acoustical enclosure can be analyzed in terms of acoustical power balance of the system under steady state conditions. Figure 4.2 depicts a structure with acoustical power injected into the inside cavity as W_i, mechanical power (acoustical and structural) absorbed by surface lining and structural loss as W_a, and, finally, acoustical power transmitted into the environment as W_t.

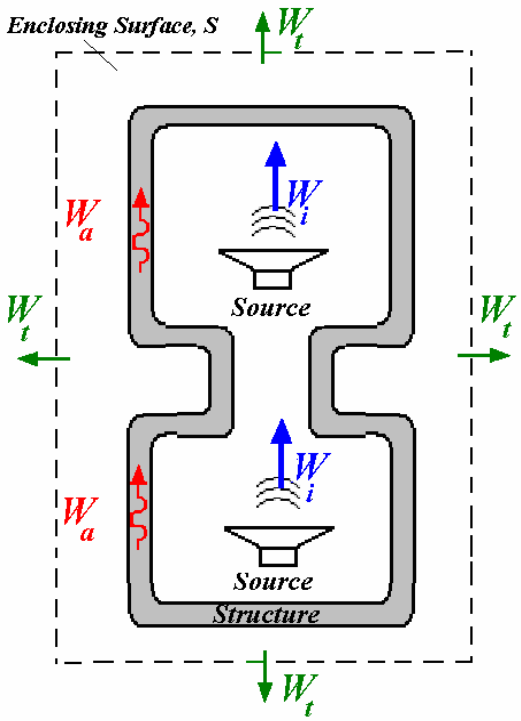

Figure 4.2 Energy Balance for an Acoustical Enclosure

The power balance, then, yields the following relation;

$$W_i = W_t + W_a \tag{4.1}$$

The overall acoustical performance of a structure as an enclosure can be best described in terms of the so-called power based Insertion Loss (IL) values. Insertion Loss in dB's is defined as

$$IL = 10\log_{10}\left(W_0 / W_E\right) = L_{W0} - L_{WE} \tag{4.2}$$

where W_0 and W_E are the sound powers radiated by the source without and with the enclosure; L_{W0} and L_{WE} are the corresponding sound power levels, respectively.

The radiation efficiency s_{rad} of a vibrating structure is defined as;

$$s_{rad} = \frac{W_{rad}}{rcA_{Total}\left\langle u_n^{\,2} \right\rangle} \tag{4.3}$$

where $\left\langle u_n^{\,2} \right\rangle$ is the space-time averaged mean-square normal vibration velocity of the radiating surface of area A_{Total} and W_{rad} is the radiated sound power, r is the equilibrium density of the medium and c is the speed of the sound in the medium.

The term radiation efficiency can sometimes be misleading as it may assume values higher than unity. For this reason the radiation ratio is also used in the literature. For an infinite rigid piston, the radiation efficiency is unity by definition. Therefore, the radiation efficiency term can be best interpreted as a comparison with an infinite rigid piston or an ideal plane wave radiator.

For an elastic, isotropic, infinite plate in bending, the radiation efficiency depends mainly on the so-called bending wavelength of the plate, which is expressed as;

$$c_B = \left(Bw^2 \big/ m \right)^{1/4} \tag{4.4}$$

where $B = EI\big/(1-n^2)$ is the bending stiffness; with E Young's modulus, n Poisson's ratio, I the cross-sectional second moment of area per unit width, about

the panel neutral axis, w is the angular frequency and $m = r_m h$ is the surface density with r_m the density of the material.

The radiation assumes its maximum value when the airborne and structure borne wave speeds are equal which is called as the critical frequency, f_c. Hence, if the speed of sound in the surrounding medium is c, speed of sound in air in this case, the critical frequency is found to be;

$$f_c = \frac{c^2}{2p}\sqrt{m/B} \qquad (4.5)$$

The frequency response of the radiation efficiency for an elastic plate can, then be approximated with respect to the critical frequency f_c, and, in terms of excitation frequency f as [3];

$$s_{rad} = 1/\sqrt{1-(f_c/f^2)} \qquad \text{for} \qquad f > f_c$$

$$s_{rad} = 0 \qquad \text{for} \qquad f << f_c \qquad (4.6)$$

The following derivations are important as qualifying descriptions of any radiating panel. At critical frequency s_{rad} assumes a maximum. Below the critical frequency s_{rad} reduces asymptotically and reaches a null value. Above the critical frequency s_{rad} reduces asymptotically and reaches to unity, that is, the panel radiates like an infinite rigid piston.

Many practical structures, being designed or acting as an acoustical enclosure, are composed of multi-layered materials. In most of the cases, the outer and the inner layers that cover and protect the porous or fibrous type acoustical materials at the inner layers, are planar metal sheets of small thickness. Therefore, an analytical solution of the radiation problem for such structures is either not available or completely impractical for most of practical engineering applications.

4.2.2 Sound Intensity and its Measurement

Over a surface element as given in Figure 4.3 with area δA, the rate of work done by the fluid can be expressed as;

$$dE/dt = \vec{F} \cdot \vec{u} = pdA\vec{n} \cdot \vec{u} \qquad (4.7)$$

where, $p = p(x,t)$ is the acoustic sound pressure, $u = \vec{u}(x,t)$ is the vector acoustic particle velocity, varying in time and space, where time and space dependence in the expressions are dropped for simplification, $\vec{F}$ is the net force applied, and finally, W is the net work done by the fluid.

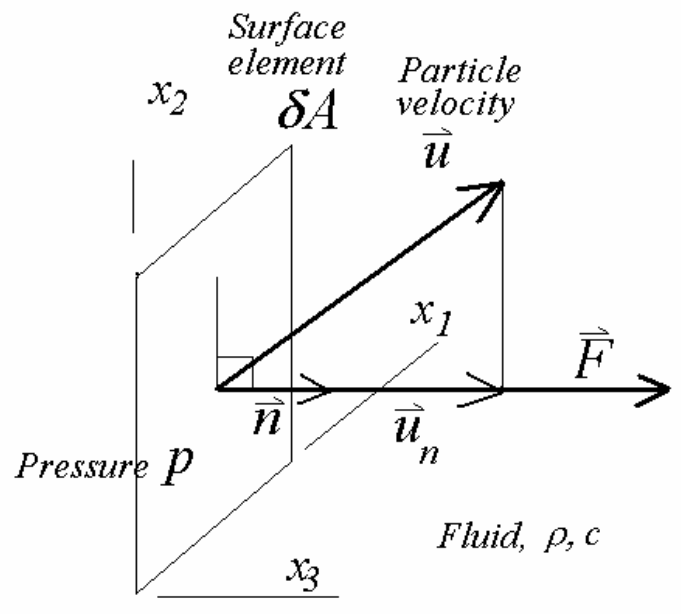

Figure 4.3 Surface Element In A Fluid With Acoustical Variables

Rearranging Equation 4.7 yields;

$$(dE/dt)/dA = p\vec{n}\cdot\vec{u} = pu_n \qquad (4.8)$$

where, $u_n = \vec{n}\cdot\vec{u}$ is the component of particle velocity normal to the surface element. The left hand side of the equation, $(dE/dt)/dA$, is the acoustical power flow over the area element. By this token, quantity $p\vec{u}$ on the right hand side of the equation is defined as the instantaneous acoustical intensity vector as $\vec{I}(x,t) = p(x,t)\vec{u}(x,t)$ and Equation 4.8 can be reconsidered as

$$\vec{I}\cdot\vec{n} = I_n = p\vec{u}\cdot\vec{n} = pu_n = (dW/dt)/dA \qquad (4.9)$$

For a time-stationary sound field, with stochastic random acoustical variables, the net rate of flow of acoustic energy per unit area can be estimated from the cross-correlation function between the pressure and the particle velocity

as;

$$R_{pu_n}(\tau) = R_{I_n}(\tau) = \lim_{T\to\infty} \frac{1}{T}\int_0^T p(t)u_n(t+\tau)dt \qquad (4.10)$$

where T is a sufficiently long interval of time. The mean value of the expression in Equation 4.10 with $\tau = 0$ will be the mean of the intensity, $\bar{I}_n$, in the normal direction as

$$R_{I_n}(0) = \bar{I}_n = \frac{1}{T}\int_0^T p(t)u_n(t)dt \qquad (4.11)$$

Most practical noise control problems involve with time stationary noise fields. In these cases, frequency domain, spectral representation of the field variables is possible and more meaningful than the transient time domain representation. The Fourier transform pairs, the single-sided cross spectral density function, G_{I_n}, and the cross correlation function, R_{I_n} are as follows:

$$S_{I_n}(w) = \frac{1}{2p}\int_{-\infty}^{\infty} R_{I_n}(\tau)e^{-jwt}\,dt \qquad (4.12)$$

$$R_{I_n}(\tau) = \int_{-\infty}^{\infty} S_{I_n}(w)e^{jwt}\,dw \qquad (4.13)$$

The mean normal intensity, from the Equation 4.14, for $\tau = 0$ can then be given as;

$$\bar{I}_n = R_{I_n}(0) = \int_{-\infty}^{\infty} S_{I_n}(w)dw \tag{4.14}$$

Hence, $S_{I_n}(w)$ is the spectral representation of mean sound intensity $\bar{I}_n$ in the frequency domain of $-\infty < w < \infty$. In order to eliminate the negative frequencies single-sided spectral density functions can be defined as;

$$G_{I_n}(w) = 2S_{I_n}(w) \qquad w > 0 \tag{4.15}$$

$$G_{I_n}(w) = S_{I_n}(w) \qquad w = 0 \tag{4.16}$$

$$G_{I_n}(w) = 0 \qquad w < 0 \tag{4.17}$$

Furthermore, any cross-spectra has the following properties;

$$Re\{S_{I_n}(w)\} = Re\{S_{I_n}(-w)\} \tag{4.18}$$

$$Im\{S_{I_n}(w)\} = -Im\{S_{I_n}(-w)\} \tag{4.19}$$

Hence, the spectrum of the mean intensity has the following relations:

$$\bar{I}_n(w) = Re\{S_{I_n}(w)\} + Re\{S_{I_n}(-w)\} + (Im\{S_{I_n}(w)\} + Im\{S_{I_n}(-w)\})j \tag{4.20}$$

$$\bar{I}_n(w) = Re\{S_{I_n}(w)\} + Re\{S_{I_n}(-w)\} + (Im\{S_{I_n}(w)\} - Im\{S_{I_n}(w)\})j \tag{4.21}$$

$$\bar{I}_n(w) = 2Re\{S_{I_n}(w)\} = Re\{G_{I_n}(w)\} \tag{4.22}$$

That is, the mean intensity is composed of the real part of the instantaneous intensity, which is named as the active intensity, as well. The imaginary part of intensity, which is also named as the reactive intensity, sums up to zero identically for all the frequencies of mean intensity. The reactive intensity, therefore, represents the oscillating part of the acoustical energy field without any net transfer of power, whereas, the active part represents the net, actively drifted acoustical power from a point of interest, as the name implies.

Consider the following Fourier transforms pairs for pressure and particle velocity given as;

$$P(w) = \frac{1}{2p}\int_{-\infty}^{\infty} p(t)e^{-jwt}dt \tag{4.23}$$

$$p(t) = \int_{-\infty}^{\infty} P(w)e^{jwt}dw \tag{4.24}$$

$$U(w) = \frac{1}{2p}\int_{-\infty}^{\infty} u(t)e^{jwt}dt \tag{4.25}$$

$$u(t) = \int_{-\infty}^{\infty} U(w)e^{-jwt}dw \tag{4.26}$$

Substituting the corresponding time domain expressions in Equation 4.11, one obtains;

$$\bar{I}_n(w) = \lim_{T\to\infty} \frac{1}{T} \int_0^T P(w) e^{jwt} U_n(w) e^{jwt} dt \qquad (4.27)$$

The time averaging operation can be reduced into the well-known power relationship for two complex quantities as;

$$\bar{I}_n(w) = \frac{1}{2} Re\left[P(w) U_n^*(w)\right] = -\frac{1}{2} Re\left[P^*(w) U_n(w)\right] \qquad (4.28)$$

In practice, the lack of any physical pick-up that can be used for the direct measurement of intensity, necessitates the use of two probe signals, generally a pressure and a particle velocity probe (p-u combination), or double pressure probes (p-p combination) where the particle velocity is estimated via signal processing.

The signal detection with a p-u probe is straightforward. However, construction of particle velocity transducers are limited by many physical constraints, such as space and frequency range, as compared to pressure probe, i.e. microphones, with supreme sensitivity, frequency range, phase characteristics as well as spatial compactness. Therefore, there is a compromise between the available probe technology and the signal analysis instrumentation. The rapid advancement on the analysis equipment as a result of digital signal processing technologies eliminates the limitations on p-p technique to a great extent, hence, the method becomes the standard engineering practice in the last two decades.

The p-p approach utilizes a first order approximation to the linearized momentum equation for an expression of the particle velocity as;

$$\frac{\partial u_n}{\partial t} = -\frac{1}{r}\frac{\partial p}{\partial x_n} \approx -\frac{1}{r}\frac{p_2 - p_1}{d} \tag{4.29}$$

where d is the distance between the nodes 2 and 1 of the finite difference element with the sound pressures p_2 and p_1, respectively. Hence, the time rate of change of particle velocity can be expressed as,

$$u_n \approx -\frac{1}{rd}\int_{-\infty}^{t}\left[p_2(t) - p_1(t)\right]dt \tag{4.30}$$

For a spectral representation, the Fourier Transform of Equation 4.30 yields,

$$U_n(w) \approx -\frac{1}{iwrd}\left[P_2(w) - P_1(w)\right] \tag{4.31}$$

Furthermore, taking the linear average of the nodal pressures as the mean sound pressure of the element, the sound intensity can be expressed in frequency domain as,

$$I_n(w) \approx \frac{1}{2}Re\{\frac{1}{2}(P_2(w) + P_1(w))\frac{i}{wrd}(P_2(w) - P_1(w))^*\} \tag{4.32}$$

Arranging the terms and dropping ω dependence for the sake of simplicity;

$$I_n(w) \approx \frac{1}{2}Re\{\frac{-i}{2wrd}(P_2P_2^* + P_1P_2^* - P_2P_1^* - P_1P_1^*)\} \tag{4.33}$$

The auto-power spectra $P_1 P_1^*$ and $P_2 P_2^*$ in the bracket which are real do not contribute to the intensity. Hence,

$$I_n(w) \approx \frac{1}{2} Re\{ \frac{-i}{2wrd} (P_1 P_2^* - P_2 P_1^*) \} \quad (4.34)$$

However, $P_1 P_2^* = \left| P_2 P_1^* \right|^*$, hence the terms in the bracket is the difference between a complex number and its conjugate, which is twice the imaginary part.

$$I_n(w) \approx \frac{1}{2} Re\{ \frac{-i}{2wrd} 2\, jIm\{ P_1 P_2^* \} \} \quad (4.35)$$

After simplifications one obtains;

$$I_n(w) \approx \frac{Im\{ P_1 P_2^* \}}{2? rd} \quad (4.36)$$

Equation 4.36 is the fundamental relation for the estimation of sound intensity by two-microphone cross-spectral method. Sound intensity measurements have found applications in noise control engineering where energy based estimations are required, such as sound power determination, source location, insertion loss, transmission loss and radiation efficiency problems related to machinery noise.

4.2.3 Use of sound intensity on the determination of IL

Analytical methods for the determination IL are complicated and basically

restricted to some general cases which fell short in modeling many enclosure structures of practical importance. They are limited mainly by the improper boundary conditions and material properties not complying with the real physical cases. The general practice, as usual, is the measurement of this value under specified laboratory conditions.

The standard method is the use of a reverberation chamber with spatially uniform sound power distribution that fulfills diffuse sound field conditions. Although they can supply a rough figure for the acoustical performance, one basic problem with such measurements is the loss of any information on the local sound transmission characteristics of the structure. On the other hand, a through inside into the local vibro-acoustic behavior of the structure is of crucial importance for the determination of transmission paths.

$$DW_0 = \frac{W_0}{A_{Total}} DA \tag{4.37}$$

$$DW_E = \vec{I} \cdot \vec{n}\, DA = I_n DA \tag{4.38}$$

where DA is the area element of the surface that encloses the structure with a total area of A_{Total}. Using the definition of IL as introduced in Equation 4.2, the insertion loss of the differential DIL, element can be written as;

$$DIL = L_I - L_W - 10log_{10} A_{Total} \tag{4.39}$$

Equation 4.39 simply states that if an enclosure is excited internally by an

air-borne noise source, the distribution of the Insertion Loss over any enveloping surface can be estimated from the normal, active intensity measurements.

4.2.4 Determination of Radiation Efficiency Sound Intensity

Use of energetic expressions obtained from a near-field intensity mapping can be used at the evaluation of this kind of structures. The definition of the radiation efficiency can be used for a differential area element DA as,

$$s_{rad} = \frac{I_n DA}{rcDA\langle u^2{}_n \rangle} = \frac{I_n}{rc\langle u^2{}_n \rangle} \qquad (4.40)$$

where, I_n is the active intensity component in surface normal direction, $\langle u^2{}_n \rangle$ is the velocity of the differential area and, rc is the characteristic impedance. Taking logarithms to the base 10 of both sides by using reference values and constants;

$$I_{ref} = 10^{-12}\, W/m^2,\ u_{ref} = 5 \cdot 10^{-8}\, m/s,\ \ rc \approx 400 rayls, \quad (4.41)$$

Using reference values given in Equation 4.40, Equation 4.41 can be expressed in terms of levels in dB as.

$$10log_{10}(s_{rad}) = 10log_{10}(I_n) - 10log_{10}(u_n^2) \qquad (4.42)$$

and, with the usual convention of $L_X = 10log_{10}X$ one gets;

$$L_{s_{rad}} = L_{I_n} - L_{u_n^2} \tag{4.43}$$

On the boundary of the vibrating surface, the acoustic particle velocity equals to normal component of the surface vibration velocity. Therefore, particle velocity terms obtained from the near-field intensity can be used as an excellent approximation for the surface velocity levels. In practice, it is not possible measure the particle velocity in the close vicinity of the radiating surface due to the probe dimensions. The estimated particle velocity, then, has always a lower value than the true surface vibration velocity, the error changing with the second order of the velocity magnitude. Noting that, propagating part of the intensity vector, that is the active intensity, is due to the phase gradient of the pressure field, but not due to the magnitude gradient which is practically constant in the probe vicinity, the magnitude of the intensity changes only to the first order of the estimated velocity errors. Therefore, the overall effect on the radiation efficiency will be to the first order of particle velocity errors.

4.2.5 Implementation of the Methodology: Measurements

The measurement set-up for the determination of near-field intensity is given schematically in Figure 4.4. The measurements are carried in a fully-anechoic room environment with 10 x 10 x10 m dimensions form the tip of the open cell polyurethane foam origin absorptive wedges with 1.4 m in effective length. The room has a cut-off frequency (lower frequency bound where the room satisfies free-field conditions) at 50 Hz for sound power measurements conducted with respect to ISO 3745 for precision grade measurements. Therefore, the reactivity index of the room for intensity measurements can totally be neglected down to a lower frequency bound of 50 Hz.

The enclosure, however, is placed on a rectangular plate out of thick plywood for the measurements. The plane acts as an acoustically hard surface, with 3 x 3 m dimensions. The theoretical conditions in this case can be simulated by free field over a reflecting plane.

The measurement grid encloses the structure around its four lateral surfaces. Preliminary measurements have shown that the radiation from the top surface is lower than 10 dB compared to the lateral surfaces. Hence, the top of the surface is neglected due to this low transmission characteristic. The grids of the surfaces have 12 rows (vertical direction), and 6 columns (horizontal direction) with 15cmx15cm elements. The measurement points are located at the mid point of these square grid elements.

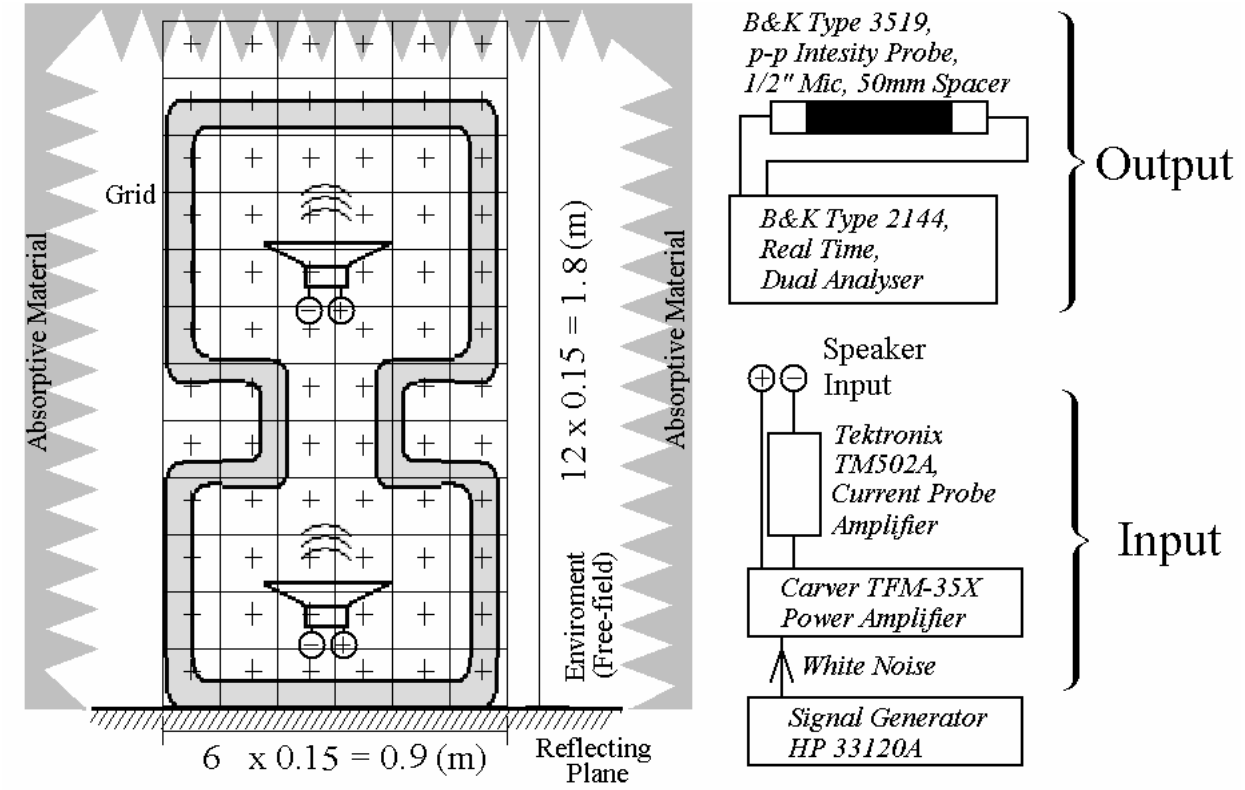

Figure 4.4 Measurement Set-up for Near-field Acoustical Intensity Measurements

The room is equipped with a microphone positioning system of five degrees of freedom, three rectangular, two angular, which gives the capacity to locate the probe in three dimensions specified in rectangular, spherical and cylindrical coordinates via a computer software.

The face to face, p-p intensity probe, B&K Type 3519, is composed of two 12 mm (nominal) or ½ inch phase matched condenser type microphones. A 50 mm microphone spacer (2 inches or 4 times the microphone diameter), is used for the separation of microphones. The choice of 50 mm is related to the upper bound of the frequency range of interest. The plane wave theory is used in order to estimate this separation distance theoretically [15]. For a 50mm spacer, the calculated error is less than 0.6 dB up to the frequency of 1000 Hz, and less than 3 dB when the frequency bound is 2000 Hz. The latter is too high to be acceptable. However, it can still be used for the determination of energetic characteristic of an enclosure.

The lower bound is related to the phase matching of the microphones. A B&K Type 3541 Intensity calibrator is used for the phase mismatch check and the microphone pair is found to have less than 0.7 dB error for frequencies higher than 50 Hz.

A B&K Type 2144, dual channel real time signal analyzer is used for signal processing. The analysis is carried out in Constant Percentage Bandwidths (CPB) with 1/12 Octave band resolution. The preference of CPB analysis, where frequency domain is logarithmic, is the common practice in acoustical

engineering due to hearing characteristics of the human ear. The human ear itself processes the sound pressure signal logarithmically, where the whole concept of musical perceptions are related. Therefore, 1/12 Octave Band resolution has a technical value related to the equally tempered scale of Western musical system, with octave intervals divided into 12 half tones forming a harmonic series.

Two commercially available, 4 Ω, mid-way loudspeakers are placed in each of the main compartments of the enclosure as input sound sources. Speakers are driven by an audio amplifier. An input band-limited white noise signal (DC to 20k Hz), that is random noise with flat power spectral density all over the frequency range, is supplied by a signal generator. At the input, the time domain signals of input current and voltage are monitored by means of a set of current and voltage probes.

Loudspeakers used in the experiment are calibrated in an anechoic room environment by means of sound power measurements carried out in a hemispherical enclosing surface with 10 microphone positions conforming with ISO 3745 standard. The calibration curves for different voltage settings are then used for insertion loss and radiation efficiency calculations.

4.2.6 Results and Analysis

The Insertion Loss values in 1/12 Octave Bands are given for four of the lateral surfaces, and their mean as an overall indicator of the enclosure behavior in Figure 4.5. The panels are named in accordance with the construction of the enclosure under investigation as LEFT and RIGHT, which have similar material properties, DOOR which is composed of two panels that can operate as two separate doors. These doors are closed during the experiments, so that there are no acoustical leak paths.

Finally, the fourth panel is named as BACK, which is the door standing part of the enclosure when serving as a refrigerator cabinet. This side is different from the rest of the walls, as it has no outer layer of metal origin. The design idea behind this alteration is to provide better heat transfer characteristics during the refrigeration.

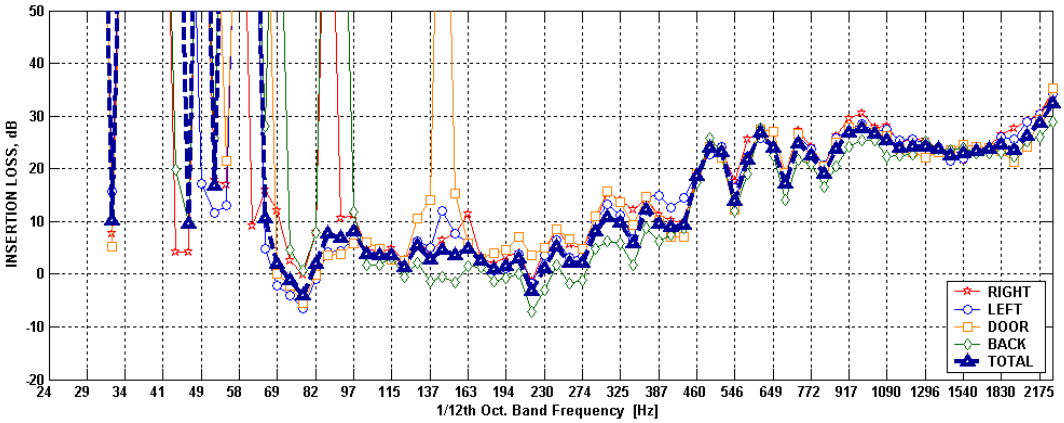

Figure 4.5 Insertion Loss (IL) of the Enclosure (20-2200 Hz)

As a check for the measurement quality the upper bound of the frequency range in Figure 4.5 is extended to 2000 Hz . Although the level values in dB's may not have required precision with an error more than ±3dB, the shape of the IL curve conforms well with the theoretical expectations. On the other hand, below 200 Hz all measurements are contaminated by errors due to abrupt sign changes in active intensity measurements. A through examination of the local values, i.e. the values at individual points of the grid, have shown that these are mostly due to values taken at the edge of the grid surfaces where intensity flow may be due to either one of the panel surfaces. This behavior is more dominant when one of panels is the DOOR panel. Therefore, it may be concluded that acoustical leaks at the overlapping surfaces of the door edges are responsible for such deviations.

The individual panel behaviors are not much different from each other as far as the shape of the spectral distributions are concerned. However, there is a systematic difference of 1-2 dB between the other three panels and the BACK panel, which is an expected result considering the weakness of the construction as mentioned above.

Figure 4.6 introduces the trend of the experimentally found IL curve by smoothing (averaging in the frequency) the corresponding data on the mean of the panels. At the lower frequency region (f < 200 Hz, Region I), the enclosure behaves like a so-called small enclosure, where the IL is almost independent of the frequency. The bulk compliance characteristics of the enclosed air volume and the enclosure walls are effective in this region.

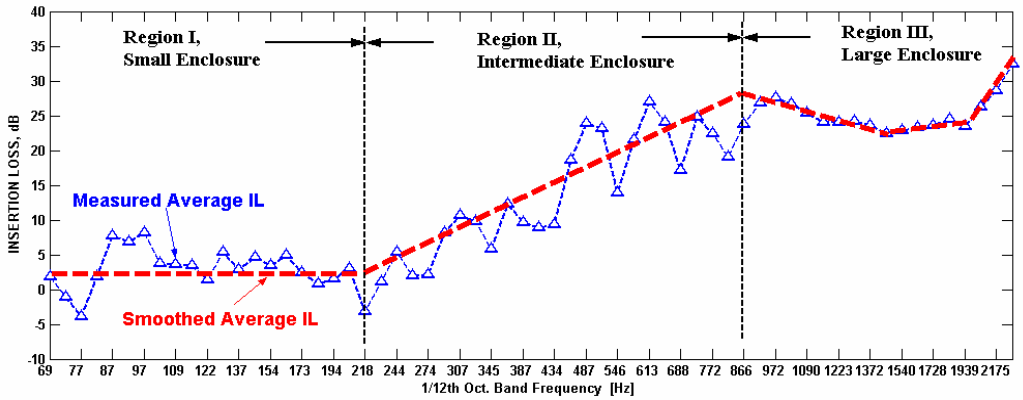

Figure 4.6 Identification of Enclosure Transmission Characteristics

At the frequency range of 200 Hz<f<800 Hz (Region II), the enclosure acts as a so-called intermediate one. This region is dominated by the modal behavior of the inside air volume and the structural walls, which give rise to the corresponding dips in the insertion loss curve. In case they have coupled modal behavior, the effect is more severe and it is possible that IL can assume values smaller than zero where the enclosed noise source becomes more effective if it were not enclosed at all.

In the frequency range where f > 800 Hz (Region III), the structure acts like a so-called large enclosure where the modal density of the inside air volume and the panel structures are very high. The Insertion Loss curve presents no distinct dips at this region except at the coincidence frequency as discussed before.

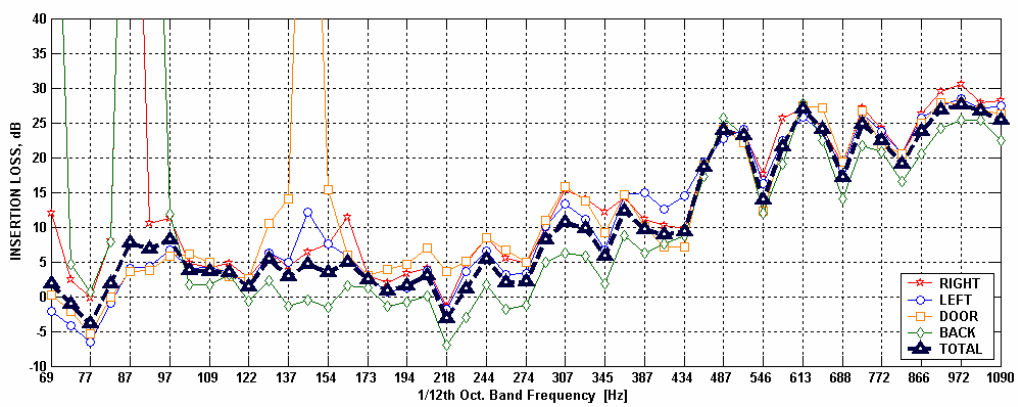

Figure 4.7 Insertion Loss (IL) of the Enclosure (70 1000 Hz)

Figure 4.7 shows the same IL curve for the frequency range of 70 Hz to 1000 Hz with a better resolution in order to present the so-called IL dip frequencies. An IL dip frequency can be observed as a frequency where the IL curve has a recession compared to its general monotonically increasing trend. At these frequencies, the enclosure is acoustically weak with lower transmission loss values compared to the behavior at the neighboring frequency bands.

IL dips are determined and presented at Table 4.1. The values are tabulated in accordance with the corresponding 1/12 Octave Band center frequencies. The widths of these bands with the standard labeling of the 1/3 Octave Band center frequency labels are also presented for narrow band (FFT) comparisons.

The local energetic behavior of the enclosure is investigated, as example cases, in three distinct 1/12 Octave Band Frequencies. Corresponding to the small enclosure region the band with 153.99 Hz center frequency, and with 9 Hz bandwidth is chosen. Note that the figures for the center frequency band have

nothing to do with precision, but are kept as they are used nominal 1/12 Octave band labels in acoustical signal processing applications.

Table 4.1 Insertion Loss (IL) Dip Frequencies

Insertion Loss (IL) Dip Frequencies								
1/12 Octave Frequency Bands, [Hz]						Corresponding 1/3 Octave Frequency Bands, [Hz]		
Band No	*Lower*	*Center*	*Upper*	Rounded Center Frequency	Band Width	Lower	Center	Upper
94	*74.98*	***77.18***	*79.44*	**77**	4	71.3	**80**	89.8
97	*89.12*	***91.73***	*94.42*	**92**	5	89.1	**100**	112.2
99	*99.99*	***102.92***	*105.94*	**103**	6	89.1	**100**	112.2
102	*118.84*	***122.32***	*125.90*	**122**	7	111.4	**125**	140.3
104	*133.34*	***137.25***	*141.27*	**137**	8	111.4	**125**	140.3
106	*149.61*	***153.99***	*158.50*	**154**	9	142.5	**160**	179.6
109	*177.81*	***183.02***	*188.38*	**183**	11	178.2	**200**	224.5
112	*211.33*	***217.52***	*223.89*	**218**	13	178.2	**200**	224.5
115	*251.16*	***258.52***	*266.10*	**259**	15	222.7	**250**	280.6
120	*334.94*	***344.75***	*354.85*	**345**	20	280.6	**315**	353.6
123	*398.07*	***409.73***	*421.74*	**410**	24	356.4	**400**	449.0
128	*530.84*	***546.39***	*562.40*	**546**	32	445.4	**500**	561.2
132	*668.28*	***687.86***	*708.02*	**688**	40	561.3	**630**	707.2
135	*794.25*	***817.52***	*841.48*	**818**	47	712.7	**800**	898.0
140	*1059.14*	***1090.18***	*1122.12*	**1090**	63	890.9	**1000**	1122.5
145	*1412.39*	***1453.78***	*1496.38*	**1454**	84	1425.4	**1600**	1795.9
150	*1883.46*	***1938.65***	*1995.46*	**1939**	112	1781.8	**2000**	2244.9

Four of the acoustical parameters related to intensity measurements, namely, active intensity, particle velocity, reactive intensity and sound pressure

are presented in these figures for the values of the four lateral panels. For the sake of better visualization, the measured values are logarithmically interpolated between the measurement points.

At every surface, the local z direction is out of the plane and local x, and y coordinates correspond to horizontal and vertical directions, respectively. The vector quantities, namely, active, reactive intensities and the particle velocity are plotted for out of plane z direction with contours where colors are scaled for logarithmically as dB levels of the acoustical quantity with references given in Equation 4.41, and in plane components in x and y direction are plotted in vector representation.

Figure 4.8 presents the results for the IL dip frequency of 153.99 Hz. The energetic properties clearly reveal out that the upper and lower parts of the cabinet are out of phase at these frequencies, whereas, all the lower and upper cavity boundaries are in phase in themselves. This is a clear indicator of a bulk motion of the structure where compliance of the air volume and the structure is responsible.

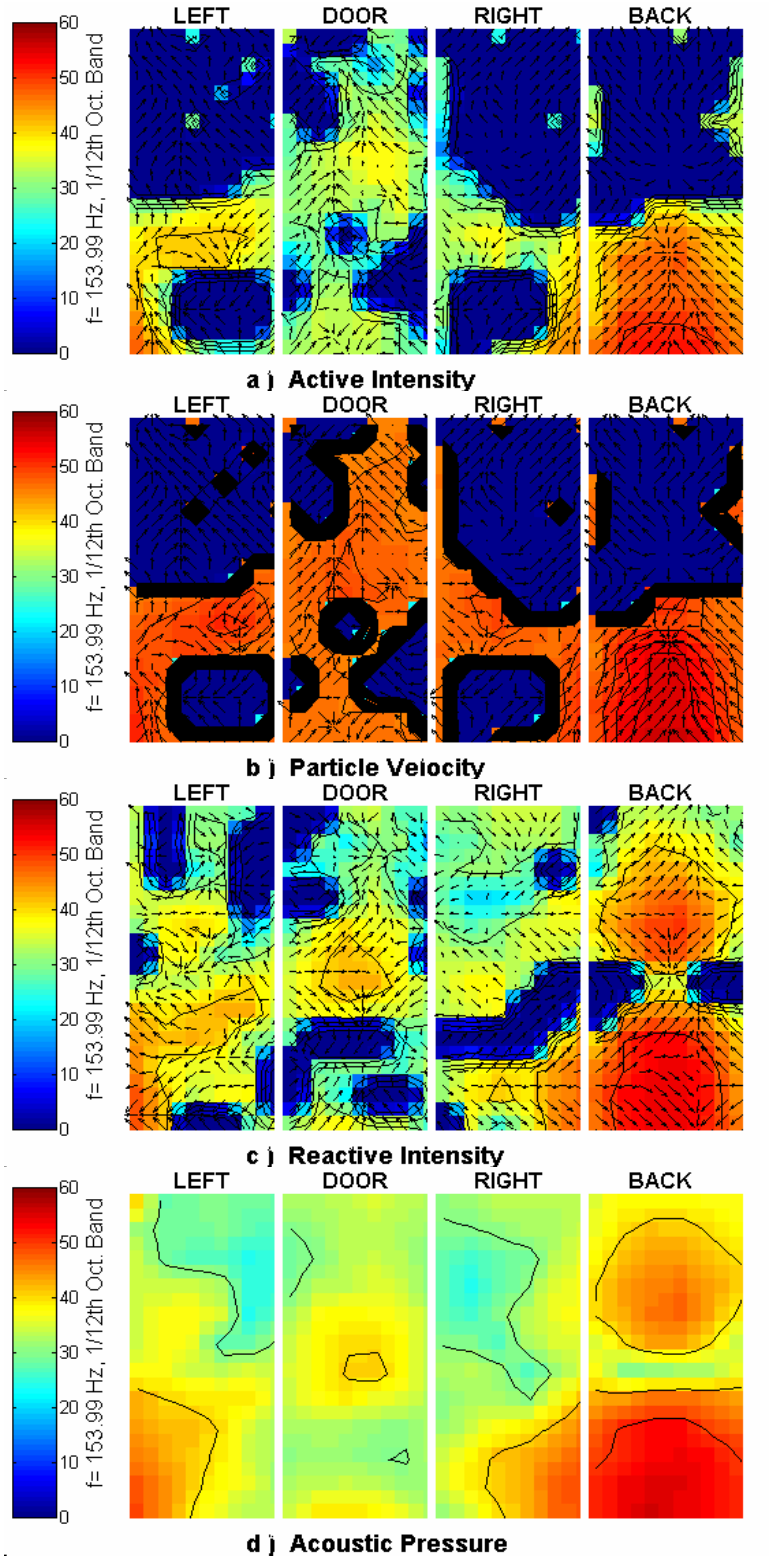

Figure 4.8 Near field Distribution of Acoustical Variables over the Structural Surfaces, 1/12 Octave Band Frequency=153.99 Hz

The Insertion Loss of an acoustically sealed enclosure can be expressed in terms of volume compliances as;

$$IL = 20log_{10}\left(1 + C_V \Big/ \sum C_{panel}\right) \tag{4.44}$$

where,

$$C_V = V_0 \Big/ rc^2 \tag{4.45}$$

is the compliance of the gas volume inside the enclosure, with V_0 the volume of the gas in the enclosure volume, $\sum C_{panel}$ is the sum of the volume compliances of all the enclosure panels with panel volume compliance defined as;

$$C_{Panel} = DV_{Panel} \Big/ p \tag{4.46}$$

Equation 4.46 can be integrated as the amount of volumetric displacement DV_{Panel} to the uniform pressure distribution p over the panel surface. Clearly, this value can either be calculated analytically or obtained experimentally. For the enclosure in hand, which is non-homogenous, non-isotropic and multi-layered, there is available analytical methodology to estimate this property. There is no standard acoustical measurement, that may be used to estimate this value directly either. Hence, the results of such an experiment can be exploited for this purpose, provided that, the frequency of the dip, and the related IL values are correctly estimated as;

$$\sum C_{panel} = C_V \Big/ (10^{IL/20} - 1) \tag{4.47}$$

In the case study, the estimated value, on the average, is IL= 4-3.5 dB at 153.99 Hz 1/12 octave band. The air volume of the structure is found to be (through IDEAS solid modeling module) as 0.4335 m^3. For r_0 =1.21 kg/m, and c=331.5 m/s at 20^{o}C, the calculated value for the air volume compliance is;

C_V =3.3 x x10^{-6} m^5/N

and, the total panel compliance is;

$\sum C_{panel}$ =6.6-5.6 x10^{-6} m^5/N

Note that the air volume and the panel compliances are in the same order of the magnitude at this particular frequency range for this enclosure. As a conclusion, it can be inferred that when compliance of an enclosure is not achievable analytically, an IL experiment of this type can easily be used for an estimation of rough value at correct orders of magnitude. This is an invaluable design input for the interested noise control engineer.

In Figure 4.9 the same acoustical parameters are presented in the same format for 687.86 Hz, 1/12 Octave Band Frequency, which corresponds to an IL deep at the intermediate region. The modal behavior can be observed at the vector plot of active intensity where sinks and sources of sound energy are distinctly observable especially at the BACK panel. Obviously, there are no physical sources or sinks injecting active power to acoustical field at those locations, hence these energetic behavior can only be explained by the resonance of the structure, coupled with the enclosed air volume.

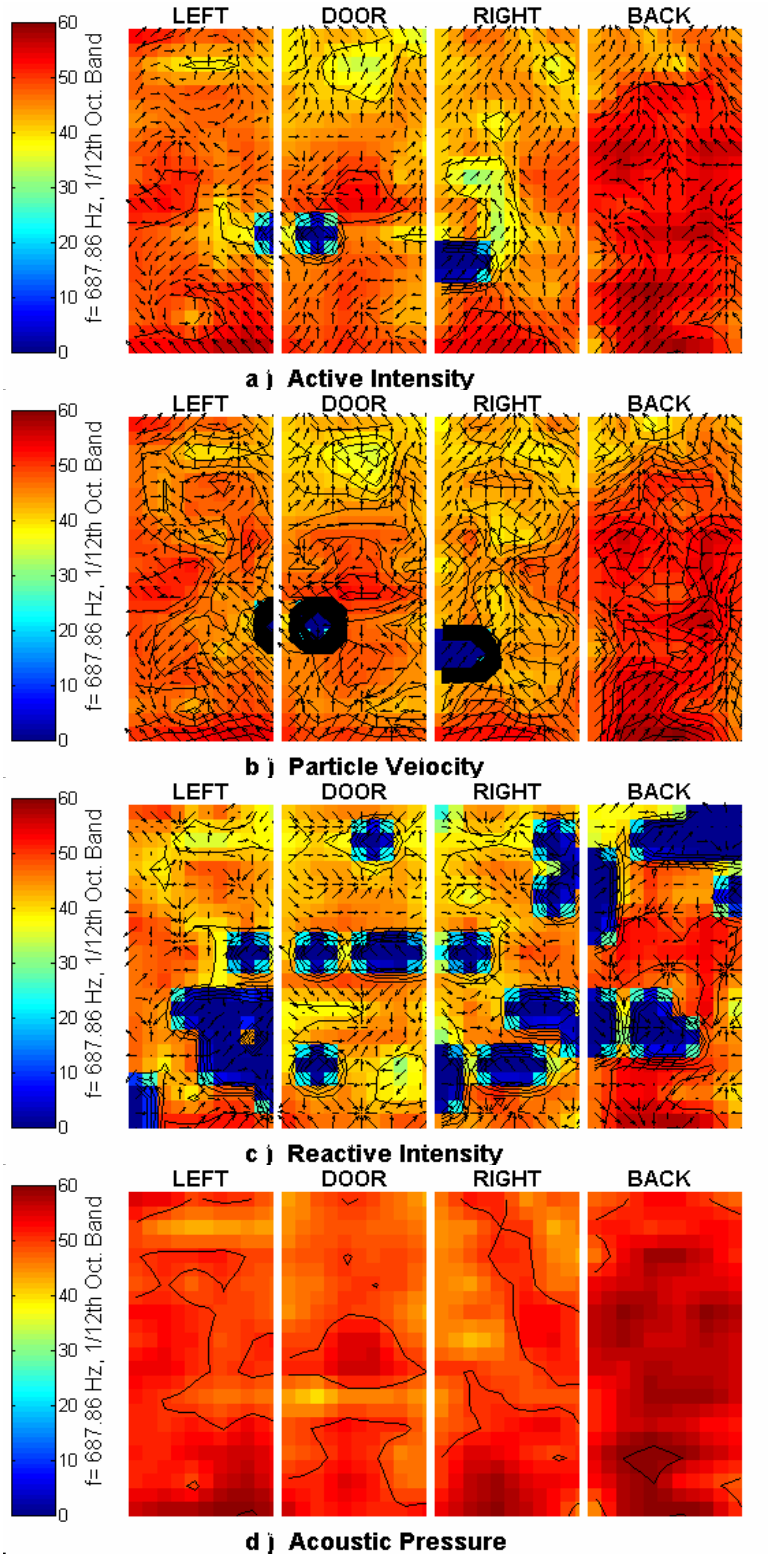

Figure 4.9 Near field Distribution of Acoustical Variables over the Structural Surfaces, 1/12 Octave Band Frequency=687.86 Hz

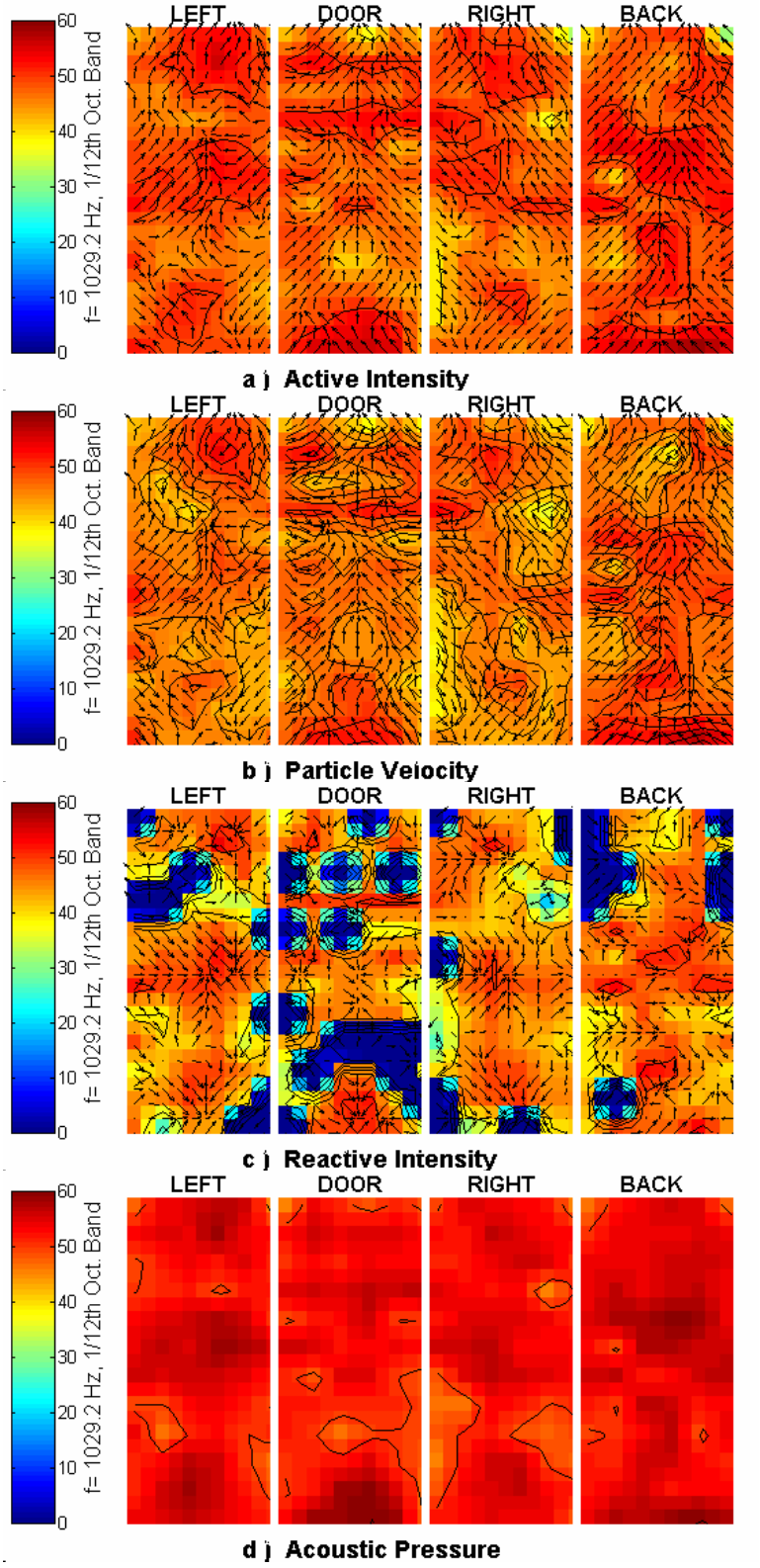

Figure 4.10 Near field Distribution of Acoustical Variables over the Structural Surfaces, 1/12 Octave Band Frequency=1029.20 Hz

Figure 4.10 is to depict the behavior at 1029.20 Hz 1/12 Octave Band Frequency from Region III for large enclosures. No distinct modal behavior is observable at the vector plots. Moreover, the sound pressure is almost uniform all over the structure with no more than 3 dB deviation.

The final output of this experimental investigation is the radiation efficiency presented in Figure 4.11. The frequency range is extended at the lower and upper bounds in order to gain some physical insight at these margins (below 50Hz, above 1000 Hz), with a reservation on the precision. The frequency scale is 1/12 Octave Band standard center frequencies rounded to the next integer value.

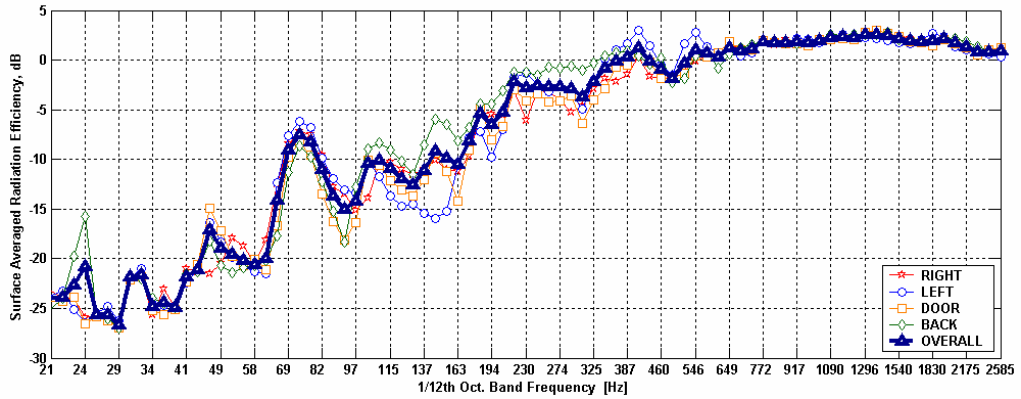

Figure 4.11 Radiation Efficiency of the Enclosure

The radiation efficiency curve of the enclosure has typical characteristics such as; below –20 dB values at the very low frequency region ($f < 50$ Hz), then monotonically increasing to the value of 0 at around 800 Hz. At the higher frequencies, this trend of monotonic increase diminishes and the curve becomes flat. This is a theoretically expected behavior, unless, the coincidence frequency is not reached. It is observed from the IL measurements that this is not the case for

this particular enclosure. This observation is verified by the radiation efficiency characteristics, as well.

On the other hand, the radiation efficiency of the structure is not related to the volumetric properties of the enclosure, but to the vibro-acoustic properties at the outer, radiating surface of the enclosure. However, at around any resonance frequency of the enclosure, where the impedance of the surface structure matches with that of the inside bulk impedances of the solid and/or the air volume, the radiation efficiency may severely increase. In the frequency region of 70-80Hz or 100-110 Hz such behavior can be observed very clearly as the radiation efficiency jumps to a value of –7 dB from the expected value of –15 dB in the former frequency range, and to a value of –9 dB from an expected value of –13dB.

Identification and explanation of this behavior requires the solution of the interior cavity acoustics, which is the subject of the following sections of this chapter.

4.3 Acoustical Modal Analysis of Coupled Cavities

4.3.1 Theory of Cavity Acoustics

A brief discussion on the modal behavior of an enclosed space is presented. Consider the wave equation, which can be expressed for the acoustic pressure p as,

$$\nabla^2 p(x,t) = \frac{1}{c^2}\frac{\partial^2 p(x,t)}{\partial t^2} \tag{4.48}$$

where c is the speed of sound. After taking the Fourier transform, the equation becomes the so-called Helmholtz Equation as

$$(\nabla^2 + k^2)P(x) = 0 \tag{4.49}$$

where $k = w/c$ is the so-called wave number with w, the angular velocity related to the frequency f as, $w = 2pf$.

A modal decomposition of the acoustic pressure P can be obtained by considering the characteristic functions (e*igenmodes*) of Equation 4.49 so that,

$$P(x) = \sum_{n=1}^{\infty} P_n Y_n(x, k_n) \tag{4.50}$$

where, $Y_n(x, k_n)$ are eigenfunctions satisfying,

$$(\nabla^2 + k_n{}^2)Y_n(x) = 0 \qquad (4.51)$$

with some boundary conditions specified over the enclosing surface.

There exist closed form solutions for coordinate systems defined by $x = (x_1, x_2, x_3)$, x_i denoting orthogonal directions of some three-dimensional coordinate frames, such as $x = (x, y, z)$ for Cartesian, $x = (r, q, z)$ for cylindrical coordinates, where Equation 4.51 is separable. The simplest case of such a coordinate system is the Cartesian coordinates, where the volume enclosed by the level surfaces, i.e. $x_1 = const.$, $x_2 = const.$, $x_3 = const.$, form a rectangular room. Equation 4.51 is subject to some boundary conditions over the room surfaces, and the simplest one is the rigid wall assumption, that is;

$$\nabla Y_n(x) \cdot n_{out} = 0 \quad \text{on } S \qquad (4.52)$$

where S is the enclosing boundary surface and n_{out} is the normal vector of the surface S.

Solution to Equation 4.51 with the boundary conditions given in Equation 4.52 is;

$$Y_n(x) = \sqrt{e_x e_y e_z}\cos\left(\frac{n_x p x}{L_x}\right)\cos\left(\frac{n_y p y}{L_y}\right)\cos\left(\frac{n_z p z}{L_z}\right) \qquad (4.53)$$

with

$$Y_n(x) = Y_{n_x n_y n_z}(x) = Y(x, n_x, n_y, n_z) \quad (4.54)$$

where, with $i = x, y, z$ e_i's are arbitrary constants, n_i's are integers extending from 0 to infinity, with L_i as the length of the corresponding edge of the rectangular volume enclosed by the Cartesian coordinates of the acoustical cavity, are the so-called modal numbers

Modal numbers are related to the wave number k as,

$$k^2 = k_x^2 + k_y^2 + k_z^2 = p^2((n_x/L_x)^2 + (n_y/L_y)^2 + (n_z/L_z)^2) \quad (4.55)$$

where, $k_i = p\, n_x/L_x$ are separation constants related to the i[th] coordinate. The special case of $n_x = n_y = n_z = 0$, that is $(0,0,0)$ mode, corresponds to a purely compliant behavior of the air in the cavity due to its bulk modulus.

The eigen-functions $Y_n(x, k_n)$ are orthogonal over the volume V, and they can be normalized to form an orthonormal set of functions by choosing $e_{ni} = 1,$ if $n_i = 0,$ and $e_{ni} = 2,$ if $n_i \rangle 0,$ in Equation 4.53. This yields the following equation;

$$\frac{1}{V}\int_V ?_m(x)?_n(x)dV = d_{nm} \quad (4.56)$$

where d_{nm} is the Kronecker delta function defined as d_{nm} =1 if *n*=*m*, and d_{nm} =0

if $n \neq m$.

Finally, modal eigenfunctions constitute a complete set, hence any well-behaved function $f(x)$ for points x can be expressed as a linear combination of $Y_n(x, k_n)$. This property can be exploited to obtain a Green's function satisfying the same boundary conditions, i.e. rigid walls, in terms of $Y_n(x, k_n)$'s.

By definition, the Green's function $G(x,y)$ can be expressed as,

$$(\nabla^2 + k^2)G(x,y) = -\delta(x - y) \tag{4.57}$$

where x and y represent the field coordinates for the receiving and source points, respectively, and $\delta(x - y)$ is the Dirac's delta function. Using the completeness property of the modal eigen-functions, $G(x,y)$ can be expressed as;

$$G(x,y) = \sum_{m=0}^{\infty} b_m Y_m(x) \tag{4.58}$$

Substitution of Equation 4.58 into Equation 4.57, and considering that $Y_n(x,k_n)$ satisfies the homogenous Helmholtz equation, the following expression is obtained,

$$\sum_{m=0}^{\infty} b_m (k^2 - k_m^2) Y_m(x) = -\delta(x - y) \tag{4.59}$$

Multiplying both sides by $Y_n(x)$ and integrating over the volume, V of the cavity,

that is;

$$\int_V \sum_{m=0}^{\infty} b_m (k^2 - k_m^2) Y_m(x) Y_n(x) dV = \int_V -d(x-y) Y_n(x) dV \tag{4.60}$$

Using the definition of the Dirac delta function, and orthonormal properties of the eigenfunctions, Equation 4.60 gives for b_n' s as;

$$b_n = \frac{Y_n(y)}{V(k_n^2 - k^2)} \tag{4.61}$$

Hence, the Green's function can be expressed as;

$$G(x,y) = \sum_{n=0}^{\infty} \frac{Y_n(y) Y_n(y)}{V(k_n^2 - k^2)} \tag{4.62}$$

Green's function formulation is fundamental for the forced solution of the Helmholtz equation as in the case of acoustical response of a cavity to a volume velocity source excitation.

4.3.2 Acoustical Response of a Cavity to a Volume Velocity Source Excitation

Consider the acoustical cavity given in Figure 4.12 with a cavity volume V, and boundary surface S where locally reactive impedance type boundary conditions are valid. The acoustical cavity includes distribution of volume flow sources $Q_{vol}(y)$ exciting the cavity at some domain of the total volume V.

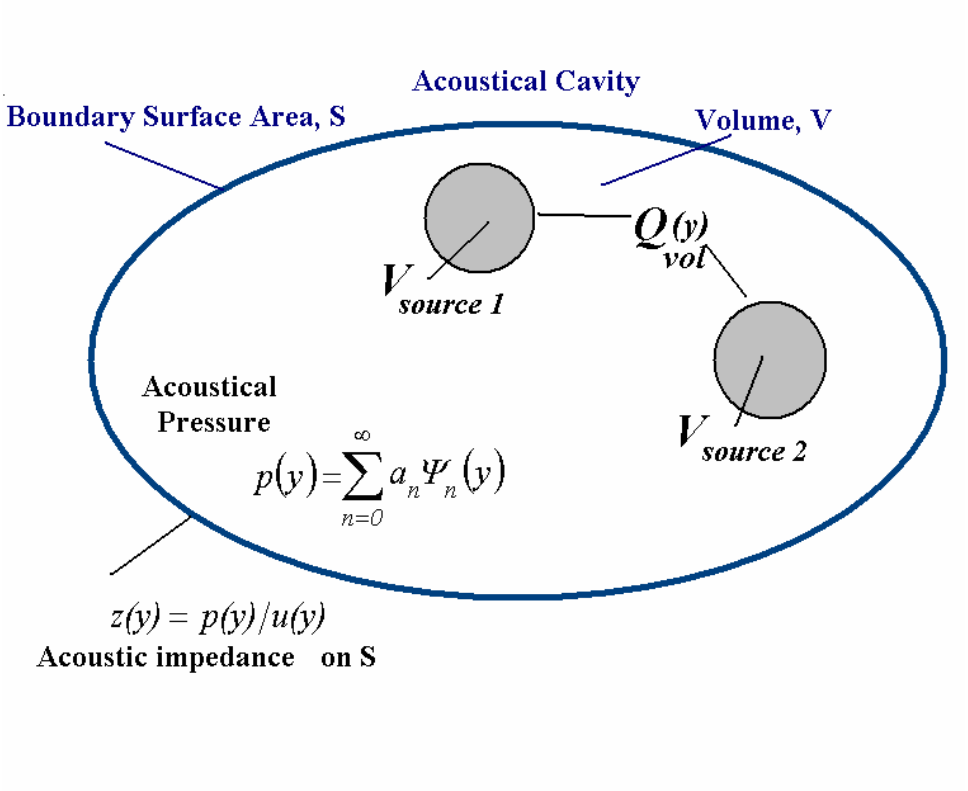

Figure 4.12 Acoustical Cavity with Acoustic Impedance Specified on the Boundary Walls, Excited by Volume Velocity Sources

The solution of the inhomogeneous wave equation for a volume velocity forcing function of Q_{vol}, that is

$$(\nabla_y^2 + k^2)p(y) = -Q_{vol}(y) \tag{4.63}$$

can be constructed from any properly chosen Green's function with $\nabla G(x,y) = 0$ on S as;

$$p(x) = \int_V Q_{vol} G(x,y) dV + \int_S G(x,y) \nabla p(y) n dS \tag{4.64}$$

A special case arises when the surfaces of the enclosed volume are locally reactive as opposed to bulk reactive surfaces, meaning that wall-cavity mode coupling is important. For a locally reactive surface subject to a harmonic sound field, the boundary condition at each point on the surface S can be described as a continuous impedance function. Acoustic impedance z(y) at point y of the surface can be expressed in terms of p(y) and u(y), the complex acoustic particle velocity normal to the enclosing surface as;

$$z(y) = p(y)/u(y) \quad \text{on S} \tag{4.65}$$

For harmonic excitations with the angular velocity ω, acoustic pressure and particle velocity are related to each other via the linearized momentum equation as;

$$\nabla p(y) \cdot n = -jwr_0 u(y) \tag{4.66}$$

where $j = \sqrt{-1}$, and r_0 is the density of the medium. Normalized specific acoustic admittance $b(y)$ can be defined from the acoustic impedance $z(y)$ and the characteristic impedance $r_0 c$, as;

$$b(y) = \frac{r_0 c}{z(y)} \tag{4.67}$$

Hence, the boundary condition on the surface S can be given as;

$$\nabla p(y) \cdot n = -jkb(y)p(y) \text{ on S} \tag{4.68}$$

The acoustic particle velocity over the boundary surface is the some of normal velocity u imposed by the boundary walls as expressed by the momentum equation and the due the admittance of the wall surfaces. Hence

$$\nabla_y p(y) = jwr_0 u_i(y) \cdot n - jkb(y)p(y), \text{ on S} \tag{4.69}$$

Placing this expression in the integral equation for p(x), one obtains;

$$p(x) = \int_V Q_{vol} G(x,y) dV + \int_S G(x,y)\left[jwr_0 u_i(y) \cdot n - jkb(y)p(y)\right] dS \tag{4.70}$$

Furthermore, p(x) can be decomposed into eigenfunctions as;

$$p(x) = \sum_{n=0}^{\infty} a_n Y_n(x) \tag{4.71}$$

Following the usual procedure of volume integration over the cavity volume and

leaving the terms alone at the left hand side of the expression yields;

$$a_n = \frac{1}{V(k_n^2 - k^2)}\left[\int_V Q_{vol} G(x,y) Y_n(y) dV + \right.$$

$$\left. \int_S jwr_0 Y_n(y) u_i(y) \cdot n dS - \int_S jk Y_n(y) b(y) \sum_{m=0}^{\infty} a_m Y_m(y) dS \right] \tag{4.72}$$

Defining a term which normalizes complex specific admittance values in terms of eigenfunctions as

$$D_{nm} = \frac{1}{V}\int_S b(y) Y_n(y) Y_m(y) dS \tag{4.73}$$

However, for n ≠ m the eigenfunctions are orthogonal, therefore, the integration approaches to zero if $b(y)$ is uniform over the domain, which is a constant. Uniform and small admittance values are common to many practically important structures, as in the case of refrigerator cabinet. Consequently, retaining only the D_{nn} terms the expression will be further simplified to;

$$a_n(k_n^2 - k^2) = \frac{1}{V}\left[\int_V Q_{vol} Y_n(y) dV + \int_S jwr_0 Y_n(y) u_i(y) \cdot n dS - a_n D_{nn}\right] \tag{4.74}$$

Upon arranging for a_n;

$$a_n(k_n^2 - k^2 + jkD_{nn}) = \frac{1}{V}\left[\int_V Q_{vol} Y_n(y)dV + \int_S jwr_0 Y_n(y)u_i(y)\cdot ndS\right] \tag{4.75}$$

Finally using them in the modal decomposition expression $p(x)$ can be expressed as;

$$p(x) =$$

$$\sum_{n=0}^{\infty} \frac{wr_0 c_0^2 Y_n(x)}{V(wc_0 D_{nm} + j(?^2 - ?_n^2))}\left[\int_V Q_{vol} Y_n(y)dV + \int_S Y_n(y)u_i(y)\cdot ndS\right] \tag{4.76}$$

Equation 4.76 can be exploited for experimental determination of modal behavior of acoustical cavities. Terms in the brackets describe the excitation mechanism of the system, either as a distribution of volume sources, or as wall excitations specified as a velocity distribution. A loudspeaker placed in the acoustical cavity of interest can be decomposed in the modal domain, in terms of modal functions in two different ways: a volume velocity with source strength specified or with the specified diaphragm velocity as vibrating.

In any case, the expression assumes a constant at the particular mode of interest as;

$$Q_n = \int_V Q_{vol} Y_n(y)dV + \int_S Y_n(y)u_i(y)\cdot ndS = Const. \tag{4.77}$$

for a given mode of interest. Similarly, the acoustical pressure can be expressed

as;

$$p(x) = \sum_{n=0}^{\infty} K_n \frac{?}{(?_n ? + j(?^2 - ?_n^2))} \qquad (4.78)$$

where; K_n and h_n are defined as modal gain and dissipation constants as.

$$K_n = \frac{Q_n r_0 c_0^2 Y_n(x)}{V} \qquad \text{and} \qquad h_n = c_0 D_{nm} \qquad (4.79)$$

Hence, the response of an acoustical cavity to a volume source excitation can be expressed as sum of responses of second order systems. This physical concept is exploited for the experimental acoustical modal analysis presented in the following sections.

4.3.3 Finite Element Method Applied to Acoustical Cavities

Acoustic cavities are modeled and meshed in IDEAS Solid Modeling Toolbox. A finite element analysis of the cavity is conducted by means of a commercial FEM solver (SYSNOISE). Linear-order (four-nodes), iso-parametric, tetrahedral elements are chosen for meshing. The structure is compound of two sub-sections. The lower room is the first sub-section and, the rest of the cavity, that is the coupling neck and the upper cold sections, builds up the second sub-section.

The upper section, with structural complexities, is handled with a mesh size of L_{up}=16mm, whereas, the lower cabinet which has a simple and rough geometry is handled with a mesh size of L_{down}=40mm. These lengths are also a compromise between the computer capacity and the required upper frequency band for this analysis. It is advised to have at least six elements in one wavelength of interest. Therefore, the frequency bounds can be found from;

$$L_i = l/6 \quad \text{and} \quad f = c/l = c/6L_i \tag{4.80}$$

Hence, considering a speed of sound 340 m/s at around ambient temperature of 20^{o}C, the upper frequency bounds are found to be; F_{up}=3.5 kHz and F_{down}=1.4 kHz. These values are sufficient for the purposes sought in the study. The cavity walls are considered rigid. Hence, the particle velocity at the boundaries, or the gradient of the acoustic pressure, is taken to be zero. This

means the solutions are completely uncoupled from the enclosing structural walls.

Figure 4.13 presents the geometry of the enclosure together with c some concepts related of FEM analysis. The internal volume of the enclosure in hand is composed of two main cavities, namely, upper and lower rooms, connected with a coupling neck with complex geometric details due to its function as an air handling passage.

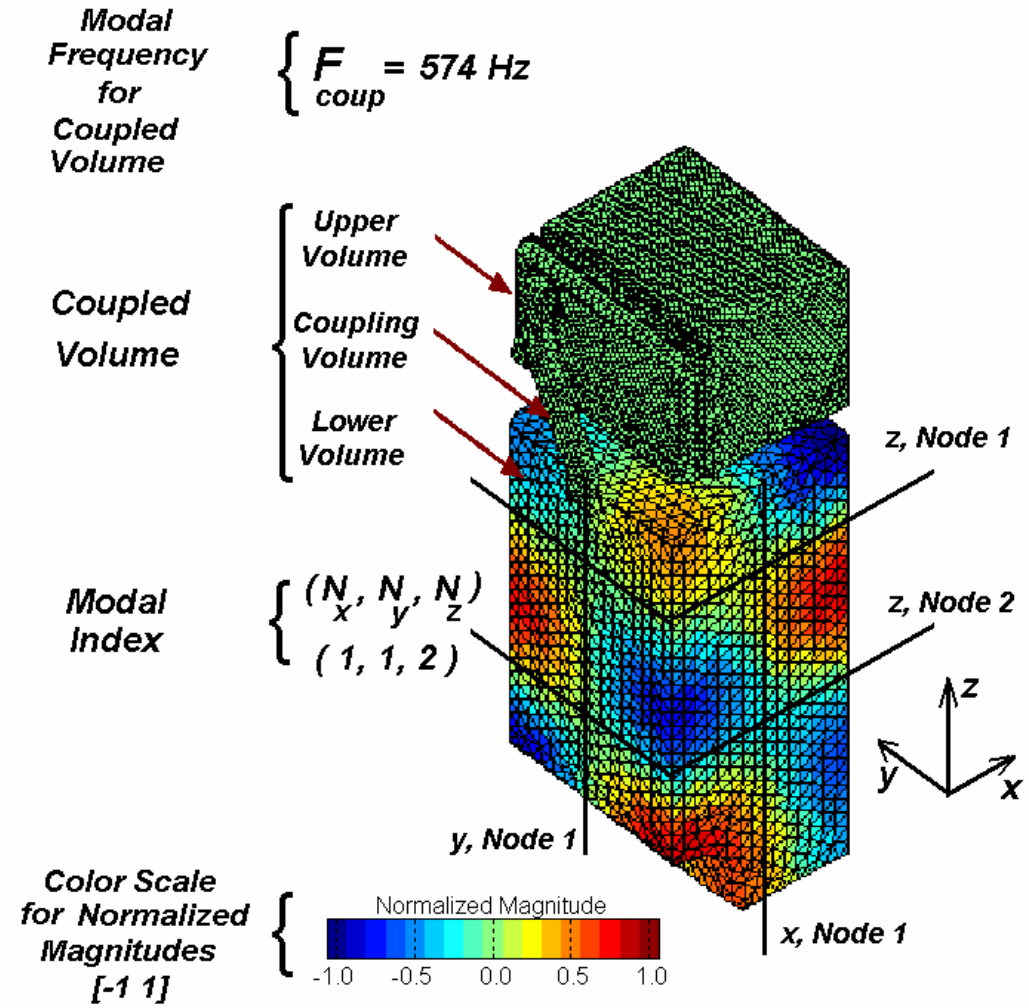

Figure 4.13 Enclosure Case Study. Key to FEM Solutions

One basic aim of this analysis is to investigate the acoustic behavior of sub-sections separately, as they are considered part of two different paths of transmission. The effect of the cavity coupling on the global description of the structure is also important. Hence, three different solutions are taken care of; upper cavity alone, lower cavity alone, and the coupled system together. However, the coupling region is included in the upper volume due to the complexity of its geometry. This is justified by the fact that, if it is treated alone, the coupling neck acts as one dimensional plane wave duct and the modal frequencies will be above 1000Hz.

The finite element solutions are valuable if they could be identified with some theoretically predictable mode shapes. Owing to the geometry of the structure, which may be the case of many practical noise emitting machinery enclosures, the cavity can be approximated as a collection of rectangular prismatic volumes, or sub volumes. Hence, modal decomposition procedures presented in the theory section can be used for this purpose.

The modes are named according to their corresponding modal numbers in the lower room and upper room. For the lower, a further simplification must be done due to the complexities at the coupling region. The modal identification is done in accordance with the un-interrupted compartment of the upper section, avoiding the coupling complexities.

Taking the orientation of the coordinates as the x axis running along the depth of the enclosure, while the y axis extending along the width, and finally z

axis stretching along the height of it, the modal shapes are mapped to the theoretical ones by considering the number of modal lines in the solutions (Figure 4.13). That is, a solution without a nodal line denotes a (0) mode number, whereas, n_i number of nodes corresponds to n_i'th mode number along that axis. In Figure 4.13, the modal shape corresponding to the (1, 1, 2) modal index is given with nodal lines indicated on the normalized equal magnitude contours.

It is worth mentioning some of the details related to the post-processing of the results generated by the FEM solver. In this study, solutions of the software are exported in Universal File Format (UFF) to MATLAB. Consequently, data processing and visualization are done in the latter environment. The routines developed can be generalized to any geometry and solver provided that input data are created in UFF 's, which is the commercial standard in Computer Aided Engineering (CAE) market.

Finally, from the theory, it is known that, modal behavior with modal shapes parallel to the walls, that is, the modes with either one of the modal numbers equal to zero; the interaction with the walls is less compared to cases if it is the other way around. Due to the practical importance, these waves have specific names as [**2**],

- Axial waves for which two of the modal indices are zero
- Tangential waves for which one modal index is zero
- Oblique waves where none of the modal index is zero

Hence, the effect of any dissipation or absorption mechanism bears an importance with the complexity of the modal behavior. For noise control purposes, this means, care must be given to vibro-acoustic characteristics of the structure that cannot be attenuated within the structure.

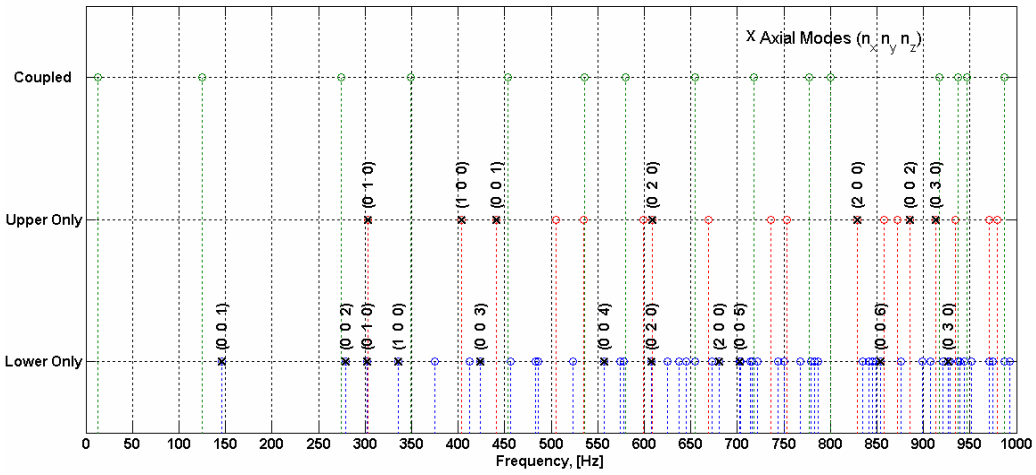

Figure 4.14 Axial Modal Frequencies of the Acoustical Cavities

Extracted modal frequencies and corresponding modal numbers for axial modes within the frequency range of interest are summarized in Figure 4.14 for better visualization. It should be noted that some modal frequencies and shapes do not have any correspondence with any one of the uncoupled solutions. This is an expected result with two mechanisms for explanation.

1. The first reason is related to the effect of the complex cavity structure that connects the upper un-interrupted, simple upper room cavity to that of the lower compartment. The connections are through narrow passages; those actually serve as air passages for the air-handling system.

The second mechanism is partly a consequence of the first one. These sections are effective either at very high frequencies or at some lower frequencies where all or some part of the structure acts with bulk properties.

Table 4.2, presenting the overall results of the FEM analysis, is constructed out of the three aforementioned results of FEM analysis. The modal frequencies are numbered with respect to the over all cavity behavior, with the corresponding frequencies given at the column with the header "all". The columns headed with "Lower" and "Upper and Coupler" gives the complete solutions for the uncoupled subsections. Finally, the last group of columns presents the corresponding modal numbers determined from the aforementioned investigation of the modal shapes.

The modal behavior related to the coupling effects are investigated in further detail. In Figure 4.15, first four modal shapes related to this coupling effect are presented side by side for comparison. The first modal shape is at F_{coup}=13Hz with the upper and lower compartments acting totally out of phase. The next modal shape with frequency F_{coup}=125Hz. In this case, however, the large cavities are almost in phase, but the coupling neck is 90^{o} behind this phase. These behaviors can only be explained by the bulk behavior of the system. This suggests that in the former case the system is acting like a Helmholtz resonator (a mass and a spring system) or a dynamic vibration absorber, whereas, in the latter case the coupling neck is resonating alone. The bulk behaviors are examined in detail in the related section.

Table 4.2. FEM Analysis Results and Modal Number Identification

Mod #	Modal Frequencies [Hz]			Modal Index		
	All	*Lower*	*Upper And Coupler*	*Nx*	*Ny*	*Nz*
1	13	10		0	0	0
2	125		114	0	0	0
3	146	146		0	0	1
4	274					
5	279	278		0	0	2
6	302	302		0	1	0
7	303		302	0	1	0
8	336	336		0	1	1
9	336	339		1	0	0
10	349					
11	375	374		1	0	1
12	404		402	1	0	0
13	412	412		0	1	2
14	424	424		0	0	3
15	441		442	0	0	1
16	454					
17	456	456		1	1	0
18	483	483		1	1	1
19	486	486		1	0	2
20	505		505	1	1	0
21	523	523		0	1	3
22	535		535	0	1	1
23	536					
24	557	557		0	0	4
25	574	574		1	1	2
26	578	578		1	0	3
27	580					
28	599		599	1	0	1
29	608	609		0	2	0
30	609		609	0	2	0
31	625	627		0	2	1
32	637	636		0	1	4
33	645	646		1	0	4
34	655	655		1	1	3
35	655					
36	669		669	1	1	1
37	673	672		0	2	2
38	681	676		2	0	0
39	703	703		0	0	5
40	704	702		1	2	0
41	714	714		2	0	2
42	716	716		1	1	4
43	718					
44	722	720		1	2	2
45	736		736	1	2	0
46	744	744		2	1	0
47	750	748		0	2	3
48	753		753	0	2	1
49	768	768		0	1	5
50	777					

Table 4.2 (continued)

	Modal Frequencies [Hz]			Modal Index		
Mod #	***All***	***Lower***	***Upper And Coupler***	***Nx***	***Ny***	***Nz***
51	779	779		2	1	1
52	783	781		0	2	3
53	787	786		1	2	3
54	787	787		1	2	3
55	800					
56	829		827	2	0	0
57	835	835		0	2	4
58	841	841		2	1	3
59	845	845		1	1	5
60	849	849		1	2	3
61	854	854		0	0	6
62	858		858	1	2	1
63	872		873	2	1	0
64	876	876		2	0	4
65	886		886	0	0	2
66	899	899		1	2	4
67	908	908		0	1	6
68	913		913	0	3	0
69	917					
70	921	923		2	2	0
71	927	927		0	3	0
72	929	929		2	1	4
73	934		934	2	0	1
74	937	937		1	0	6
75	937					
76	939	938		0	3	1
77	944	944		0	2	5
78	947					
79	952	953		2	2	2
80	971		972	2	1	1
81	971	971		0	3	2
82	975	975		2	0	5
83	979		980	1	0	2
84	987	987		1	1	6
85	987					
86	993	992		1	3	0

The other remaining coupled modes at F_{coup}=274 Hz and F_{coup}=279 Hz are too close to each other, the out of phase behavior at the coupling volume, but in phase behavior at the boundary volumes, again, suggests that the coupling volume is in resonance with some boundary conditions other than rigid walls. It can also be observed at $F_{coup=}$279Hz that the (0, 0, 2) mode related to the lower section becomes effective.

The next set of coupling frequencies are presented in Figure 4.16 for F_{coup}=349 Hz, F_{coup}=404 Hz, F_{coup}=454 Hz and F_{coup}=536 Hz. At all three of these frequencies, as the modal shapes display, the coupling volume is resonating and the upper and lower volumes are acting as bulk acoustical volumes as a compliance type boundary condition. The only exception is F_{coup}=404Hz where (1, 0, 0) mode like behavior is added to the coupled behavior of the whole system. This behavior has severe effects on the transmission characteristic of the enclosure, and this is discussed at the end of this section.

Figure 4.17 and Figure 4.18 are given for the modal frequencies where F_{coup}, F_{up} and F_{down} coincide with each other. The upper and lower cavities have a common dimension in y direction, hence, standing wave patterns along this direction at low frequencies must be similar with very close frequencies. At F_{coup}=F_{up}=F_{down}=302Hz, and 609Hz this phenomenon is clearly observed, where the former frequency is for (0,1,0) mode and the latter has nothing to do with the (0,2,0) mode. For F_{coup}=F_{up}=F_{down}=302Hz it is interesting to note that this coupled frequency appears twice. This suggest that these kind of coupling due to the coincidence of the coupling volume dimensions are not as severe as the coupling of the volumes via any connecting volume.

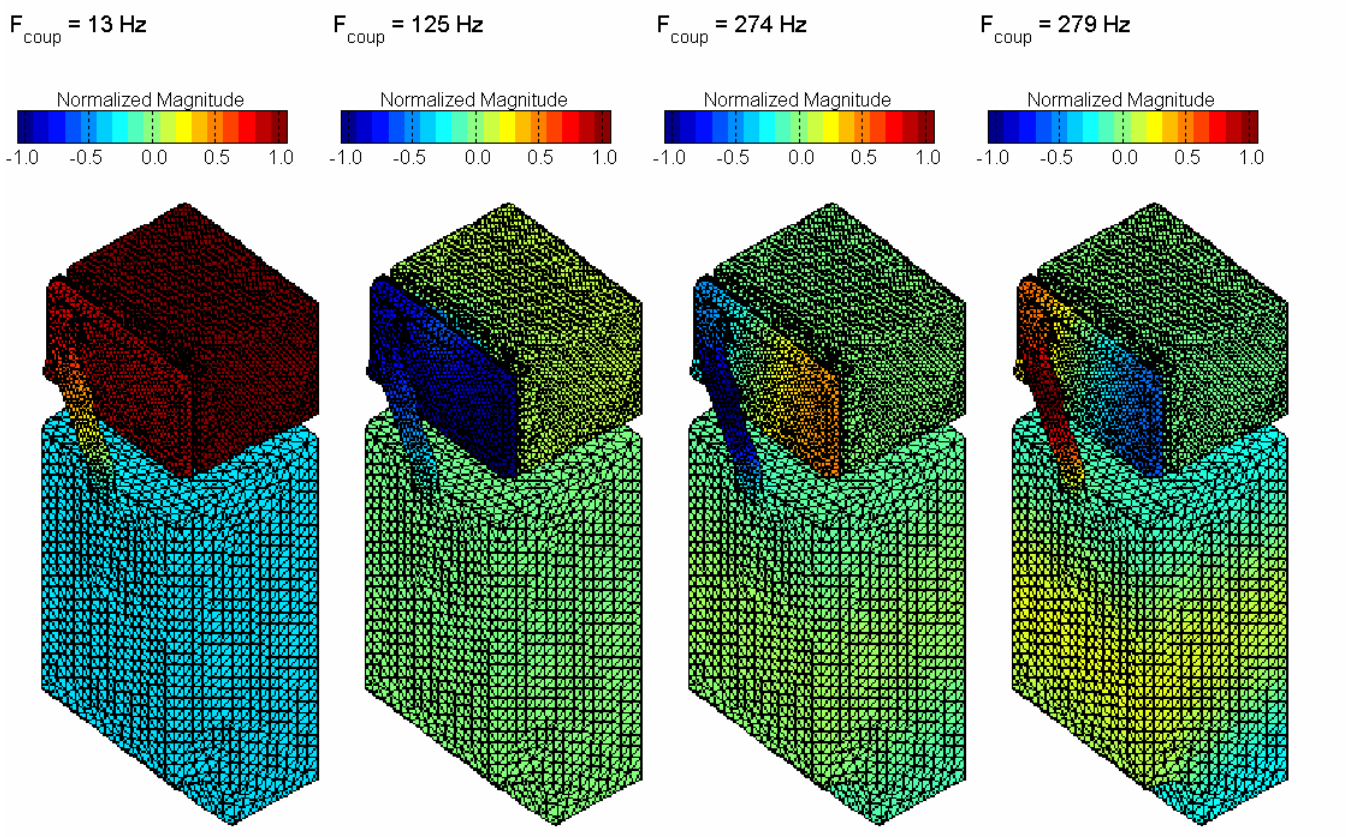

Figure 4.15 First Four Modal Shapes and Frequencies due to the Coupling Effects Only

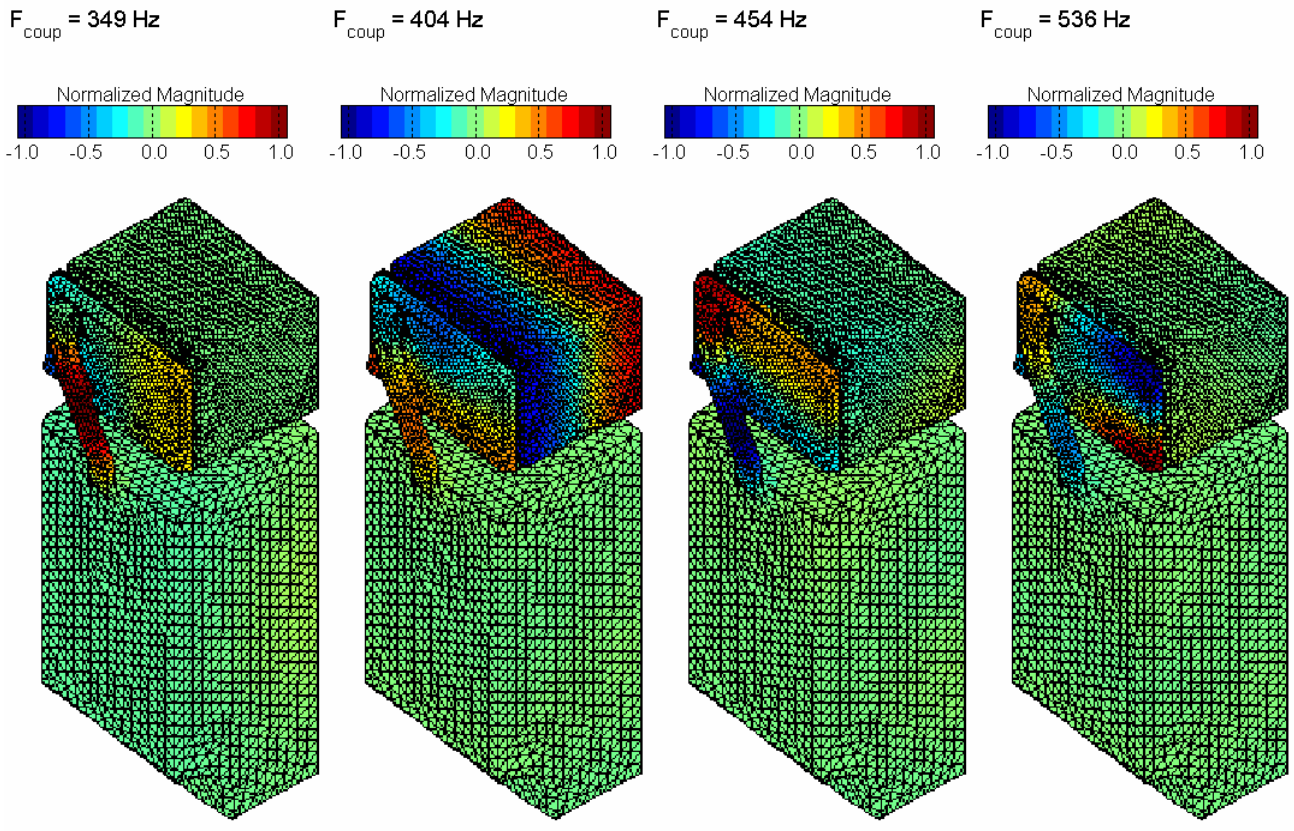

Figure 4.16. Second Four Modal Shapes and Frequencies due to the Coupling Effects Only

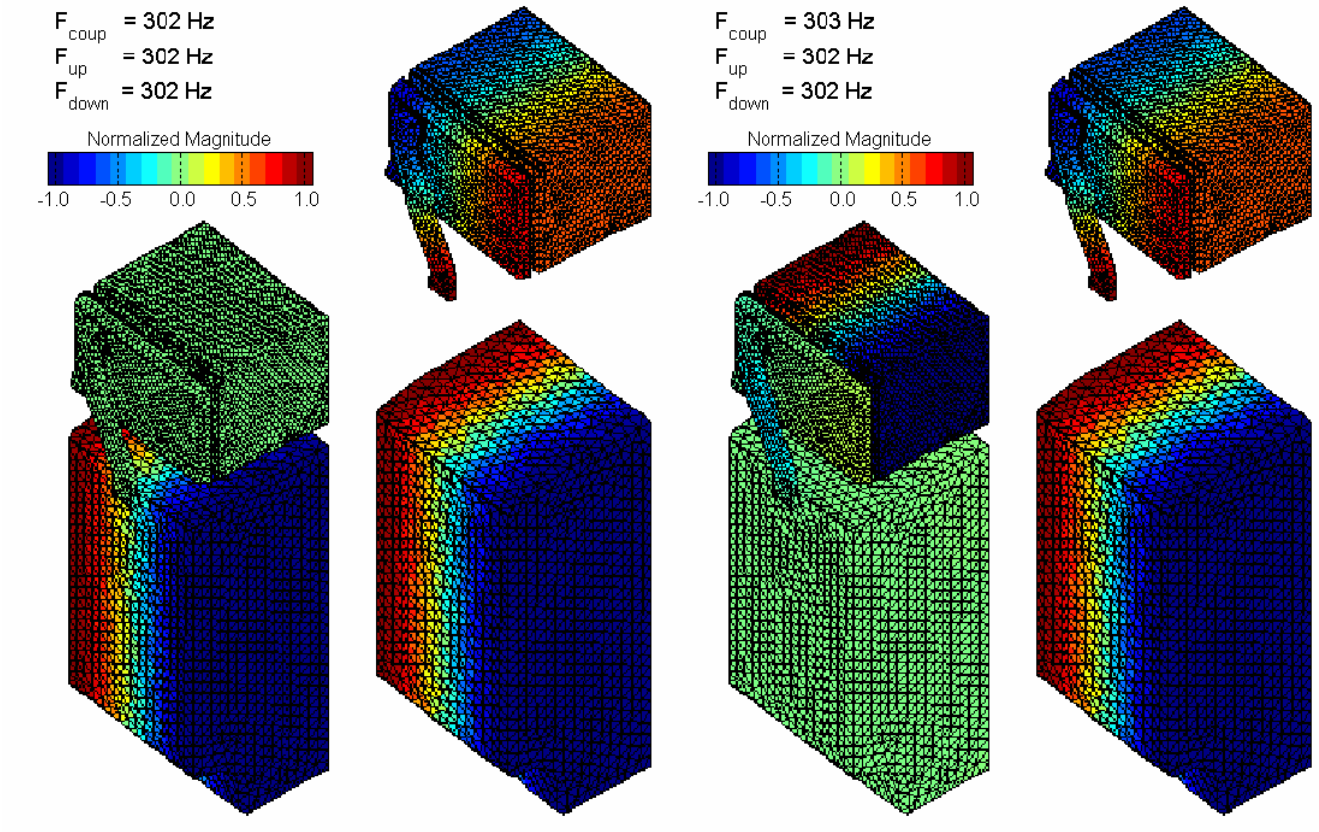

Figure 4.17. Modal Shapes at Shared Frequencies by the Upper, Lower and Coupled Cavities, F=302Hz, and 303Hz

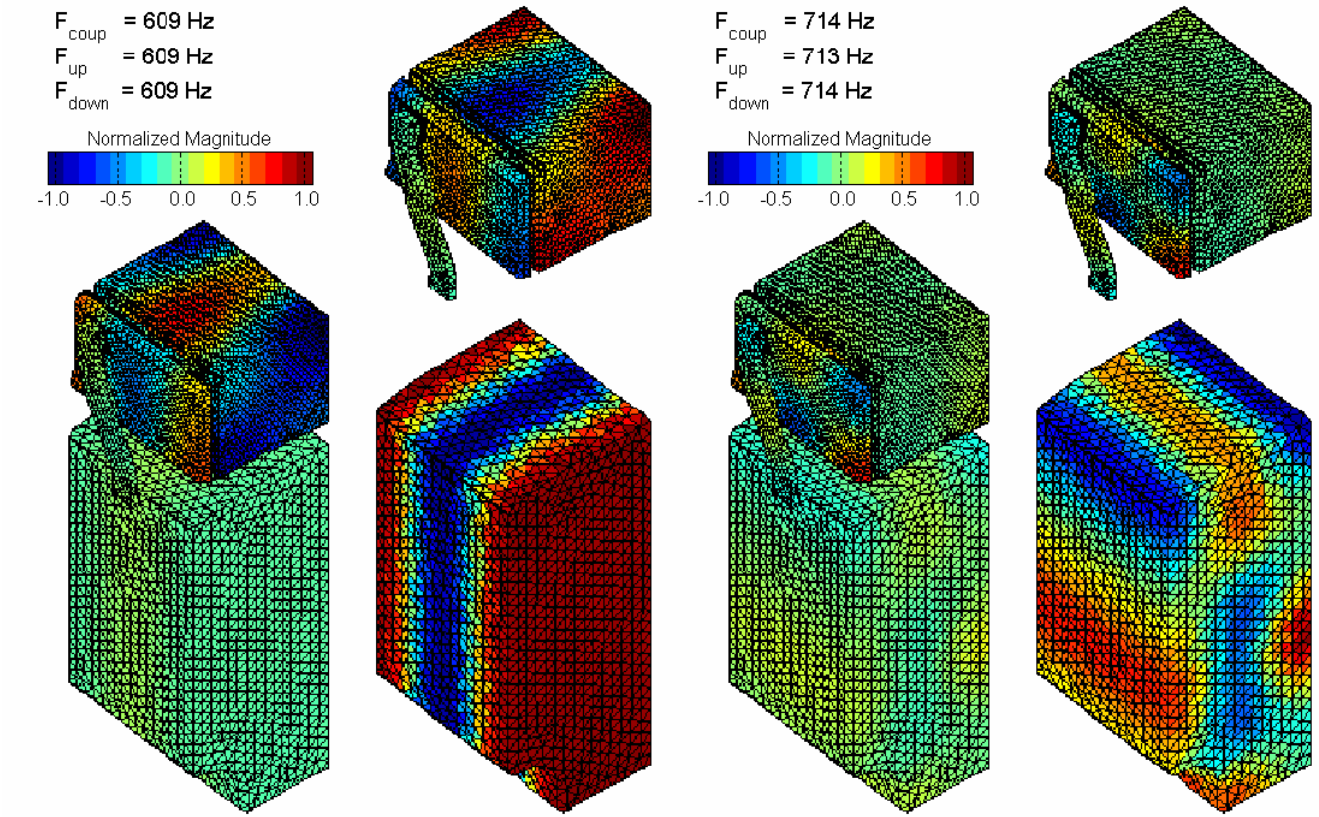

Figure 4.18. Modal Shapes at Shared Frequencies by the Upper, Lower and Coupled Cavities, F=609Hz, and 714Hz

4.3.4 Experimental Modal Analysis of Acoustical Cavities

In this section, experimental modal analysis of the acoustical cavity presented in the previous section is accomplished. The first step in this analysis is the construction and calibration of a volume source for excitation and of the system and measurement of the required Frequency Response Functions (FRF) by using this calibrated signal as input.

The experimental set-up is presented in detail for this purpose in the following section. Finally, modal extraction methodology based on the Equation 4.78 presented in the section on theory is applied for the analysis of resulting experimentally obtained FRF 's.

Volume Source Design for Experimental Acoustical Modal Analysis

Excitation of the cavity by means of volume flow source with prescribed characteristics is one of the crucial steps of experimental modal analysis. A source with known volume flow strength all over the frequency range of interest, with proper dimensions that can be fit into the refrigerator enclosure is difficult, if not impossible. To overcome this difficulty, reciprocity principle for a linear electro-acoustic transducer is used.

A volume velocity source is constructed out of a simple commercial type loudspeaker. By exploiting the principle of electro-acoustic reciprocity, the volume flow strength of the exciting loudspeaker is estimated from the input current and voltage signal in time domain, together with the output acoustic

pressure on the diaphragm. The estimated volume velocities from the measurement of electrical variables are calibrated in the frequency domain of interest by laser vibro-meter measurements on the diaphragm.

Estimation of the volume velocity of an acoustic source is essential for many practical applications that require measurement of frequency response functions of vibro-acoustical paths, or acoustic transfer impedances. System excitation for experimental acoustic modal analysis, and transfer path analysis by using vibro-acoustic reciprocity are two typical examples to be named. Construction of a known volume velocity source for a general purpose of usage involves difficulties due to size, frequency range of interest and cost effectiveness. Therefore, it is invaluable to obtain the source parameter, which is the volume velocity of a source that suits the specific application of interest. This requires an effective, flexible and robust methodology for the determination source strengths in-situ.

For a typical linear electro-acoustical transducer, as depicted in Figure 4.19, the electrical parameters, volt V current i and acoustical parameters sound pressure p and volume velocity Q are related to each other as [2],

$$\begin{bmatrix} V \\ \mathrm{p} \end{bmatrix} = \begin{bmatrix} Z_{ec} & T_{ea} \\ T_{ae} & Z_a \end{bmatrix} \begin{bmatrix} i \\ Q \end{bmatrix} \tag{4.81}$$

where, Z_{ec} is the clumped electrical impedance (V/i when $Q=0$), Z_a is the open-circuit acoustic impedance ($-p/Q$ when $i=0$).

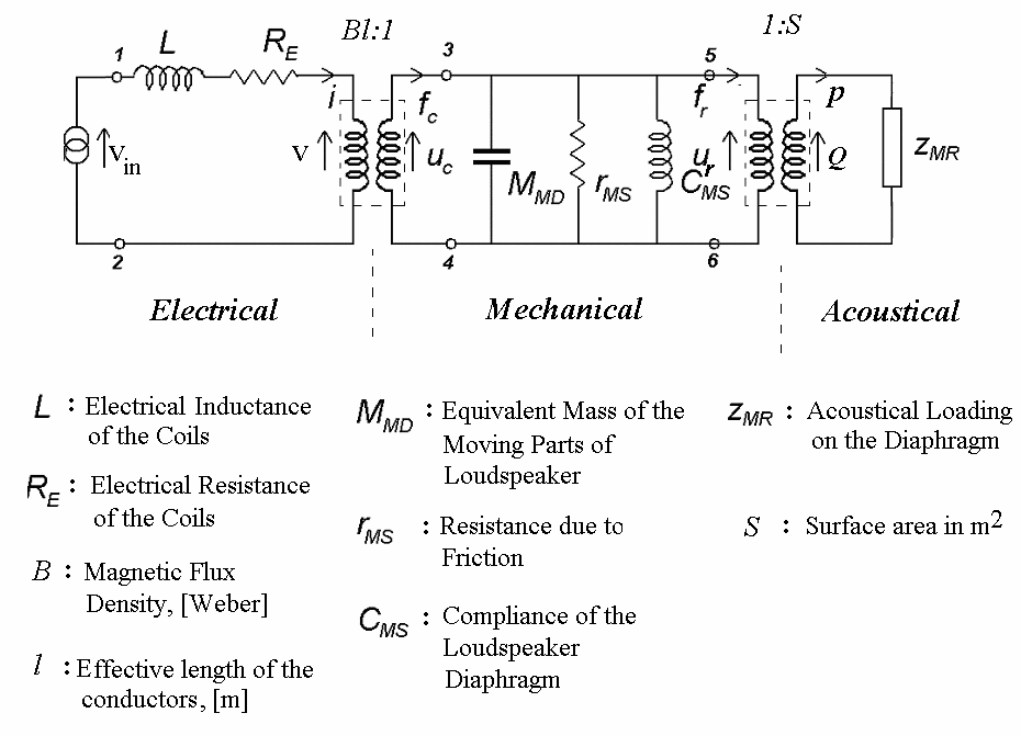

Figure 4.19 Mobility Type Representation of a Typical Electro-acoustic Transducer

If and $\left|T_{ea}\right| = \left|T_{ae}\right|$ the transducer is called reciprocal and the principle of reciprocity can be expressed in two alternative ways as;

$$\left|\frac{Q}{V}\right|_{p=0} = \left|\frac{i}{p}\right|_{Q=0} \tag{4.82}$$

$$\left|\frac{Q}{i}\right|_{p=0} = \left|\frac{V}{p}\right|_{i=0} \tag{4.83}$$

Both expressions can be used, under proper conditions, for an estimation of the volume velocity Q. Another relation of reciprocity type holds for the acoustical environments, which can be expressed as linear, time invariant systems, as

follows;

$$\left|\frac{p_2}{Q_1}\right|_{Q_2=0} = \left|\frac{p_1}{Q_2}\right|_{Q_1=0} \tag{4.84}$$

where subscripts represent two distinct points in the acoustical field, and the relation states that source and receiver points can be interchanged reciprocally. For a measurement system, where the acoustical environment and the transducers, that is, microphones and loudspeakers are reciprocal, these expressions can be used for a practical assessment of either the source strength form Q or, as important as this one, the non-linearity of the system elements, if there is any.

The primary aim of this study is the prediction of volume source strength of an electro-acoustic transducer from the input volt or current signals so that Frequency Response Function between the input volume source and the output acoustical pressure can be estimated correctly. For this; either one of Equation 4.82 or 4.83 can be exploited as;

$$H_{pQ}(f) = \frac{G_{pQ}(f)}{G_{QQ}(f)} \tag{4.85}$$

where $H_{pQ}(f)$ is the transfer function between input volume source and output acoustic pressure, $G_{pQ}(f)$ the cross spectrum of the input, output signals and $G_{QQ}(f)$ is the auto-spectrum of the input signal. The frequency dependency of these terms is omitted in the following equations for the sake of simplicity.

Equation 4.85 can be re-written by exploiting the reciprocal relations given in Equation 4.82 as follows, $H_{Qi} = H_{Vp}$ hence;

$$\frac{G_{Qi}}{G_{ii}} = \frac{G_{Vp}}{G_{pp}} \tag{4.86}$$

Equation (4.85) can be re-written as;

$$H_{pQ} = \frac{G_{pQ}}{G_{QQ}} = \frac{G_{pi}}{G_{Qi}} = \frac{G_{pi}}{G_{ii}} \frac{G_{ii}}{G_{Qi}} \tag{4.87}$$

Up on substituting the expression in given in Equation (4.86) to Equation (4.87);

$$H_{pQ} = \frac{G_{pi}}{G_{ii}} \frac{G_{ii}}{G_{Qi}} = \frac{G_{pi}}{G_{ii}} \frac{G_{pp}}{G_{Vp}} = \frac{H_{pi}}{H_{Vp}} \tag{4.88}$$

Equation 4.88 states that transfer function between the pressure and volume source can be estimated from the transfer functions between the pressure and current, and, between the voltage and the pressure. This is valid, of course, only at the diaphragm of the transducer for the magnitude of H_{pQ}.

In this study, the aim of the experimental modal analysis is not the prediction of mode shapes, but the modal frequencies. In this case, the input signal, or the volume source strength is not required as far as magnitude characteristics are concerned. On the other hand, it is crucial to measure the phase of the excitation correctly at each measurement point for the correct determination of the phase relation at every response points. Hence, the derivation given in

Equation 4.88 is used for phase relationship only. The source strength of the volume source is handled with different methodologies.

Anthony and Elliot [12] suggested three different methods for the measurement of the source volume velocity which require precise laboratory measurements, and among them surface velocity measurement of a loudspeaker diaphragm by a laser vibro-meter is the most accurate one, with considerable expensiveness. In this study, some alternative means of measuring the volume velocity of a source is investigated by exploiting the principle of electro-acoustic reciprocity for linear, time invariant transducers.

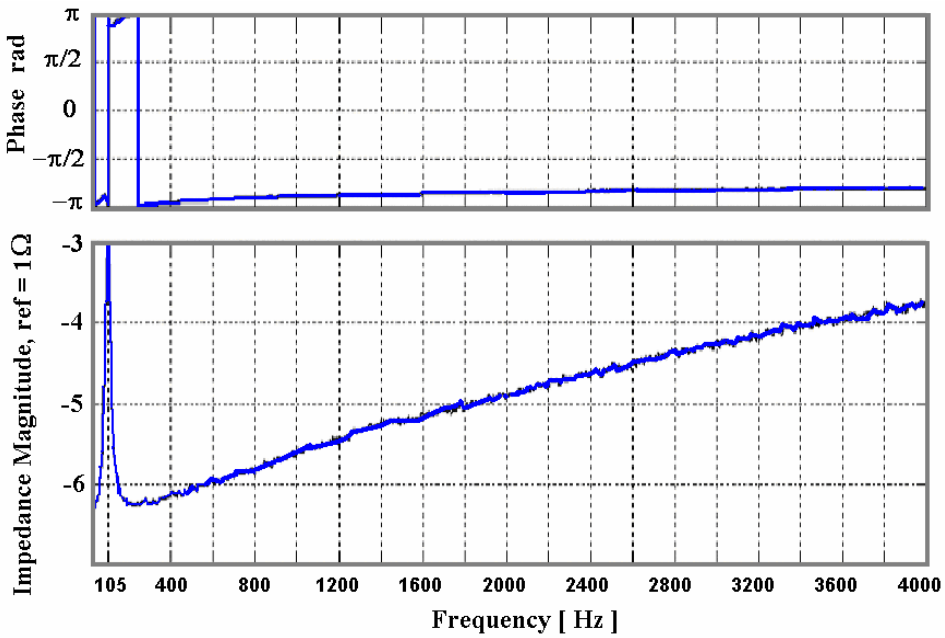

Figure 4.20 Impedance of Loudspeakers (Resonance at 105 Hz)

The sources under investigation are designed out of an ordinary, lightweight, cost effective mid-way speakers supplied from the local market with nominal impedance of 8 Ohms and diameter of 100mm. The sources are driven by

a band limited white noise, kept at $2V_{pp}$ and the current drawn by the source is measured at the output of the amplifier. The electrical characteristic of the loudspeakers is investigated via impedance measurements the frequency range of interest chosen as 20-4000 kHz. (Figure 4.20). The diaphragm resonance is found to be at 105 Hz, and the transducer has reasonable linear characteristics after 400 Hz.

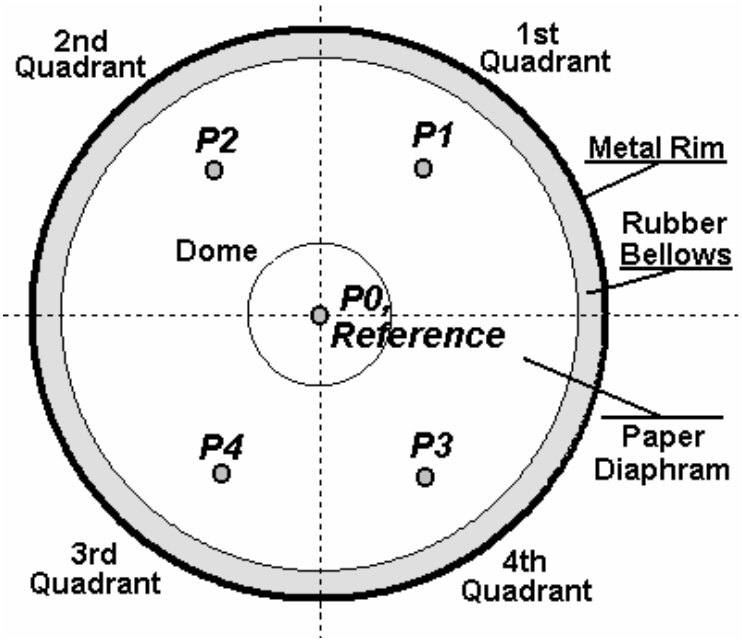

Figure 4.21 Regions of Loudspeaker Diaphragm for Laser Vibro-meter Measurements.

Laser vibro-meter measurements are conducted for the determination of diaphragm velocity at selected points as shown in Figure 4.21 the points are chosen to detect phase relation between four diaphragm quadrants via measured frequency response functions between the input loudspeaker coil voltage and surface velocity.

Figure 4.22 gives the results for H_{Qi}, the transfer function between the input current and the volume velocity, $Q = uS$, with u diaphragm normal velocity and S diaphragm area, normalized to the mid-point level. The frequency resolution of the measurements is 2Hz, at a frequency range of 0-6400 Hz. As expected, there are deviations from the ideal in-phase, piston like behavior, but these can be tolerated for the purpose of this study.

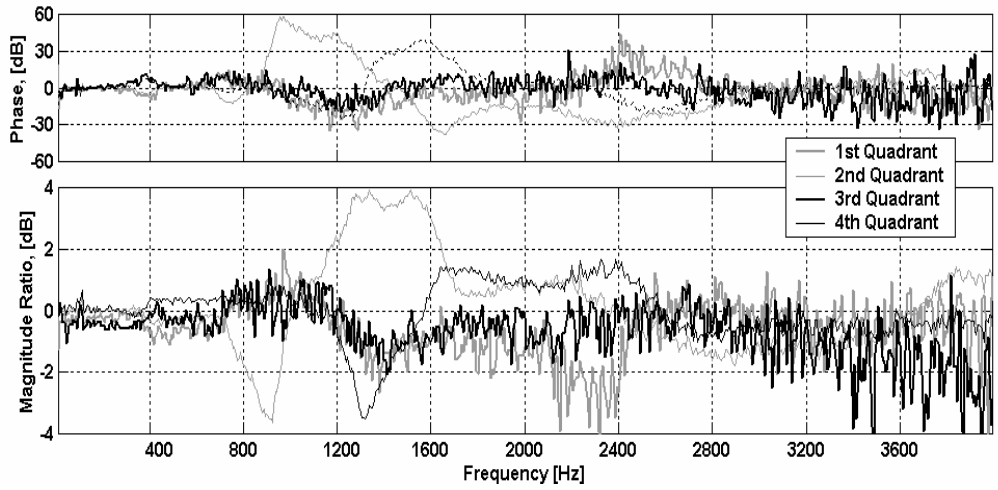

Figure 4.22 Normalized Frequency Response Functions for H_{Qi}

Set-up for Experimental Acoustical Modal Analysis

A set-up is developed for the experimental modal analysis of enclosures. It is modified for the requirements of the case study in hand and the related transducer positions are given in Figure 4.23.

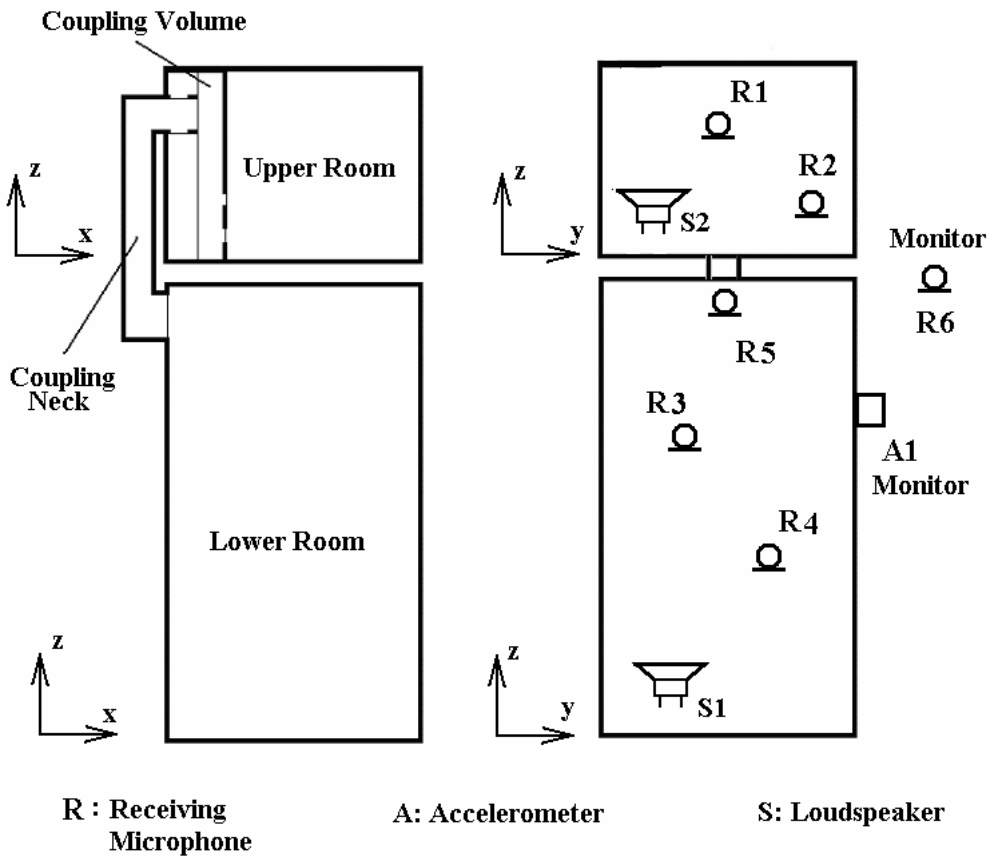

Figure 4.23 Locations of the Transducers for Experimental Modal Analysis

The upper cavity is monitored by two microphones, whereas, the lower cavity is monitored by three microphone positions. The coordinates of these microphones are tabulated in Table 4.3 together with the source positions. There are two additional transducers, namely, an accelerometer placed on the refrigerator cabinet, and a microphone at 1.5m height, at 1m distance form the

enclosure, in order to observe the background vibration and noise levels. The measurement environment is a fully anechoic chamber, as in the case of intensity measurements, with more than 80dB noise reduction between the surrounding laboratory environment and measurement room.

Table 4.3 Microphone, Source and Thermocouple Positions

	Microphones			Source
	cm			
	R1	R2		S1
x	18.4	19.8		32.0
y	14.0	39.3		47.6
z	15.8	11.9		20.5
	R3	R4	R5	S2
x	18.6	23.4	14.0	32.5
y	28.8	44.5	8.5	12.7
z	68.3	28.7	94.0	80.3

The instrumentation for the measurements is depicted in Figure 4.24. The input signal is band-limited white noise, fed to a flat response, professional audio power amplifier. The input volt and current signals are monitored, and current signal is used as input signal for the FRF estimations as explained before.

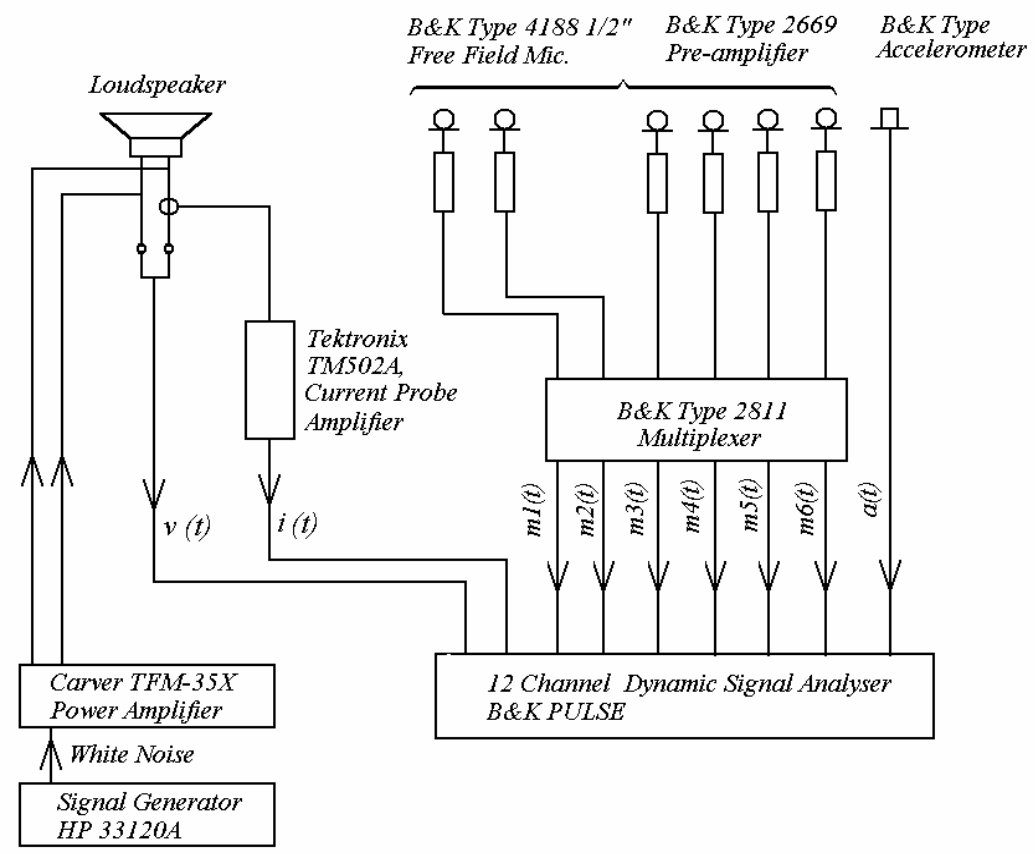

Figure 4.24 Instrumentation for Experimental Modal Analysis

Results and Analysis

The effect of cabinet temperature is investigated by running the test at different working temperatures. During the operations, time averaged bulk temperature for each room is determined by means of an array of thermocouples placed close to the microphones. There are six thermocouples for monitoring the internal cavity temperatures, two at the upper cavity, two at the lower, one at the coupling neck and finally, one at the measurement room in order to monitor the ambient temperature. The temperatures are recorded to a data logger throughout the measurements.

The frequency range of measurement in this set-up is 0-1600Hz, with 2Hz,

narrow band (FFT) resolution. A spectral overlapping of 99% is applied with 1000 linear averages for each individual measurement. Due to the frequency resolution requirement, Hanning type time window is used through out all the analysis.

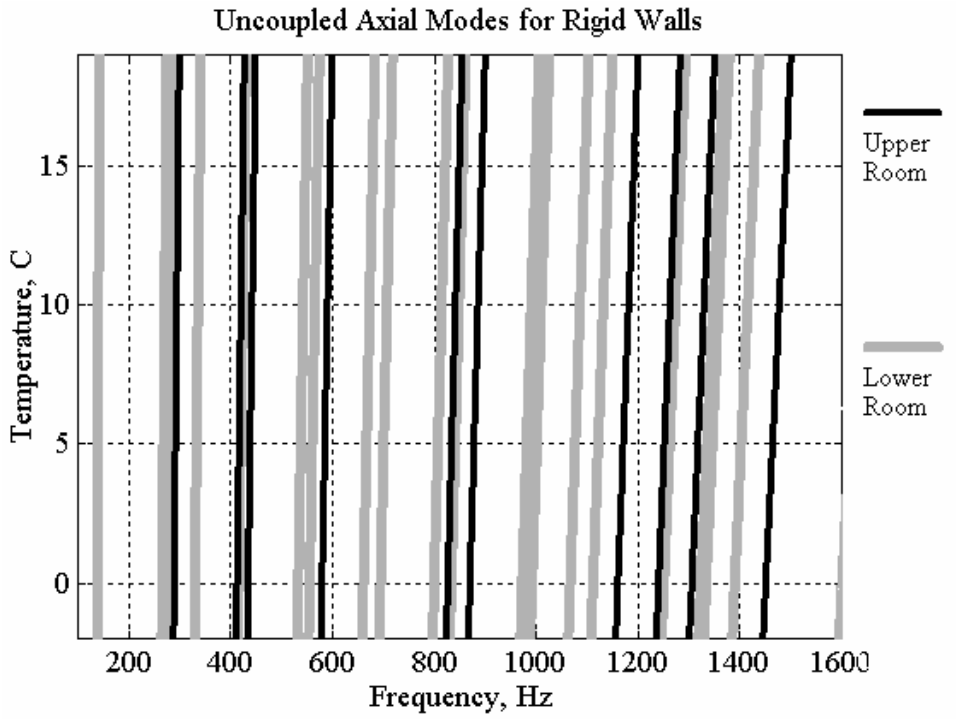

Figure 4.25 Change of Theoretical Axial Modal Frequencies with respect to Temperature

Figure 4.25 depicts the effect of average temperature on the theoretically calculated modal frequencies of the "upper" and "lower" rooms with rigid wall conditions. For an ideal gas, the speed of sound changes with the square root of temperature in Kelvin [2], $c = 331\sqrt{T/273}$. Therefore, for a fixed geometry, the standing wave pattern does not change, hence the wavelengths, but the resonance, or modal frequencies change due to the relation; $c = fl$, hence;

$$f = c/l = 331\sqrt{T/273}/l \qquad (4.89)$$

It can be concluded from Equation 4.89 that, for lower modal frequencies effect of temperature change is not as effective as it is for the higher frequency modes. Transfer function for receiving microphone 4 is presented in Figure 4.26.as a color plot after a heat-up experiment. The enclosure is cooled-down to approximately 4.1^{o}C (277.1K) by means of a compressor, and then the data is collected as the enclosure naturally heats up to room temperature 21.7^{o}C (294.7K).

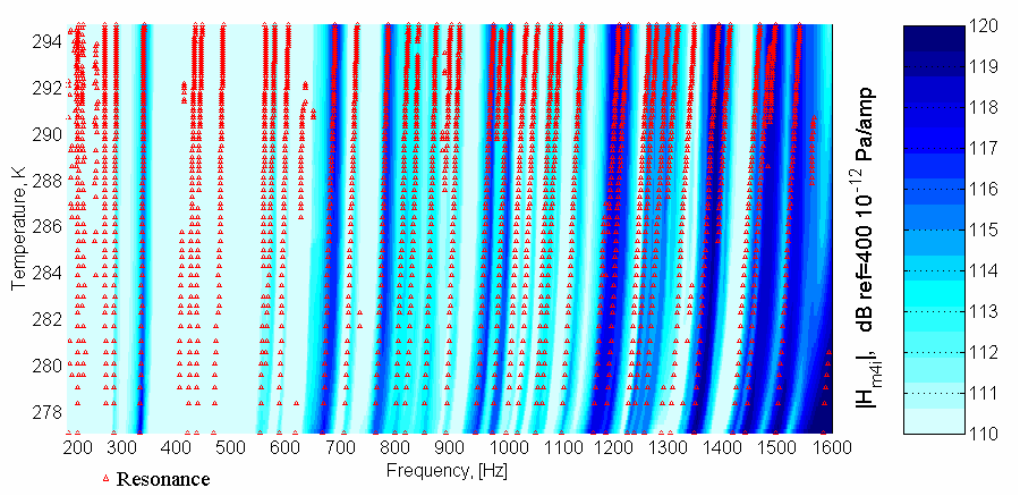

Figure 4.26 Change of Modal Frequencies with respect to Temperature

A peak search methodology, which depends on finding local extrema after low-pass filtering of the spectral data with a cut-off frequency of 5Hz is used for the enhancement of the peaks of transfer functions at possible resonance. The results are superimposed on the same plot. The measured behavior is in good

agreement with the theoretically predicted one, with the slight bending of maxima as the temperature goes up.

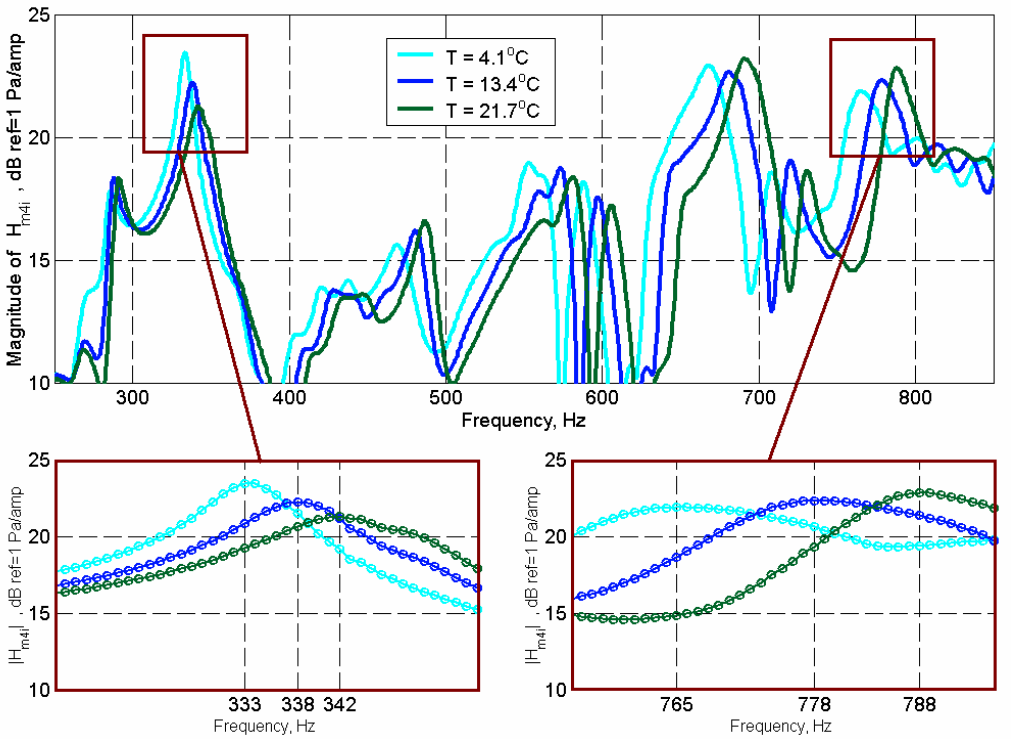

Figure 4.27 Behavior of the Transfer Functions around two Distinct Modal Frequencies at Three Different Cavity Temperatures

Figure 4.27 presents a closer investigation of this behavior for two resonance frequencies, at three different cavity temperatures. The ratios of the resonance frequencies, calculated from Equation 4.89 and from the measured data, are compared at Table 4.4. There is an excellent harmony between the measured and calculated values. Note that, for a narrow bandwidth analysis (FFT) the difference between the resonance frequencies at lower and higher temperatures gets higher as the resonance frequency increases. Hence, conformity between the calculated and measured values enhances as in the case of this study.

Table 4.4 Comparison of the Measured and Calculated Resonance Frequencies at Different Cavity Temperatures

		T1	***T2***	***T3***
Temperature	^{o}Celcius	4.1	13.4	21.7
	Kelvin	277.1	286.4	294.7
Speed of Sound	m/s	333.5	339.0	343.9
Resonance 1	Hz	333	338	342
Δf Resonance 1	Hz	0	5	9
Resonance 2	Hz	765	778	788
Δf Resonance 2	Hz	0	13	23
Theoretical Ratio (Equation 4.89)	c_{Ti}/c_{T1}	*1.000*	*1.017*	*1.031*
Calculated Ratio For Resonance 1	f_{Ti}/f_{T1}	*1.000*	*1.015*	*1.027*
Calculated Ratio For Resonance 2	f_{Ti}/f_{T1}	*1.000*	*1.017*	*1.030*

Two important conclusions can be drawn from this behavior:

1. Modal behavior is affected by the temperature of the related cavities. In general, this behavior is widely ignored in many analysis related to cavity acoustics. An enclosure designed at standard conditions of 20^{o}C may behave in a very different way at; say 100^{o}C, which may be the actual operation conditions.

2. Change of modal frequencies as a function of cavity temperatures can be used as a modal extraction tool in experimental modal analysis. The most crucial difficulty in this kind of experimental analysis, as explained in the previous sections, is the construction of a volume source with known magnitude and phase characteristics so that the vital Frequency Response Functions can be estimated.

Otherwise, a peak in the amplitude of the response function may be either due to the cavity characteristics, i.e. free response, or due to the excitation mechanism, i.e. forced response. In case, such a source of this quality is missing, a simple response measurement by means of a pressure transducer at two different temperatures can reveal any possible modal behavior that can be separated from the excitation mechanism.

For the extraction of modal frequencies, which is the main aim of this study, a methodology is developed which has the following algorithm:

- Bode plots of transfer functions of H_{pQ}'s are obtained and a peak search algorithm is conducted in order to identify possible resonance frequencies. The lower microphone near the coupling neck is omitted for low signal to noise ratio characteristics so that only R1, R2 from the upper cabinet and R3 and R4 from the lower cabinet are used. Figure 4.28 and Figure 4.29 present the corresponding Bode plots for the upper and lower rooms, respectively.

- Next, possible modal frequencies from each receiver point are grouped into six different sets with two original memberships at each set. (Set1:R1&R2, Set2:R1&R3, Set3:R1&R4, Set4:R2&R3, Set5:R2&R4, Set5:R3&R4). An algorithm is applied to each set, in order to find coinciding resonance frequencies with a frequency resolution of ±5Hz. The results are presented in Figure 4.30 for each set of frequencies. At the final stage, given at the row with the All Receivers header, these

coinciding frequencies are plotted together so as to obtain cluster of frequencies again in a neighborhood less than ±5Hz. Finally, these clusters are named with the mean frequency as given in the last row with a header Modal Frequencies. In summary, the frequencies given under this heading correspond to some resonance frequencies, shared by at least two of the receiving points in a neighborhood less than ±5Hz. The resulting experimentally found modal frequencies are tabulated in Table 4.5 for easy reference.

Table 4.5 Experimentally Found Modal Frequencies

No	Modal Frequency Hz	No	Modal Frequency Hz
1	122	16	523
2	148	17	557
3	165	18	592
4	173	19	639
5	223	20	696
6	235	21	709
7	241	22	722
8	294	23	774
9	329	24	815
10	350	25	858
11	383	26	867
12	413	27	888
13	436	28	972
14	465	29	989
15	497		

Accuracy +/- 5 Hz

- Two cases of degeneracy are possible in the methodology, namely, a possible modal frequency is not identified or a frequency identified as

possible modal frequency is not related to the modal behavior at all. In order to avoid these, the last step is to check each possible modal frequency for each receiving point in corresponding Nyquist plots for the phase behavior [42]. At about a modal frequency, the Nyquist plot must assume a circular shape, that is the phase of the transfer function must undergo a phase change of $2p$ radians.

- Figure 4.31 through Figure 4.42 present the Nyquist plots of these sorts, for each receiving points at R1 to R4. In these plots, around each resonance frequency ±15 data, that is ±15Hz with 1Hz resolution, is plotted. The center frequency (resonance frequency) is indicated by an arrow (red), the starting frequency indicated by a square (cyan) and the end frequency by an upright triangle (cyan). The frequencies which have no coincidence with any other one of the other receivers are subscripted with "solo", whereas the candidate modal frequencies as obtained at the previous step are subscripted with "coupled" at the upper corner of the these plots.

A typical discussion can be carried out by considering Figure 4.31 for the first receiving point of upper section. The frequencies F_{solo}=95Hz, 191Hz, 204Hz and 282Hz are identified only at this location as a resonance, but at none of the other receivers. A close investigation of the their behavior in the Nyquist domain clearly reveals that it is, indeed, impossible to fit any circle, i.e. the transfer functions do not have any $2p$ radians phase shift behavior at neither one of these

frequencies.

The other check is for the frequencies F_{coup}=121Hz, 149Hz, 166Hz, 234Hz, 243Hz, 327Hz, 383Hz and 416Hz, identified as possible modal frequencies. Clearly, for all of these frequencies, a circle can be fit to the data; hence, they have the validity to be considered as modal frequencies. The resulting Nyquist plots given from 4.31 to Figure 4.42 are checked for the above given criteria, and no discrepancies have been observed.

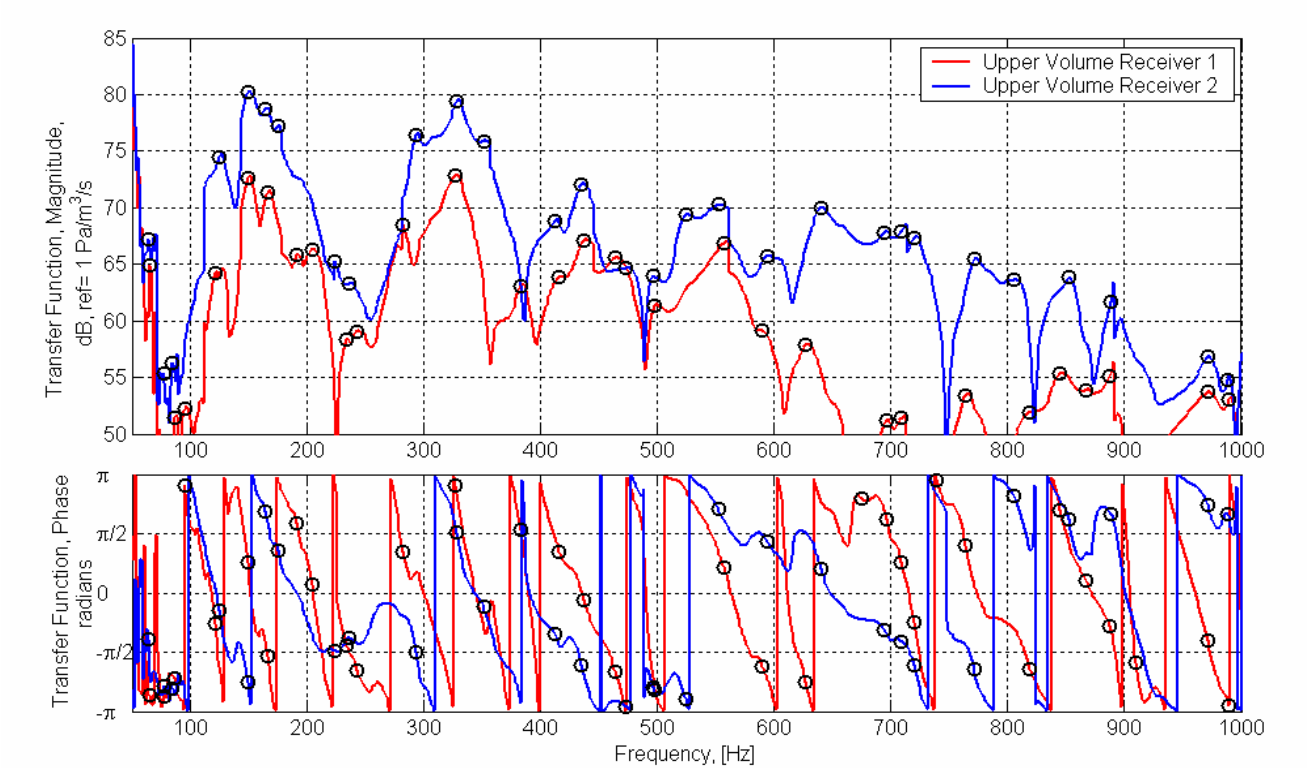

Figure 4.28 Bode Plot of Transfer Function H_{pQ} for Upper Volume Microphones

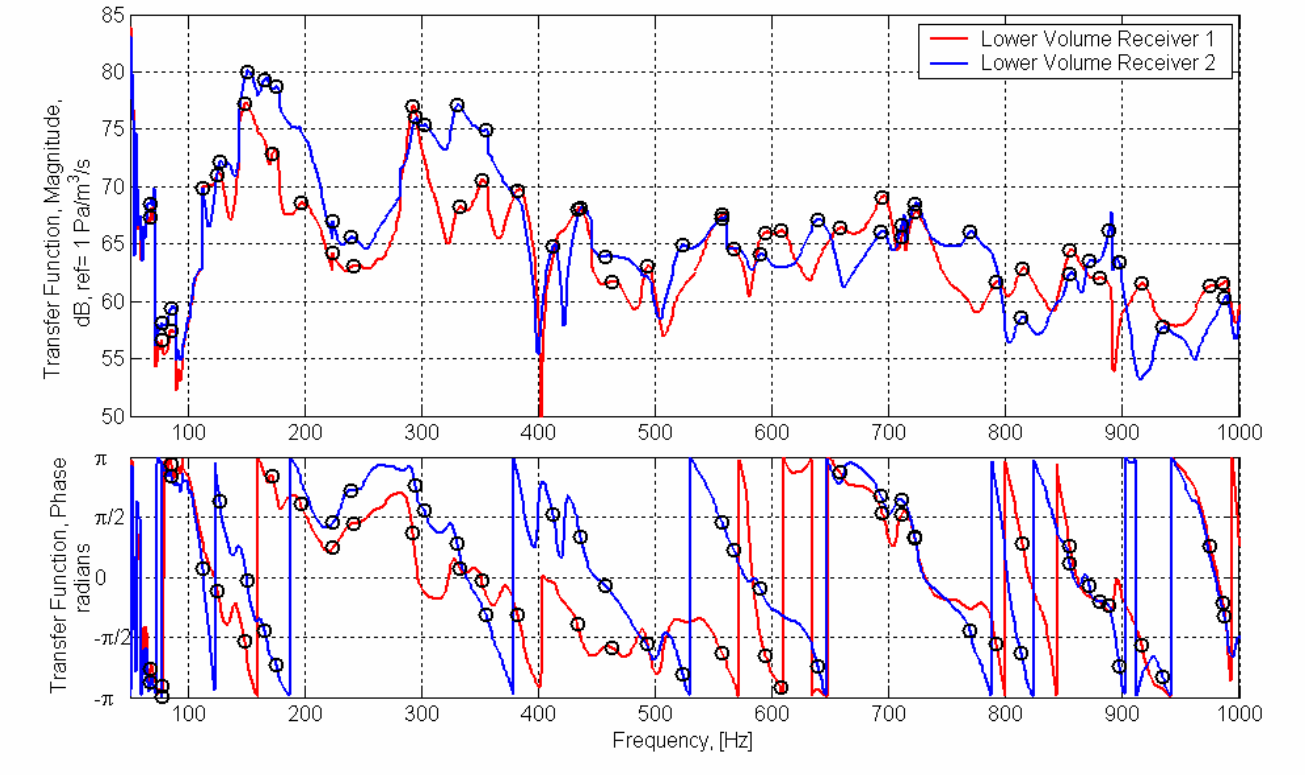

Figure 4.29 Bode Plot of Transfer Function H_{pQ} for Lower Volume Microphones

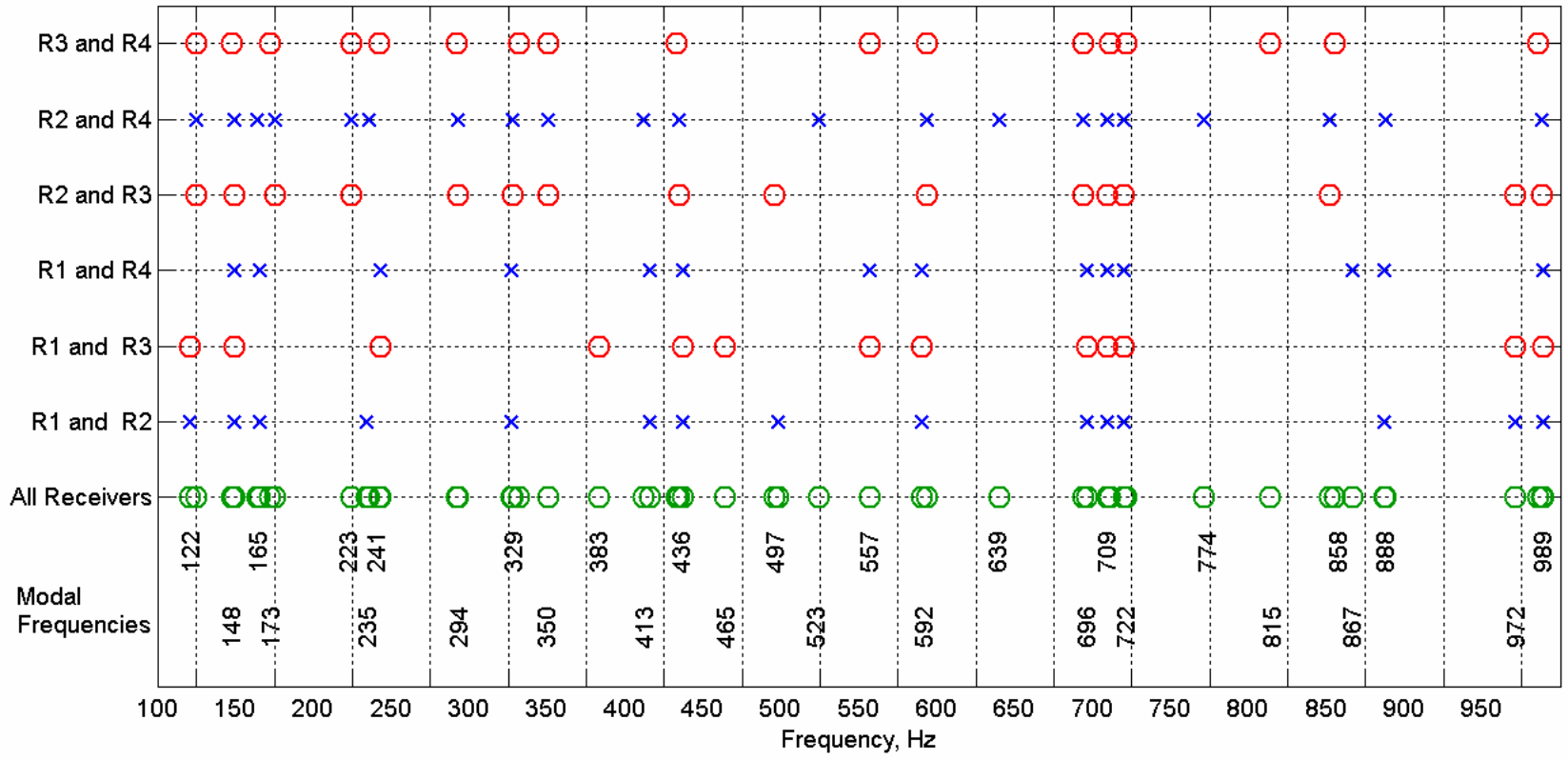

Figure 4.30 Possible Modal Frequencies extracted from H_{pQ} of Receiving Microphones

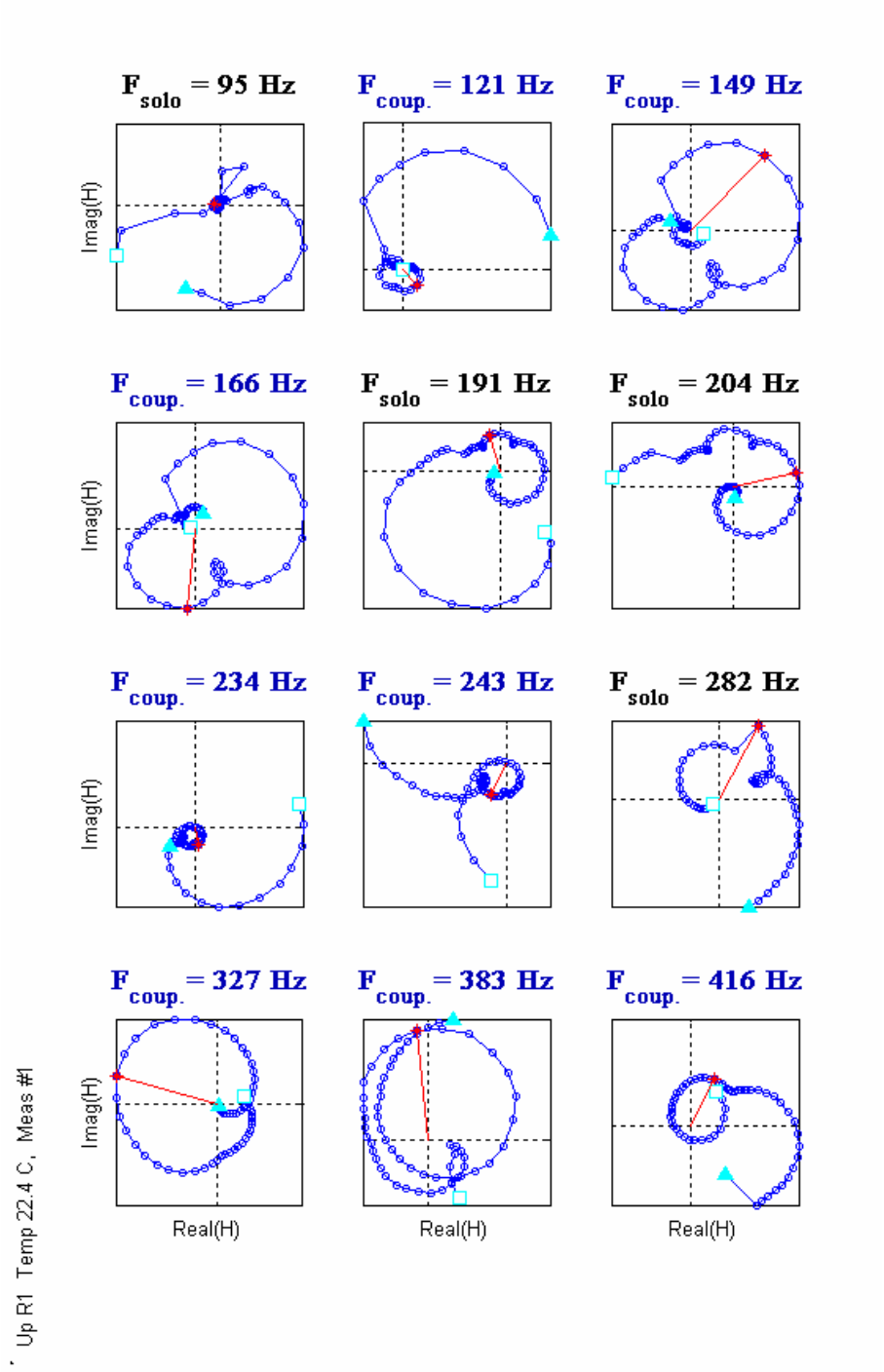

Figure 4.31 Nyquist Plot of H_{pQ} for Upper Volume Microphone R1 about Possible Modal Frequencies in 2Hz Resolution. (95Hz-416Hz)

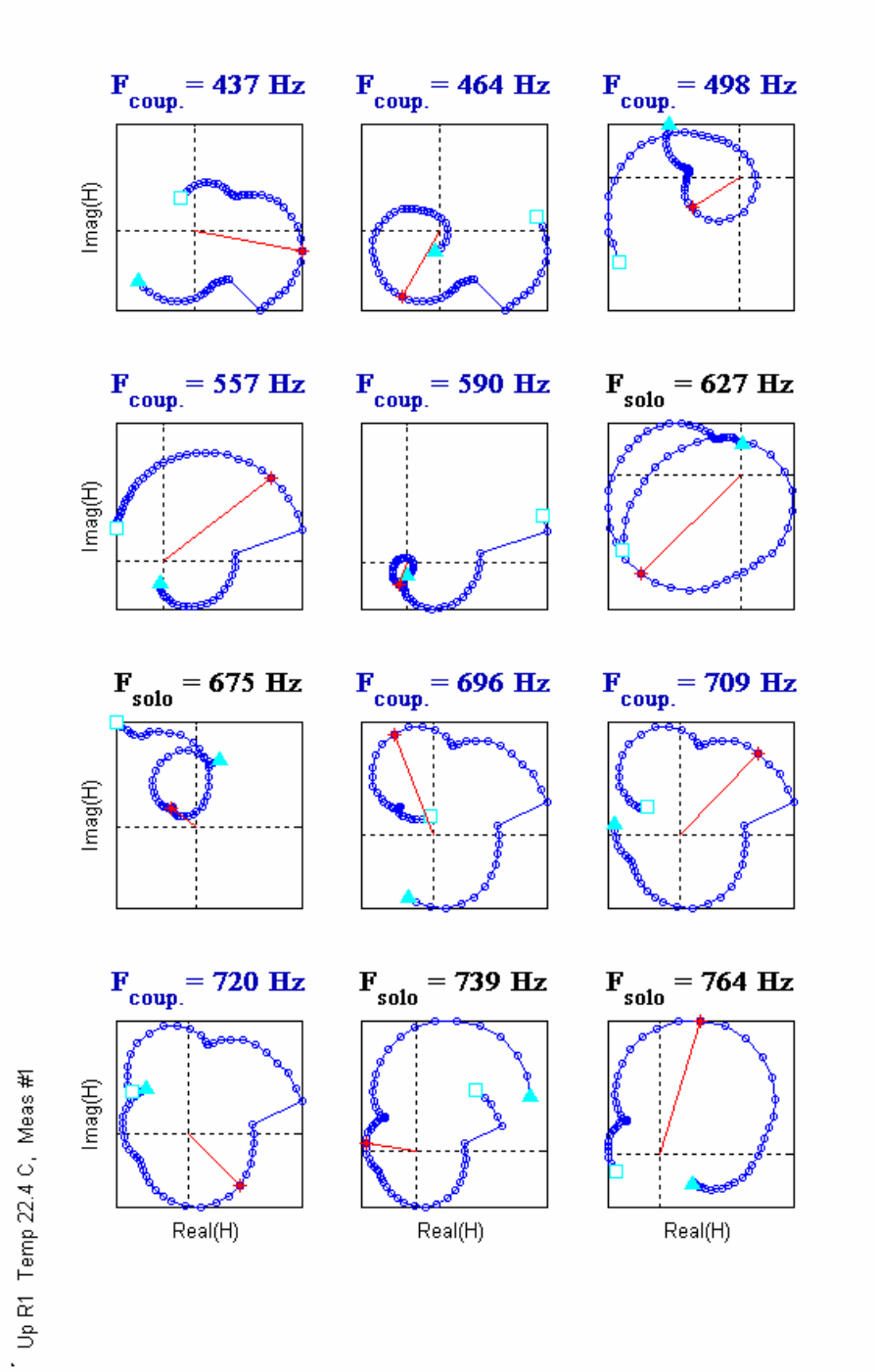

Figure 4.32 Nyquist Plot of H_{pQ} for Upper Volume Microphone R1 about Possible Modal Frequencies in 2Hz Resolution. (437Hz-764Hz)

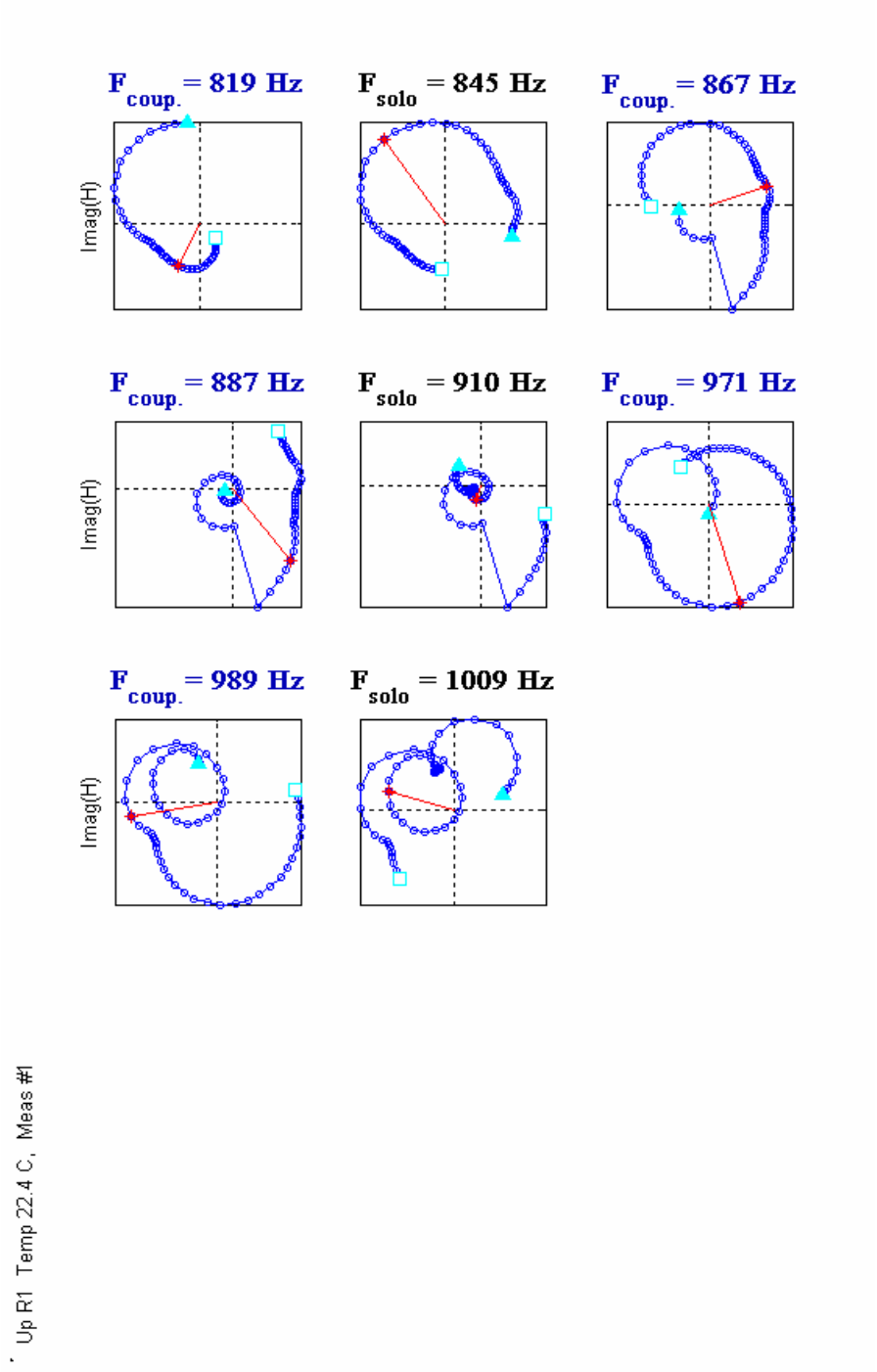

Figure 4.33 Nyquist Plot of H_{pQ} for Upper Volume Microphone R1 about Possible Modal Frequencies in 2Hz Resolution. (819Hz-1009Hz)

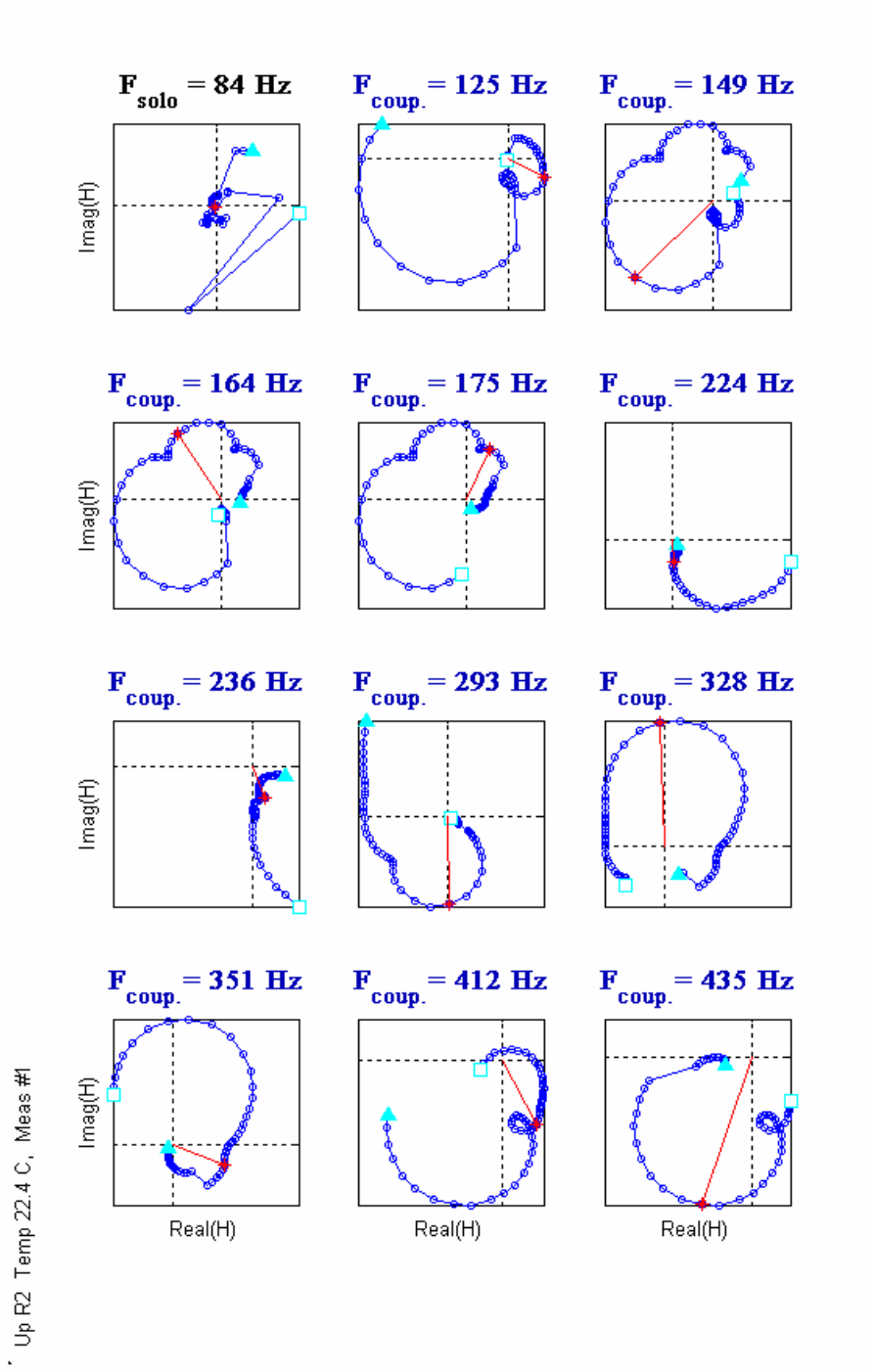

Figure 4.34 Nyquist Plot of H_{pQ} for Upper Volume Microphone R2 about Possible Modal Frequencies in 2Hz Resolution. (84Hz-435Hz)

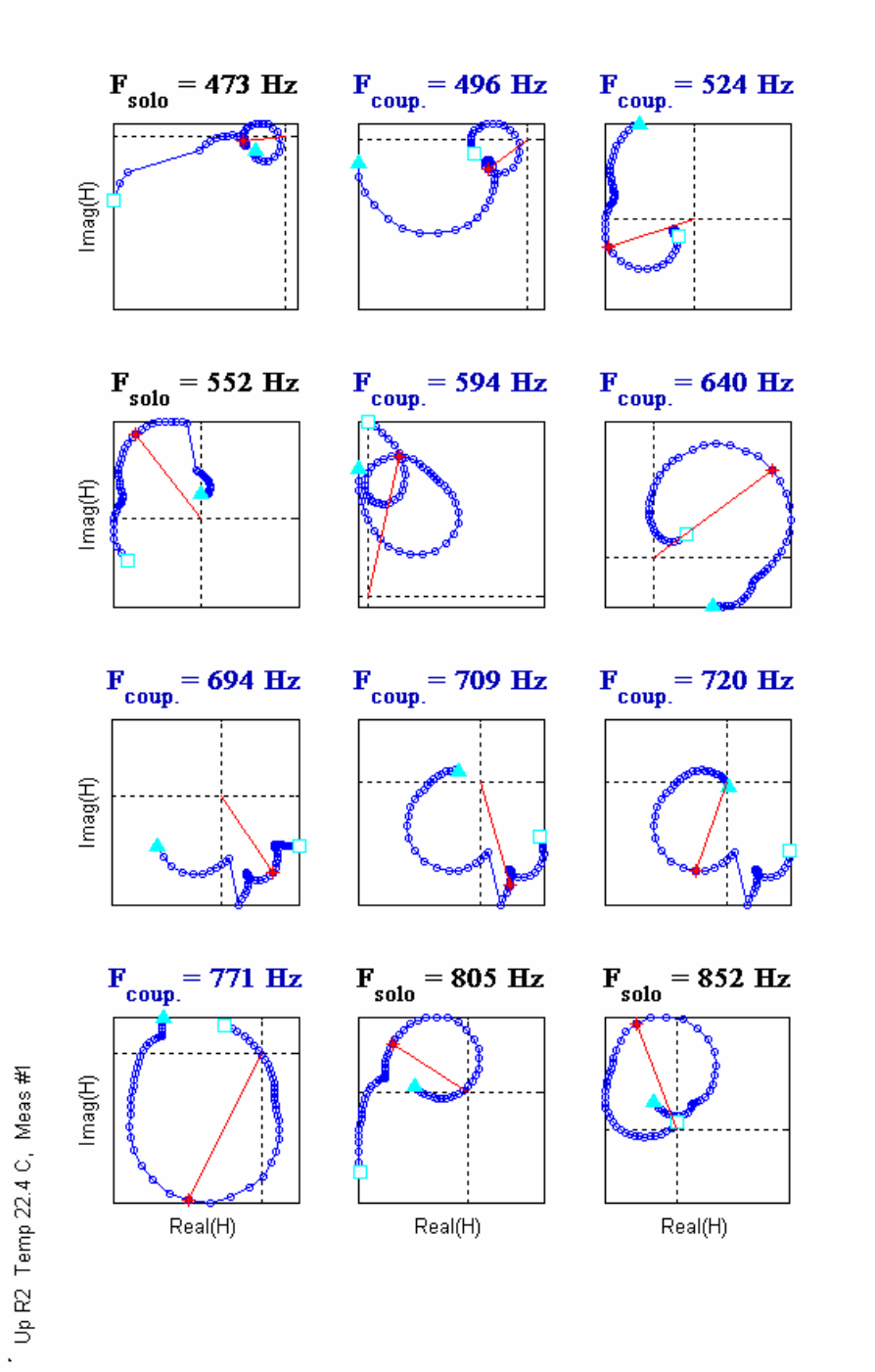

Figure 4.35 Nyquist Plot of H_{pQ} for Upper Volume Microphone R2 about Possible Modal Frequencies in 2Hz Resolution. (473Hz-852Hz)

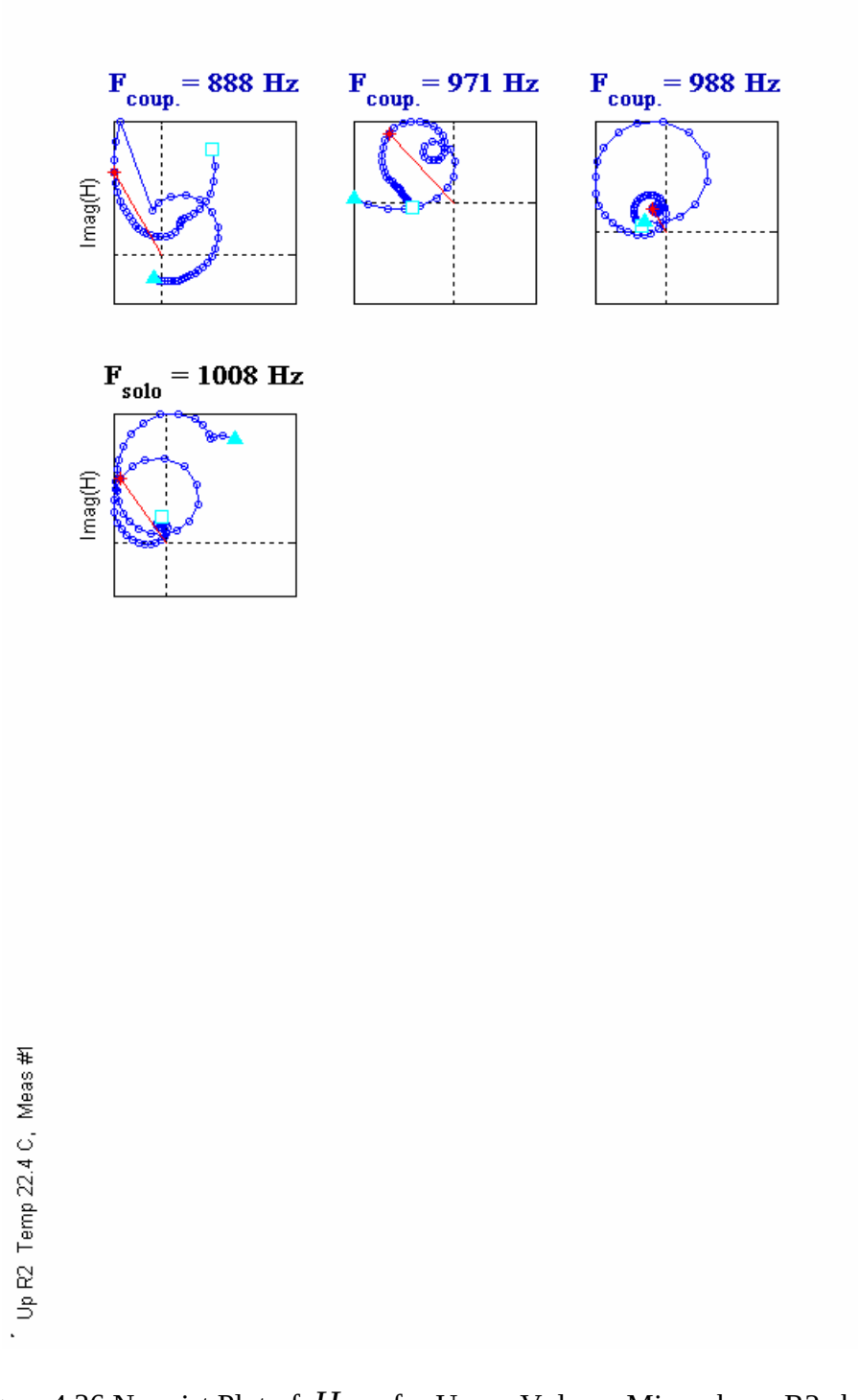

Figure 4.36 Nyquist Plot of H_{pQ} for Upper Volume Microphone R2 about Possible Modal Frequencies in 2Hz Resolution. (888Hz-1008Hz)

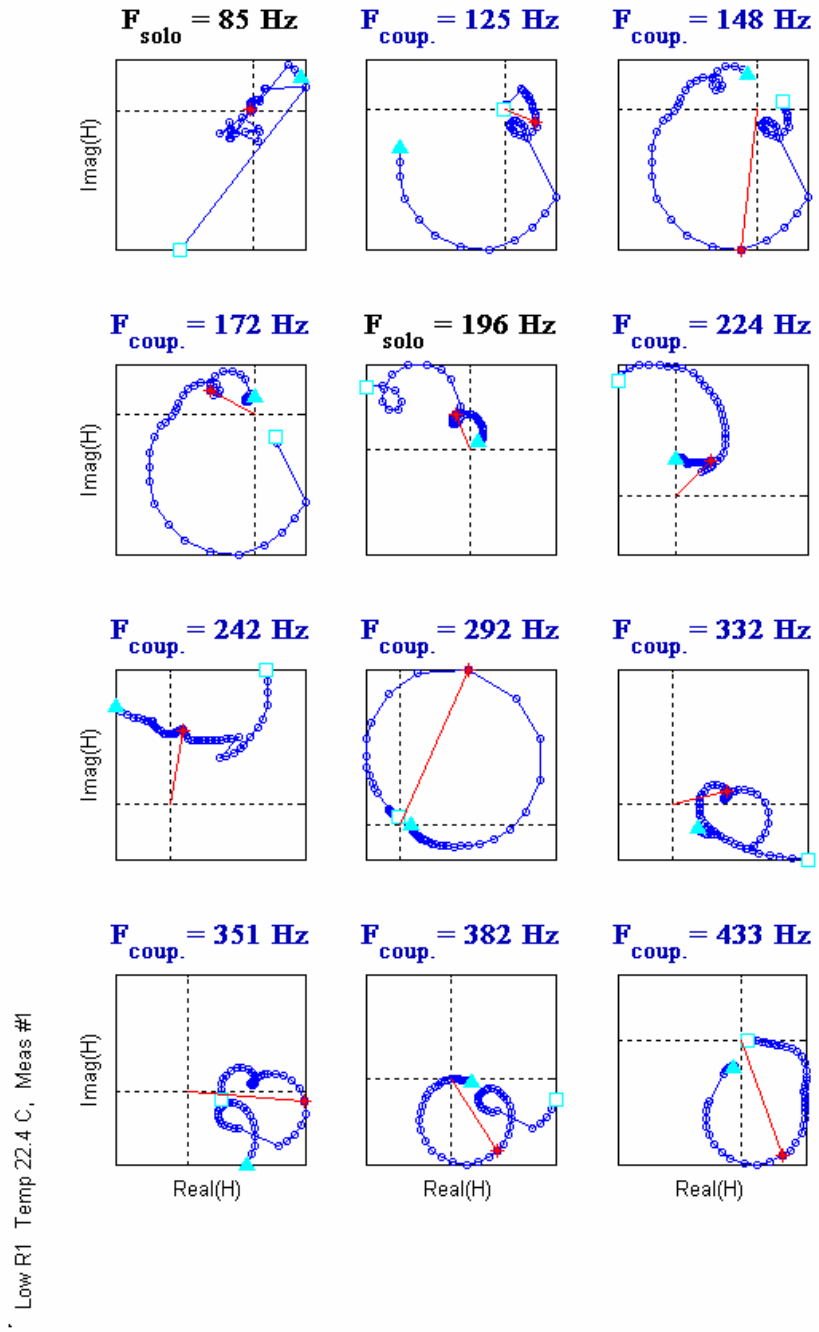

Figure 4.37 Nyquist Plot of H_{pQ} for Lower Volume Microphone R1 about Possible Modal Frequencies in 2Hz Resolution. (85Hz-433Hz)

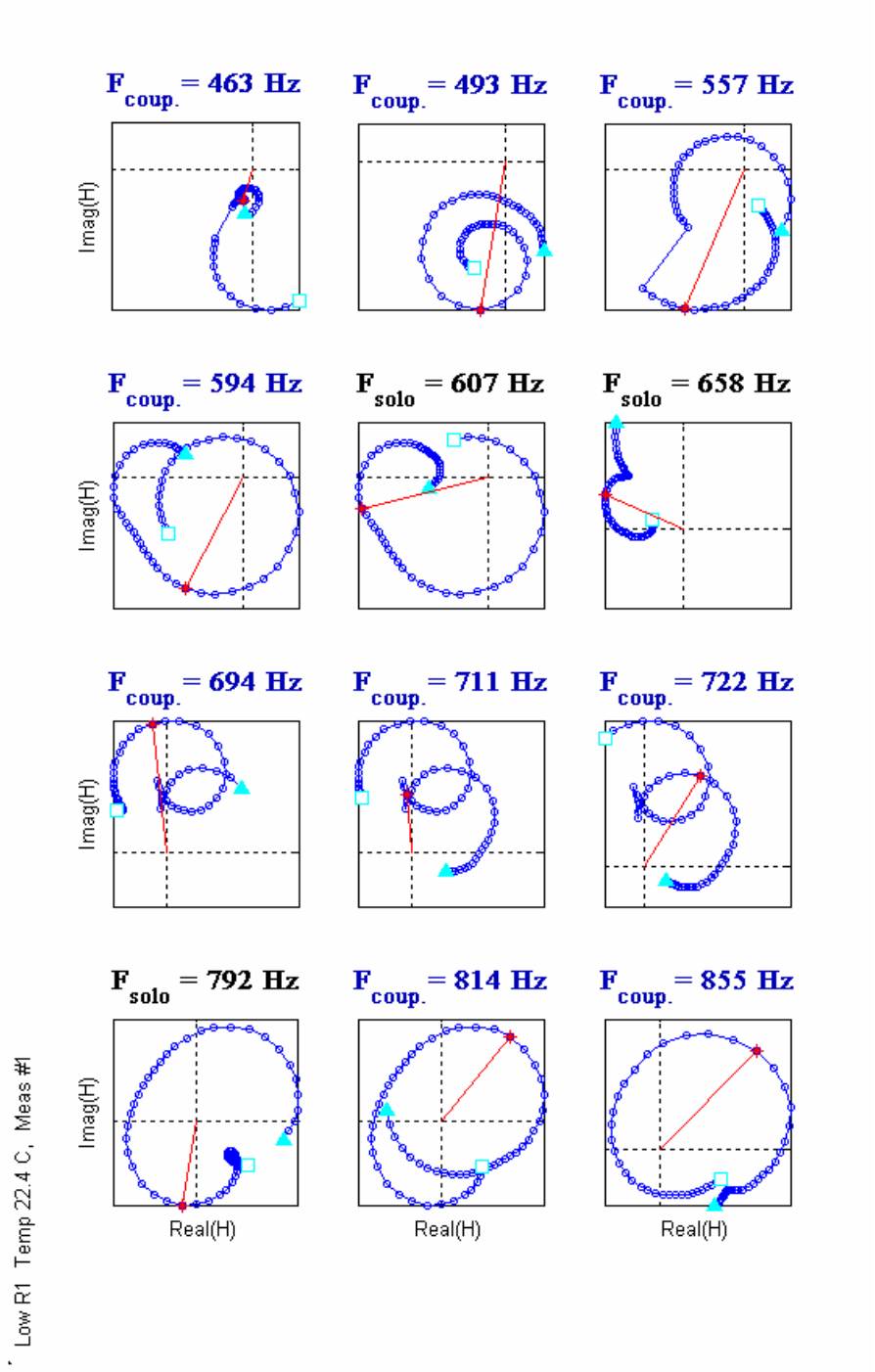

Figure 4.38 Nyquist Plot of H_{pQ} for Lower Volume Microphone R1 about Possible Modal Frequencies in 2Hz Resolution. (463Hz-855Hz)

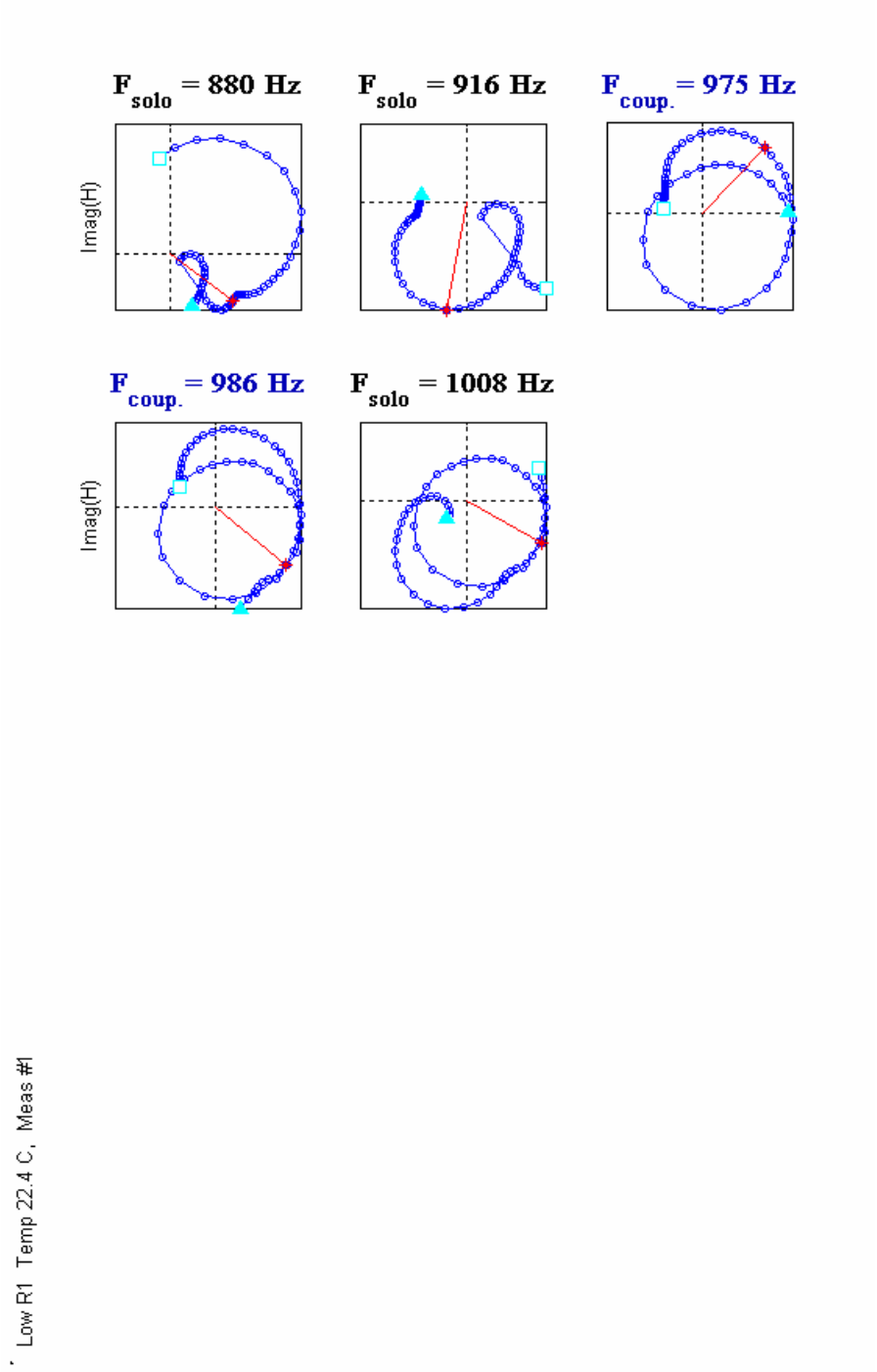

Figure 4.39 Nyquist Plot of H_{pQ} for Lower Volume Microphone R1 about Possible Modal Frequencies in 2Hz Resolution. (880Hz-1008Hz)

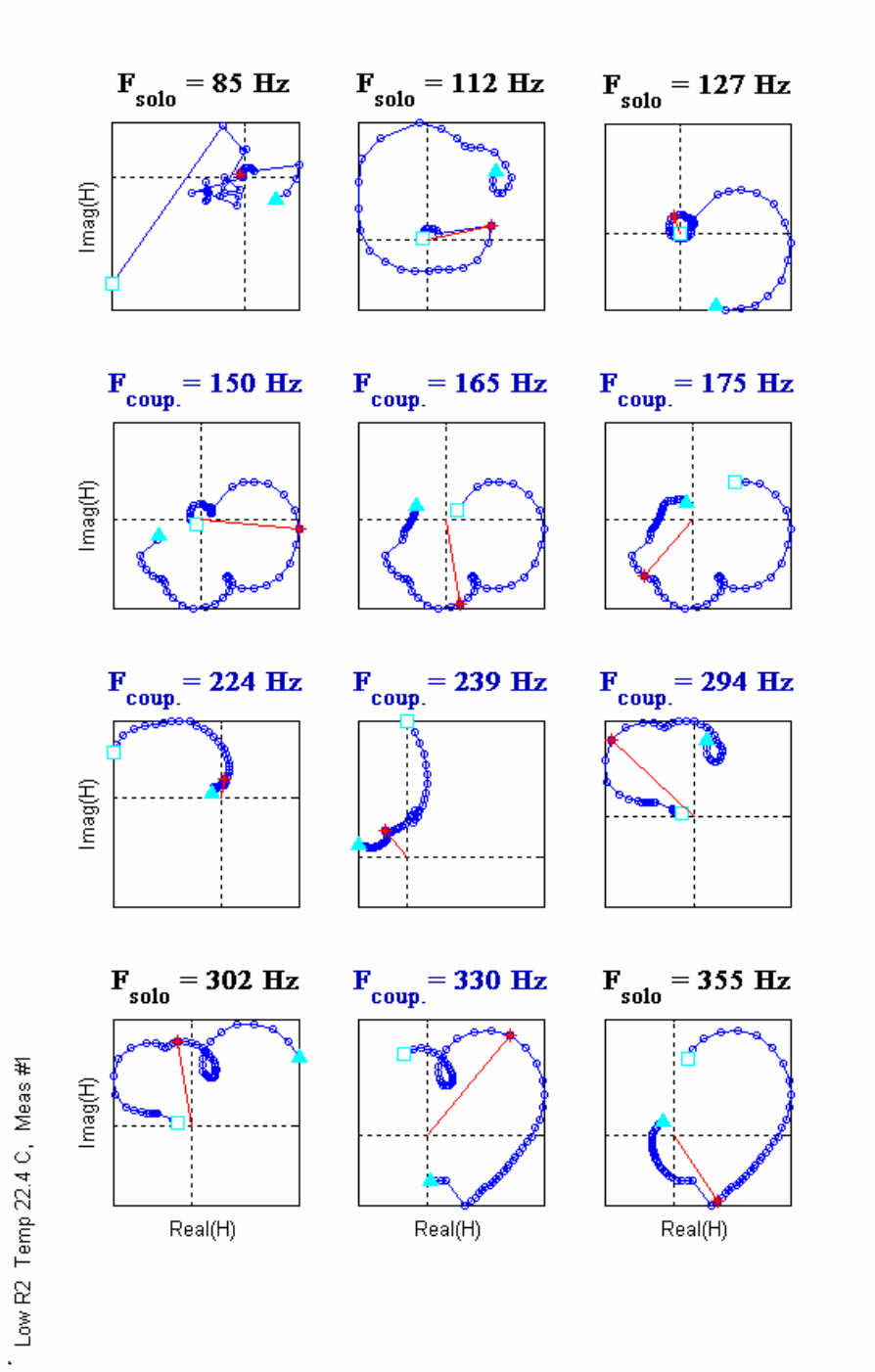

Figure 4.40 Nyquist Plot of H_{pQ} for Lower Volume Microphone R2 about Possible Modal Frequencies in 2Hz Resolution. (85Hz-355Hz)

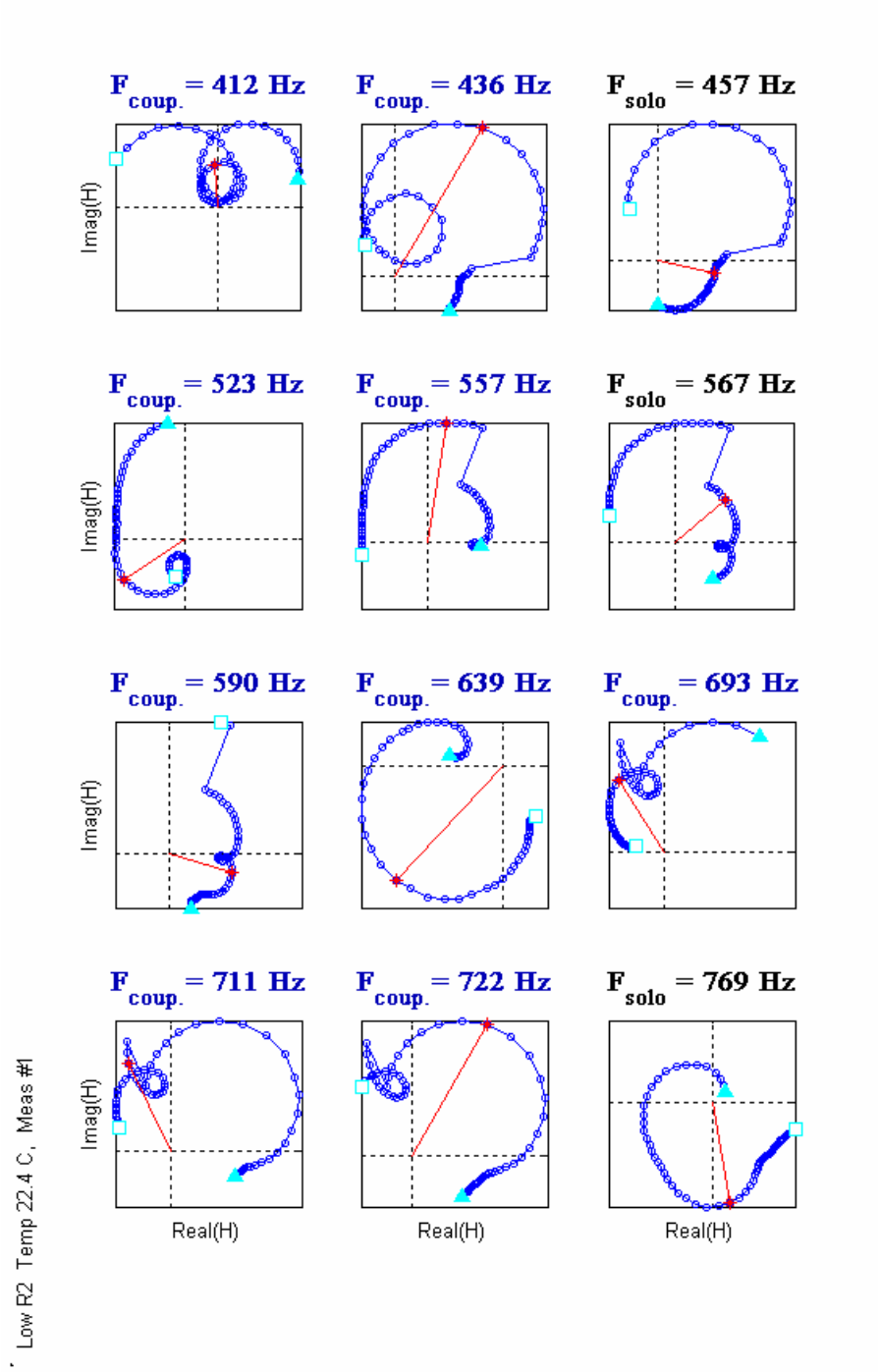

Figure 4.41 Nyquist Plot of H_{pQ} for Lower Volume Microphone R2 about Possible Modal Frequencies in 2Hz Resolution. (412Hz-769Hz)

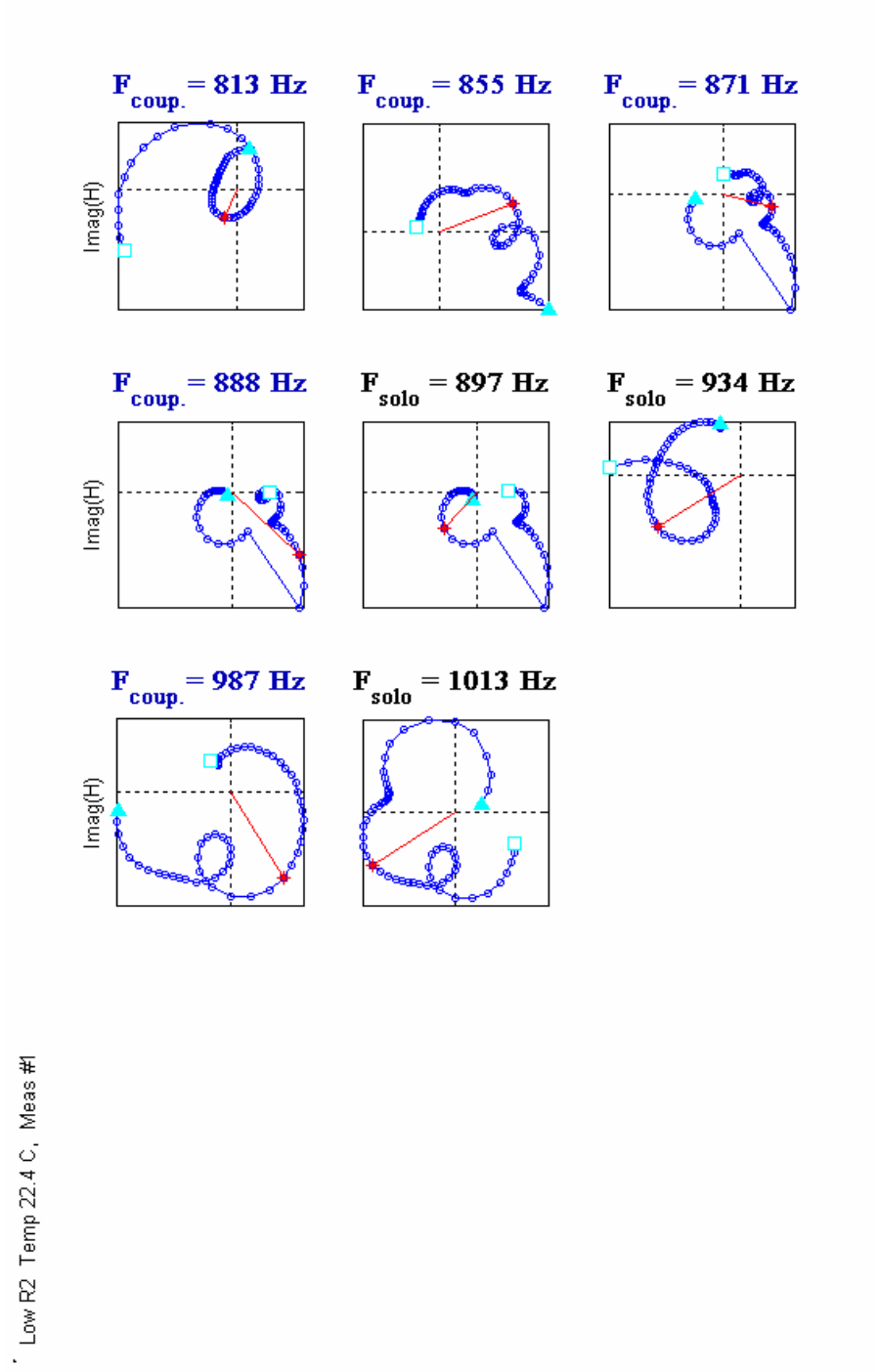

Figure 4.42 Nyquist Plot of H_{pQ} for Lower Volume Microphone R2 about Possible Modal Frequencies in 2Hz Resolution. (813Hz-1013Hz)

A Brief Discussion on Experimental Errors

Experimental errors in FRF estimates can be investigated as bias and random errors [40]. The frequency dependent random errors $\hat{e}_{xy}(f)$, on the estimation of the gain of transfer functions $\hat{H}_{xy}(f)$ can be expressed as;

$$|\hat{H}_{xy}(f)| \pm \hat{e}_{xy}(f) = |\hat{H}_{xy}(f)|(1 \pm e[\hat{H}_{xy}(f)]) \quad (4.90)$$

where $e[\hat{H}_{xy}(f)]$ represents errors normalized to measured gain of transfer function, namely $|\hat{H}_{xy}(f)|$. The head on the frequency dependent variables denotes that these are estimated values from the measurements. Similarly, random errors on the measured phase of the transfer function $\hat{F}_{xy}(f)$ can be given as;

$$|\hat{F}_{xy}(f)| \pm ?\hat{F}_{xy}(f) = |\hat{F}_{xy}(f)|(1 \pm e[|\hat{H}_{xy}(f)|]) \quad (4.91)$$

which is equal to the normalized random errors expressed for gain errors. If the number of for non-overlapped linear averages is denoted by N_a, the normalized random error for the estimation of transfer function gain is given as [40];

$$e[|\hat{H}_{xy}(f)|] = \frac{[1 - ?^2_{xy}(f)]^{1/2}}{|?_{xy}(f)|\sqrt{2N_a}} \quad (4.92)$$

where $?_{xy}(f)$ is the true value of the ordinary coherence function.

The expected value of the ordinary coherence function $\hat{?}_{xy}(f)$ defined as;

$$\hat{?}^{2}_{xy}(f) = \frac{|\hat{G}_{xy}(f)|^2}{\hat{G}_{xx}(f)\hat{G}_{yy}(f)} \tag{4.93}$$

with $\hat{G}_{xy}(f)$, $\hat{G}_{xx}(f)$ and $\hat{G}_{yy}(f)$ estimates of input-output cross-spectral density functions, input and output auto-spectral density functions, respectively. The normalized random error related to the ordinary coherence function is given in terms of true coherence function as follows;

$$e[\hat{?}^{2}_{xy}(f)] = \frac{\sqrt{2}[1-?^{2}_{xy}(f)]}{|?_{xy}(f)|\sqrt{N_a}} \tag{4.94}$$

These normalized random error terms are investigated for a typical experimental acoustical modal analysis measurement. In all these measurements, the number of non-overlapped linear averages is taken to be as N_a=1000. The receivers are considered as microphone 1 of upper-cabinet, and microphone 4 of the lower cabinet. Figure 4.43 presents random error terms for the ordinary coherence functions as given in Equation 4.94. For an order of magnitude analysis, the estimated values of the coherence spectra are assumed as required true values. Above 100 Hz, the normalized random errors on ordinary coherence functions for both microphones are below 0.01.

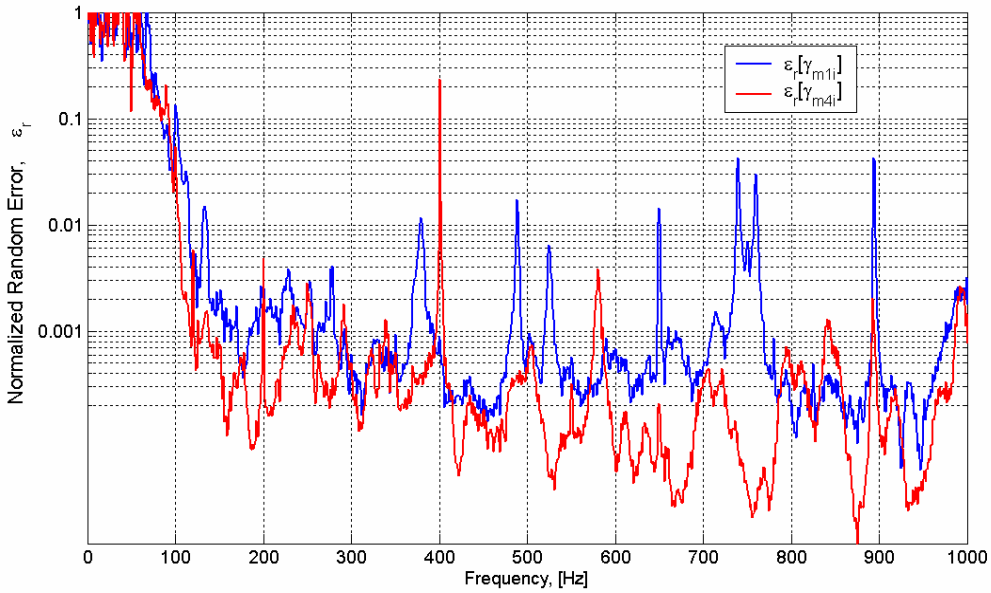

Figure 4.43 Normalized Random Error of Coherence Functions for Experimental Acoustical Modal Analysis

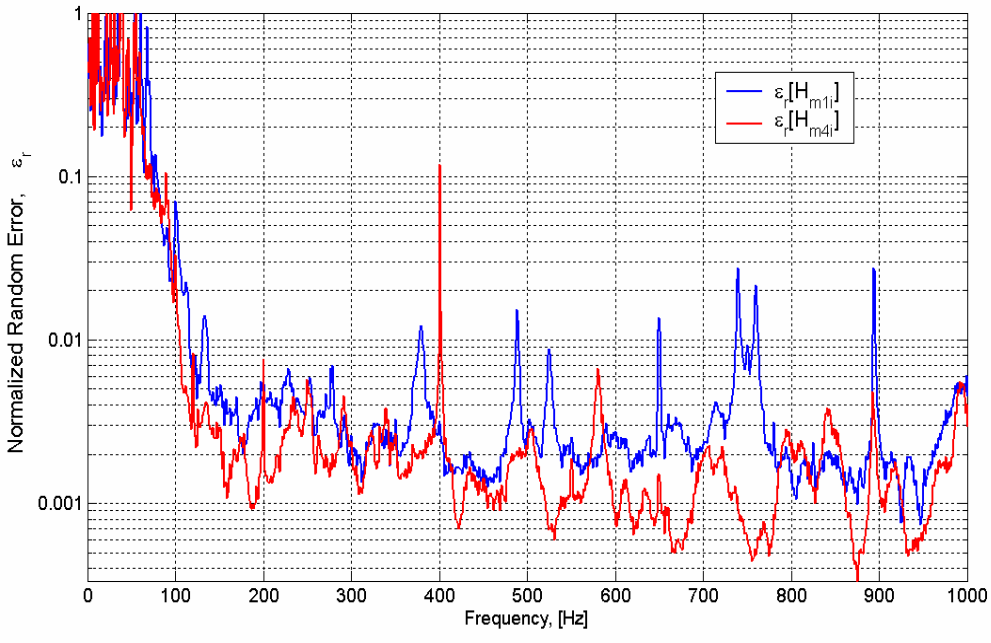

Figure 4.44 Normalized Random Error of Gain Estimates of Transfer Functions for Experimental Acoustical Modal Analysis

Figure 4.44 presents the normalized random error terms for gain estimates of the transfer functions, whereas Figure 4.45 shows the uncertainty due to random errors in phase of the transfer functions. Above 100 Hz, the errors on gain values are below 0.01 again. This corresponds to a 20 dB, at least, signal-to-noise ratio for the estimated gain of the transfer functions. The normalized random phase errors at the same frequency interval, on the other hand, are below 1 degree.

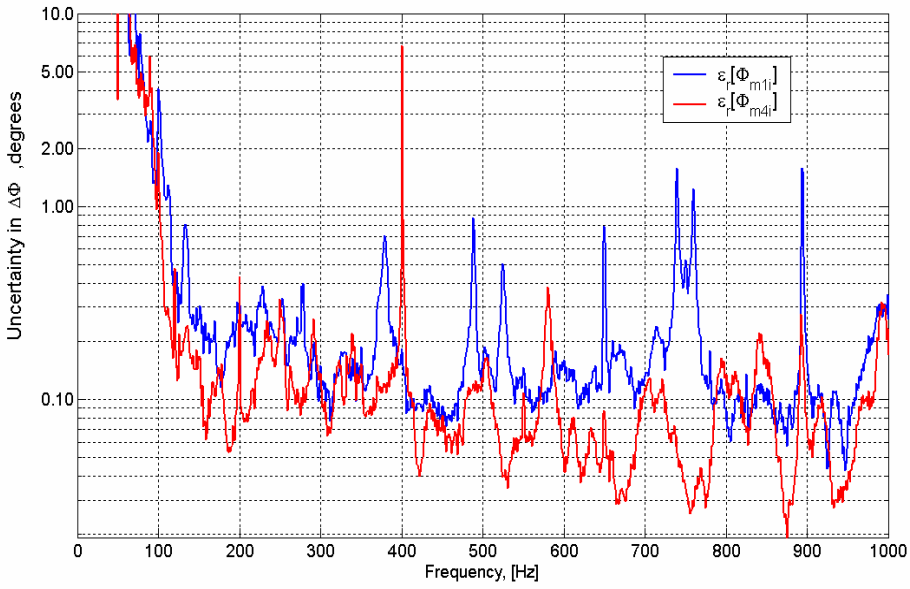

Figure 4.45 Uncertainty in Phase Estimates of Transfer Functions for Experimental Acoustical Modal Analysis

It can be concluded from this investigation that, the random error on the measurements are at reasonable levels. It is worth emphasizing that the random error terms are affected by mainly two parameters, namely, the number of averages or record length, and the coherence functions. The high value chosen as N_a=1000 ensures reasonable random error values provided that, the coherence

functions behave well at the frequency range of interest. Theoretically, the magnitude of ordinary coherence functions can assume values between zero and one. At values close to one, error levels approach to zero, and at values close to zero the error terms asymptotically approach to infinity.

The ordinary coherence functions are related to the uncorrelated noise at the output points, hence, are direct indicators of the possible bias errors in the experiment. Similar formulations are available for an order of magnitude analysis of such errors [40]. A good indicator of possible bias errors in the gain of transfer functions due to extraneous noise or non-linearity in the system can be expressed in terms of ordinary coherence functions as follows;

$$e_b[\hat{H}_{xy}(f)] = \frac{|1 - ?_{xy}(f)|}{|?_{xy}(f)|} \qquad (4.95)$$

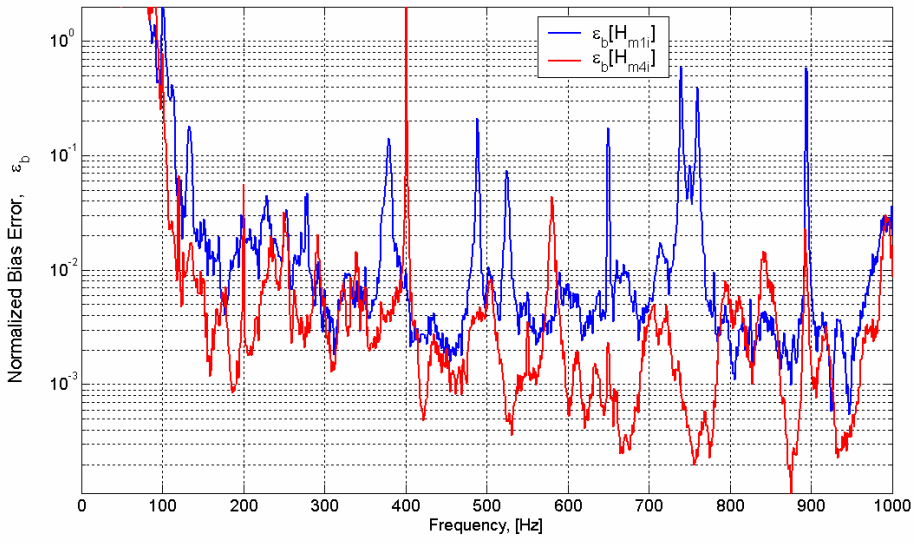

Figure 4.46 Normalized Bias Error of Gain Estimates of Transfer Functions

Figure 4.46 shows these kinds of bias errors for two receiving microphones as explained in the previous discussion on random errors. There is a considerable difference between the error levels of two receiving microphones. In this particular experiment, input volume source is placed in the lower section of the enclosure. Hence, signal to noise ratio at the position of microphone 1, which is placed at the upper section, is much lower compared to that of microphone 4, which is placed at the lower section together with the source. This indicates that location of the forcing volume source is important in experimental acoustical modal analysis applications for coupled structures. Measurements taken at different combinations of forcing and receiver positions can be considered as a possible enhancement for this kind of bias errors.

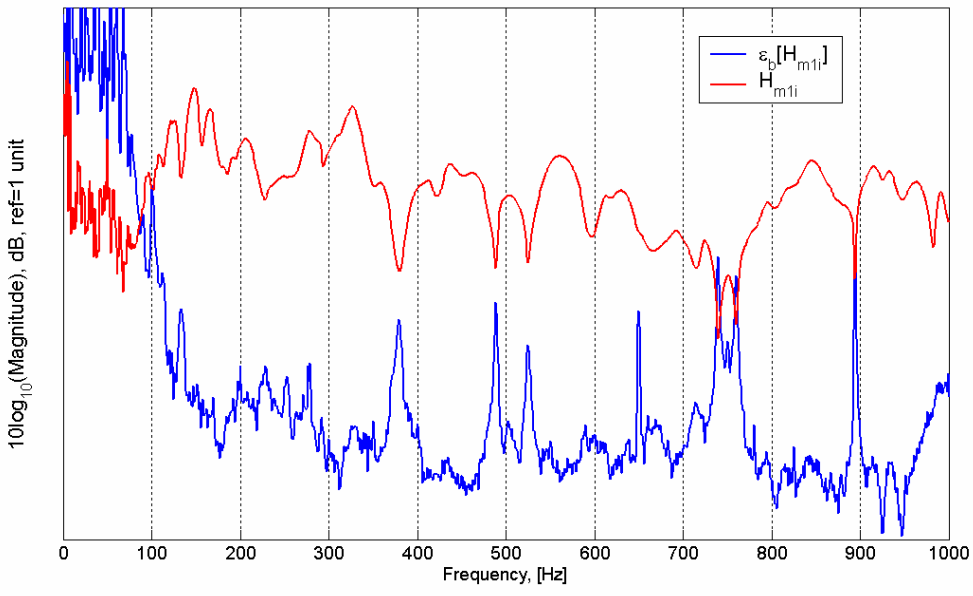

Figure 4.47 Comparison of the Magnitude of Transfer Function and Bias Error Terms at Microphone Position 1 of Modal Analysis

Although the error level is below 0.1 at the frequency range above 100 Hz, there are distinct frequencies where these values approach to values higher than this level. In Figure 4.47 magnitude of transfer function and bias error terms at microphone position 1 are compared. Almost uniformly, at the frequencies where bias error spectrum has peaks, which correspond to the notches of coherence spectrum, magnitude of the transfer function spectrum has notches. There are two possible mechanisms for this type of behavior, namely, inadequate spectral resolution or nonlinear system response. In this particular case, with a frequency resolution of 1 Hz, non-linearities in the system have more responsibility as compared the former cause.

The adequacy of frequency resolution for experimental acoustical modal analysis can be checked by considering the spectral behavior of the system transfer functions around the resonance frequencies. Normalized bias error terms for the magnitudes of auto-spectrum $\hat{G}_{xx}(f)$, and cross-spectrum $\hat{G}_{xy}(f)$ are given as [40];

$$e[\hat{G}_{xx}(f)] = e[|\hat{G}_{xy}(f)|] = (-1/3)\cdot(B_e/B_r)^2 \qquad (4.96)$$

where, B_e is the spectral resolution bandwidth and it is related to the record length of T as, $B_e = 1/T$; B_r is the half-power point bandwidth of spectral peak. Here, the minus sign indicates that the estimated values form an upper bound for the true values.

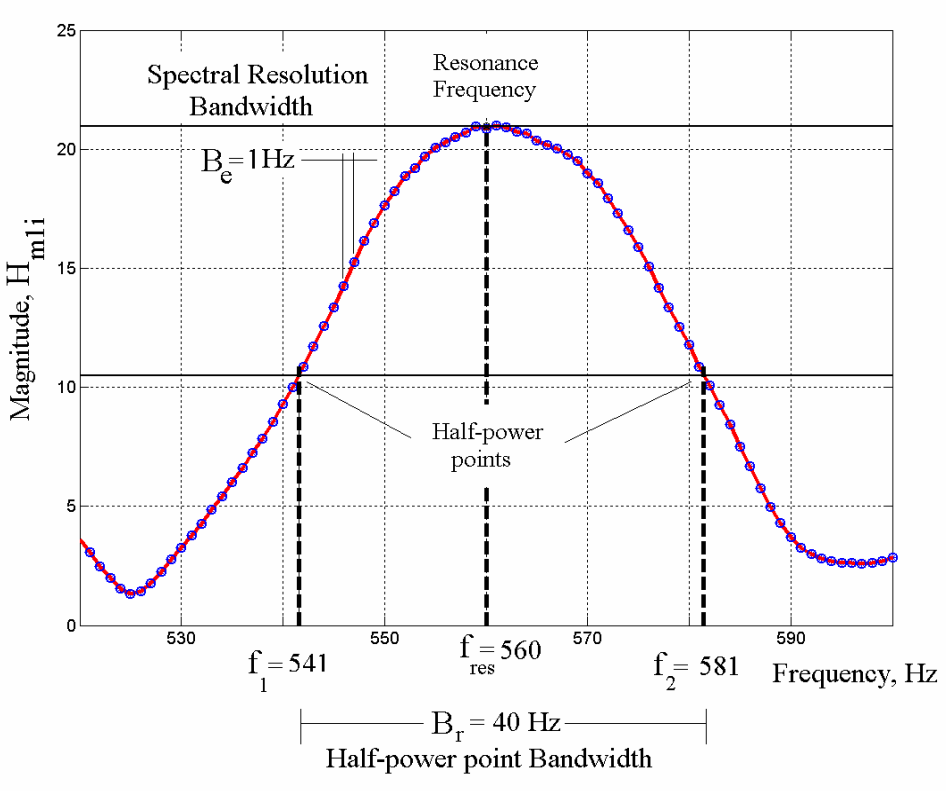

Figure 4.48 Half-power Point Bandwidth Analysis for Bias Errors

Although the error analysis should be carried out at every individual resonance frequency, a typical spectral plot around a resonance frequency at f_r =560 Hz, (557 Hz at Table 4.4) for the magnitude of transfer function is presented in Figure 4.48. The spectral resolution bandwidth of the measurement is taken as B_e =1 Hz and the corresponding half power point frequencies are found at f_1 =541 Hz and f_2 =581 Hz, hence, B_r =40 Hz.

The resulting normalized bias error term is found as;

$$e[\hat{G}_{xx}(f)] = e[|\hat{G}_{xy}(f)|] \approx 0.0002 \qquad (4.97)$$

which is almost at the order of magnitude of the random error levels of this

experiment. However, the upper limit on the bias error levels for the overall experiment is determined by the resonance frequencies where B_r is small. Values of B_r, on the other hand, are controlled by the damping of the structure as smaller modal damping values yield lower half-power bandwidths.

Table 4.6 Half-power Bandwidths and Bias Error Terms for Experimentally Found Modal Frequencies (First 15)

No	Modal Freq.	Half-power Band	e_b	e_b
	Hz	Hz	***B=1 Hz***	***B=10 Hz***
1	122	14	0.002	0.17
2	148	13	0.002	0.20
3	165	13	0.002	0.20
4	173	13	0.002	0.20
5	223	26	0.000	0.05
6	235	22	0.001	0.07
7	241	24	0.001	0.06
8	294	24	0.001	0.06
9	329	24	0.001	0.06
10	350	24	0.001	0.06
11	383	24	0.001	0.06
12	413	25	0.001	0.05
13	436	25	0.001	0.05
14	465	27	0.000	0.05
15	497	30	0.000	0.04

Table 4.6 presents the bias error analysis based on half-power point bandwidths for the first fifteen resonance frequencies of the system. For the spectral bandwidth of resolution of 1 Hz, error terms are at the order of 1/1000 of the transfer function magnitude at most. On the other hand, the modal frequency extraction developed in this study assumes a frequency resolution 10 Hz (±5 Hz). Although this procedure does not correspond to an increase of effective spectral

bandwidth to 10 Hz, as the most conservative error analysis procedure, Table 4.5 gives the resulting error terms for $\boldsymbol{B}$=10 Hz as well.

The error magnitudes dropped by a factor of 10^2 and at low resonance frequencies, decrease in accuracy is higher, whereas at higher frequencies the error terms are still at an order of 1/100, which is still an acceptable order. It is worth mentioning that, the low resonance frequencies where errors may be large, have very low damping properties without any modal over-lapping, therefore the true experimental errors in determining the resonance frequencies are much lower than this conservative analysis is indicating.

4.3.5 Lumped Parameter Solution of the Acoustical System

Resonance frequencies due to the bulk behavior of the air within the enclosure can be predicted from a simple lumped parameter model of the system. If no damping is considered for the air within the structure, then, there would be the system can be modeled by means of two type of linear lumped parameter acoustical elements, namely, acoustical mass (or inertance) and acoustical compliance [6].

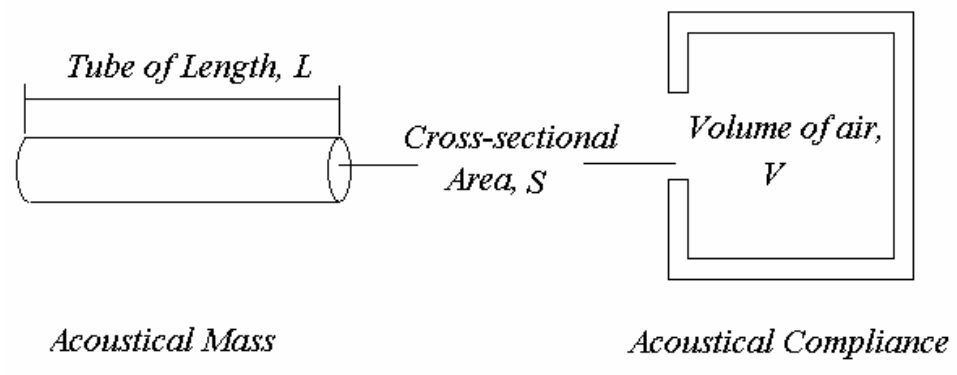

Figure 4.49 Lumped Parameter Acoustical Elements

Acoustic mass, M_A is related to the mass of air accelerated by a net force, which acts to displace the gas without appreciably compressing it. Acoustic compliance C_A, on the other hand, is associated with a volume of air that is compressed by a net force without an appreciable amount of displacement of the center of mass of the air volume. Practically, long air columns with tubular cross sections small compared to the length of the columns acts almost purely as an acoustic mass, whereas, enclosures of large volumes with almost uniform morphology, that is without any preferred direction of slenderness, act as purely acoustic compliances.

Referring to Figure 4.49, the constitutive equations for acoustical mass and compliance are as follows [6],

$$p(t) = M_A \frac{dQ(t)}{dt}, \tag{4.97}$$

$$p(t) = \frac{1}{C_A} \int Q(t)dt \tag{4.98}$$

where,

$p(t)$ is the instantaneous pressure acting over the element to accelerate or compress the air,

$Q(t)$ is the instantaneous volume velocity of the gas in cubic meters per second that is undergoing into acceleration or compression in the element. The volume velocity $Q(t)$ is equal to the acoustical particle velocity $u(t)$ multiplied by the cross-sectional area S.

M_A is the acoustic mass of the gas undergoing acceleration. For r_0 being the air density, its value for a lumped parameter ideal pure element is;

$$M_A = \frac{r_0 LS}{S^2} = \frac{r_0 L}{S} \tag{4.99}$$

C_A is the acoustic compliance of the gas undergoing compression. Again, its value for a lumped parameter ideal pure element is;

$$C_A = C_M S^2 = \frac{V_0 r_0 c^2}{S^2} S^2 = \frac{V_0}{gP_0} \tag{4.100}$$

with g the ratio of the specific heats, app. 1.4 for air, and P_0 the ambient static pressure, app. 100 kPa for practical considerations.

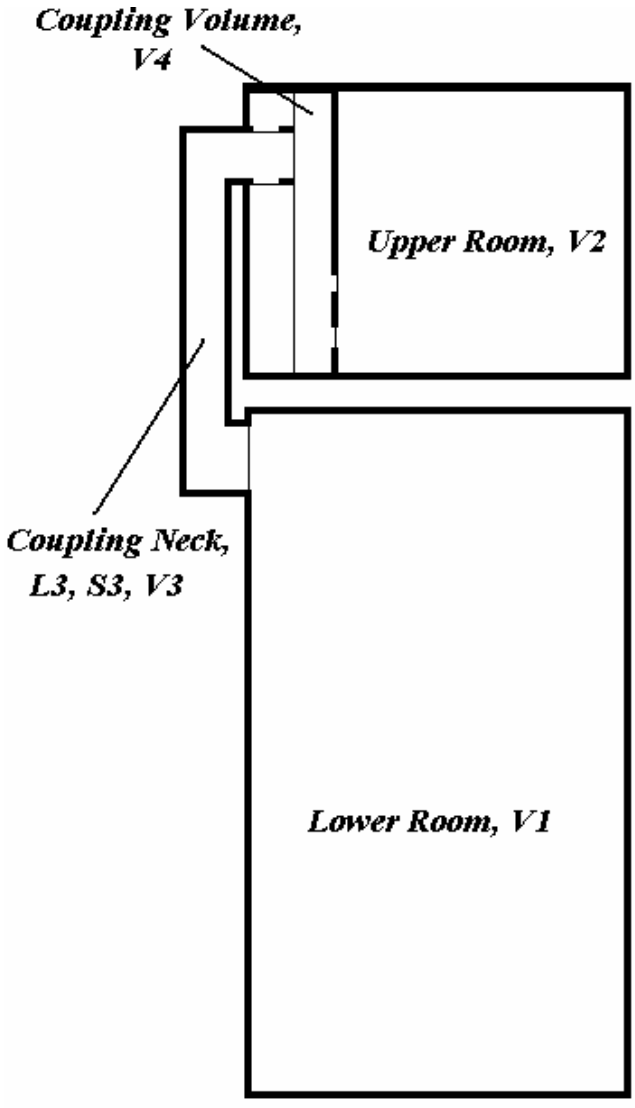

Figure 4.50 Acoustical Cavities for the Enclosure (Refrigerator)

A simplified version of the enclosure geometry is given in Figure 4.50 Upon inspection, there are two compliance type elements and one mass type element in this system, and these are, namely, air volume in upper and lower rooms and the coupling neck, respectively. The acoustical circuit diagram of this simplified system is depicted in Figure 4.51.

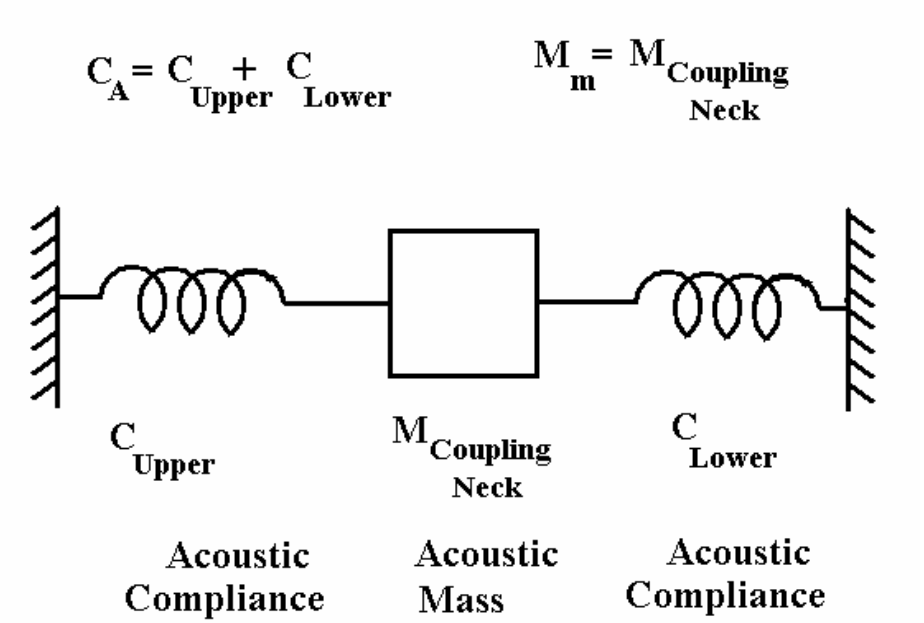

Figure 4.51 Acoustical Circuit of Cavities for the Enclosure

Table 4.7 Lumped Parameter Acoustical Elements

Acosutical Elements	Name of the Element	Effective Length	Effective Volume	Effective Surface Area	Acoustical Mass	Acoustical Compliance
		m	m^3	m^2	kg/m	m/N
Compliance Type	Coupling Volume	-	0.0101	0.0039	-	7.08E-08
	Upper Room	-	0.0915	0.0039	-	6.44E-07
	Lower Room	-	0.3339	0.0039	-	2.35E-06
Mass Type	Coupling Neck	0.5060	0.0020	0.0039	1.57E+02	1.39E-08

The coupling volume may behave in either way but due to the both small volume and comparatively large sectional area it is as effective as the other elements in the low frequency range of interest. The values for the elements are presented in the Table 4.7.

The resonance frequency for the simple circuit of compliance and mass

type elements only is given by,

$$f = \frac{w}{2p} = \frac{1}{2p\sqrt{C_A M_m}} \tag{4.101}$$

The calculated resonance frequencies for physically relevant pairs of acoustic compliances and masses are given at Table 4.8. Notice that an acoustical compliance together with an acoustic mass compounds a so-called Helmholtz resonator.

Table 4.8 Resonance Frequencies for Lumped Parameter Acoustical Elements

Elements of Mass/Compliance systems		Acoustical Mass	Acoustical Compliance	Resonance Frequency
Mass Type	Compliance Type	kg/m	m/N	Hz
Coupling Neck	Coupling Volume	1.57E+02	7.08E-08	47.7
Coupling Neck	Upper Room	1.57E+02	6.44E-07	15.8
Coupling Neck	Lower Room	1.57E+02	2.35E-06	8.3
Coupling Neck	Coupling Neck	1.57E+02	1.39E-08	107.8

These results clearly indicate that the bulk compliance mode of the complete structure at 10 Hz is related to the lower rooms acting as an acoustic compliance and the coupling neck as an acoustical mass. The bulk frequency at 125Hz for the total system is related to the bulk frequency of 114 Hz for the upper half of the structure. The only frequency close to this value is the one calculated for the coupling neck acting as both an acoustical compliance and mass. This suggests that the coupling neck is actually divided into some sub-sections to

sustain a resonance at the given frequency.

4.4 Summary of Results and Conclusions

In this chapter, experimental methods are examined on the noise transmission path identification of acoustically coupled spaces, with structurally coupled boundaries. The experimental works are applied to a real structure, namely a domestic type refrigerator cabinet, which encloses acoustically coupled cavities. The frequency bound of the problem is 1000 Hz and this frequency range is extended in the upper bound to 2000 Hz, when possible, in order to get an insight for the quality of measurements on the one hand, and for getting further insight of the problem in the mid to high frequency behavior of the enclosure.

At the first section of this chapter, the acoustical transmission problem of the structure is investigated via vector intensity measurements. Frequency depended IL values for the cabinet are obtained together with the dip frequencies where the structure exhibits weak transmission characteristics. The radiation efficiency of the structure is also analyzed and discussed for possible physical phenomenon as an explanation of observed characteristics.

Following this section, cavity acoustics problem is attacked by means of modal decomposition and lumped parameter acoustical system modeling techniques. The theory behind the modal decomposition techniques is examined at the beginning of the section, which is followed by finite element analysis and experimental acoustical modal analysis studies. The cavities assume different

temperatures during operation, which are below the environmental room temperature. The effect of this temperature difference on the modal behavior of the cavities is discussed briefly and some practical consequences of this effect are presented.

The experimental modal analysis techniques developed for the structural problems are applied to acoustical case in hand, and modal frequencies for the coupled structure are extracted successfully. Finally, a very low frequency, lumped parameter model of cavities is developed and the resonance frequencies due to this bulk behavior are obtained.

Rigid wall boundary conditions are used in finite element analysis of the cavities, which essentially ignores the structural coupling of the acoustical cavities with the enclosure walls. In addition to finite element techniques, lumped parameter analysis of the system is effectively used in modeling of the system for very low frequency characteristics of the enclosure. Experimental acoustical modal analysis, on the other hand, naturally includes these wall effects, as well as the acoustical damping of the structure via dissipation due to wall and air absorption characteristics.

The acoustical transmission problem formulated as insertion loss of the enclosure and radiation efficiency of the outer layer encompasses all these effects, together with the structural characteristics of the multi-layered enclosure walls. Therefore, all possible engineering approaches are applied to the enclosure and the remaining task is the integration of these results in order to obtain a complete

picture of the vibro-acoustical behavior of the enclosure below 1000 Hz low frequency range as set at by the definition of the problem.

Figure 4.52 presents experimentally found modal frequencies together with the experimentally determined IL frequencies. Figure 4.53 and Figure 4.54 present the comparison of finite element analysis results with experimentally determined modal frequencies and IL frequencies respectively. The values related to these plots are already given in Table 4.1 for IL values, Table 4.2 for Finite Element Analysis, Table 4.4 for experimental modal analysis results. Finally, Table 4.7 tabulates resonance frequencies for the lumped behavior of the system.

The methodologies conducted in this study can be categorized in terms of their cost as an engineering approach from low to high with increasing order. Lumped parameter modeling assumes the lowest rank as a basic engineering tool for acoustical analysis. Finite element analysis is next, provided that a reliable solver is available, with supporting computer aided engineering software for solid modeling, meshing etc.

Insertion loss estimations from intensity measurements are next to the analytical and numerical methods as an experimental methodology. Experimental modal analysis is the most costly analysis, as compared to finite element techniques not only due to the instrumentation involved, but also, due to the analysis and that must be taken care of as post-processing of the data.

For engineering applications, analytical and numerical methods are easy, inexpensive and reliable, if there are any that can handle physics of the problem as

required. On the other hand, experimental identification methodologies are usually expensive and very demanding if reliability and precision is required with a high standard. A hybrid approach which can take care of the drawbacks of both methodologies is the most cost effective one, hence, the aim of the study presented in this Chapter so far.

Some typical conclusions can be drawn from these analyses, as examples.

1. The lowest resonance frequency is at 13Hz, which is obtained form finite element (FE) analysis and predicted from the lumped parameter model as a Helmholtz resonator type behavior where the lower compartment acts like an acoustical compliance and the coupling neck acts like an acoustical inertance. However, this frequency is well below the audio frequency band (16-20 Hz at lower bound) therefore, can be omitted for noise control purposes. Nevertheless, it is clear that a slight increase in the inertance of the coupling neck, or a decrease in the compliance of the lower compartment, can easily shift this frequency up to the audible region. This can be possible by lowering the volume of the lower compartments at one hand, and increasing the length or decreasing the effective cross-sectional area of the coupling neck on the other hand.

2. Another frequency that deserves attention is 125Hz, identified very clearly in FE analysis, which is predicted with a slightly lower value as the tubular resonance frequency (organ pipe tone) of the coupling

neck. This frequency is very precisely identified by the experimental modal analysis, as well. On the other, this frequency of resonance assumes its crucial importance due to the IL curve as a dip frequency. In other words, the IL dip at 122Hz is due to the cavity resonance of the enclosure, experienced as a result of the isolated coupling neck resonance. The remedy is, obviously, the modification of this volume without destroying its primary function as part of machinery.

3. The resonance of the cavity due to the modal behavior of the lower compartment at 145Hz is identified experimentally, as well. Although, the IL curve has no distinct dip frequencies at this frequency, the dip frequencies at 137Hz and 154Hz suggest some structural coupling mechanism that can be related to this resonance behavior.

4. At 345 Hz, the enclosure has again an IL dip. At 349Hz, the FE analysis identifies a coupled mode, and the corresponding mode shape clearly indicates the effect of coupling neck. The experimental modal analysis identifies this frequency as modal resonance frequency at 350Hz with ±5Hz accuracy.

5. Similarly, at modal resonance frequencies 404Hz, 412Hz, 680Hz and 815Hz, IL dip frequencies can easily be identified with the cavity resonance of the enclosure.

In this Chapter, physical phenomenon related to the vibro-acoustical behavior of an enclosure with acoustically, structurally coupled internal cavities are

investigated via analytical and experimental tools. However, a complete description of the performance of an enclosure can be estimated when it is excited by means of a source distribution, as close as possible to its operating conditions. Moreover, the resulting noise transmission paths may assume some practical importance if they are related to some receiving points where optimization, or as in many cases minimization of noise is required. Next Chapter handles this requirement for an enclosure excited by multi noise source mechanism, with receiving points located in an environment at the end of some typical noise transfer paths.

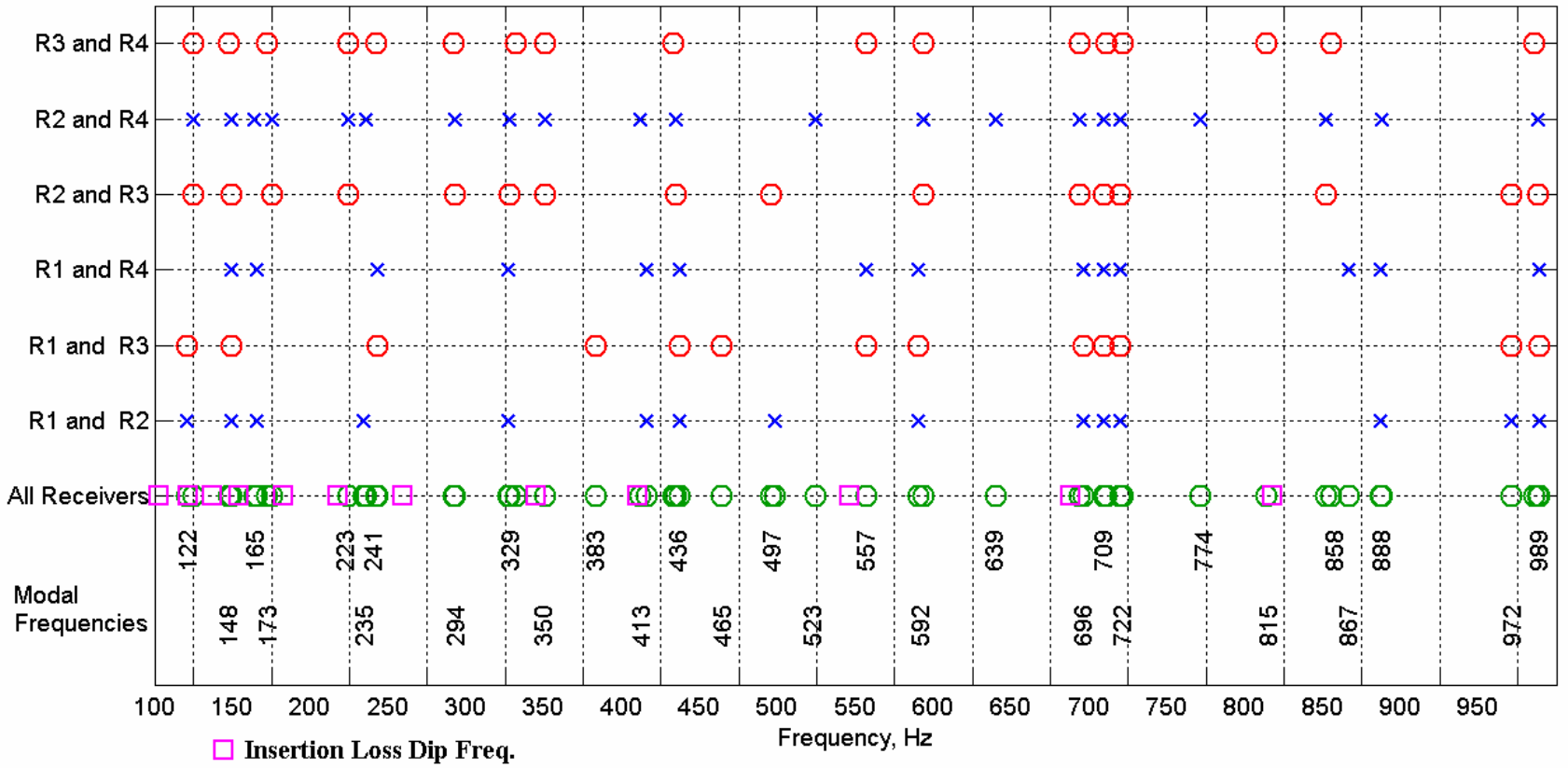

Figure 4.52 Comparison of Insertion Loss Dip Frequencies with those of Experimentally Found Modal Frequencies

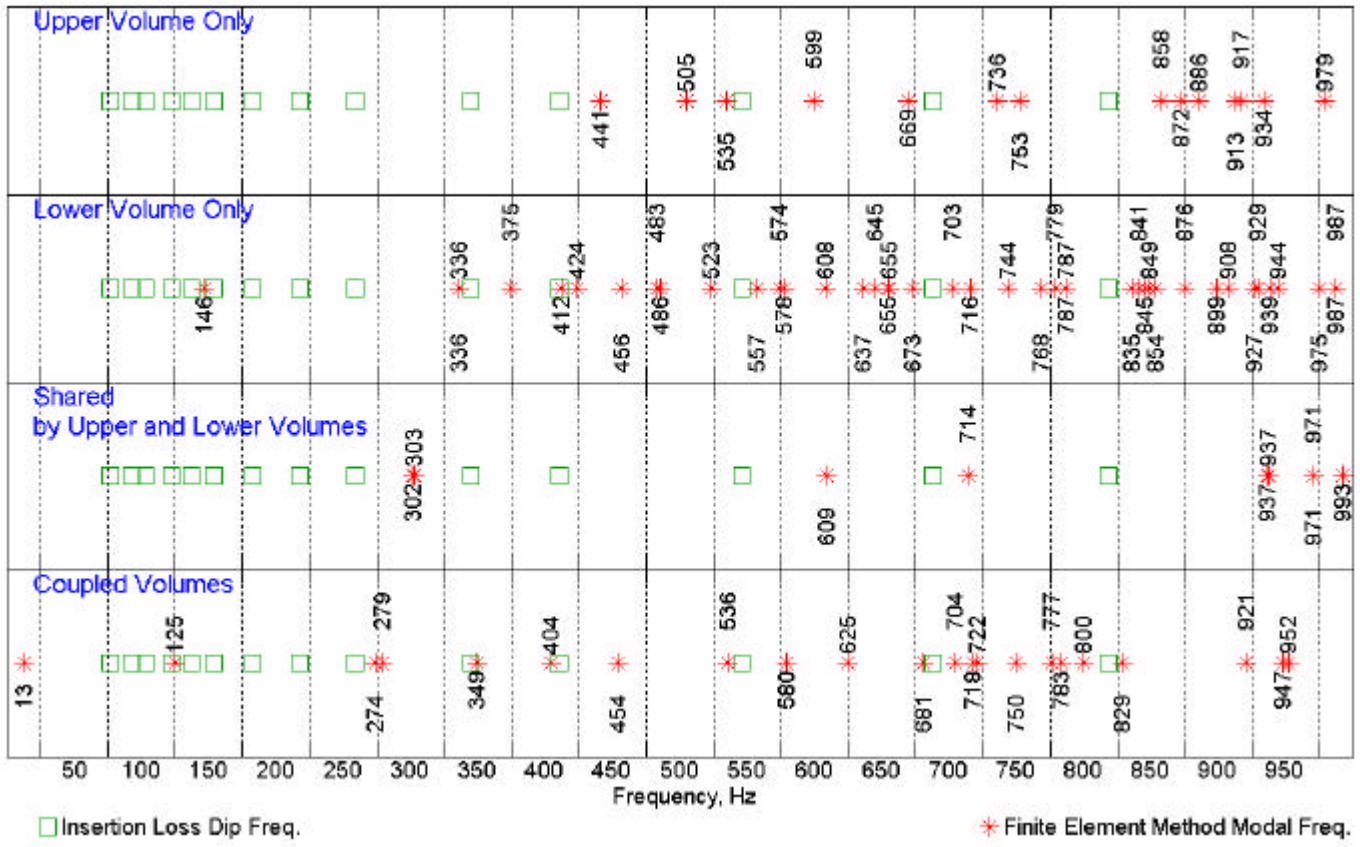

Figure 4.53 Comparison of Insertion Loss Dip Frequencies with those of FEM Frequencies

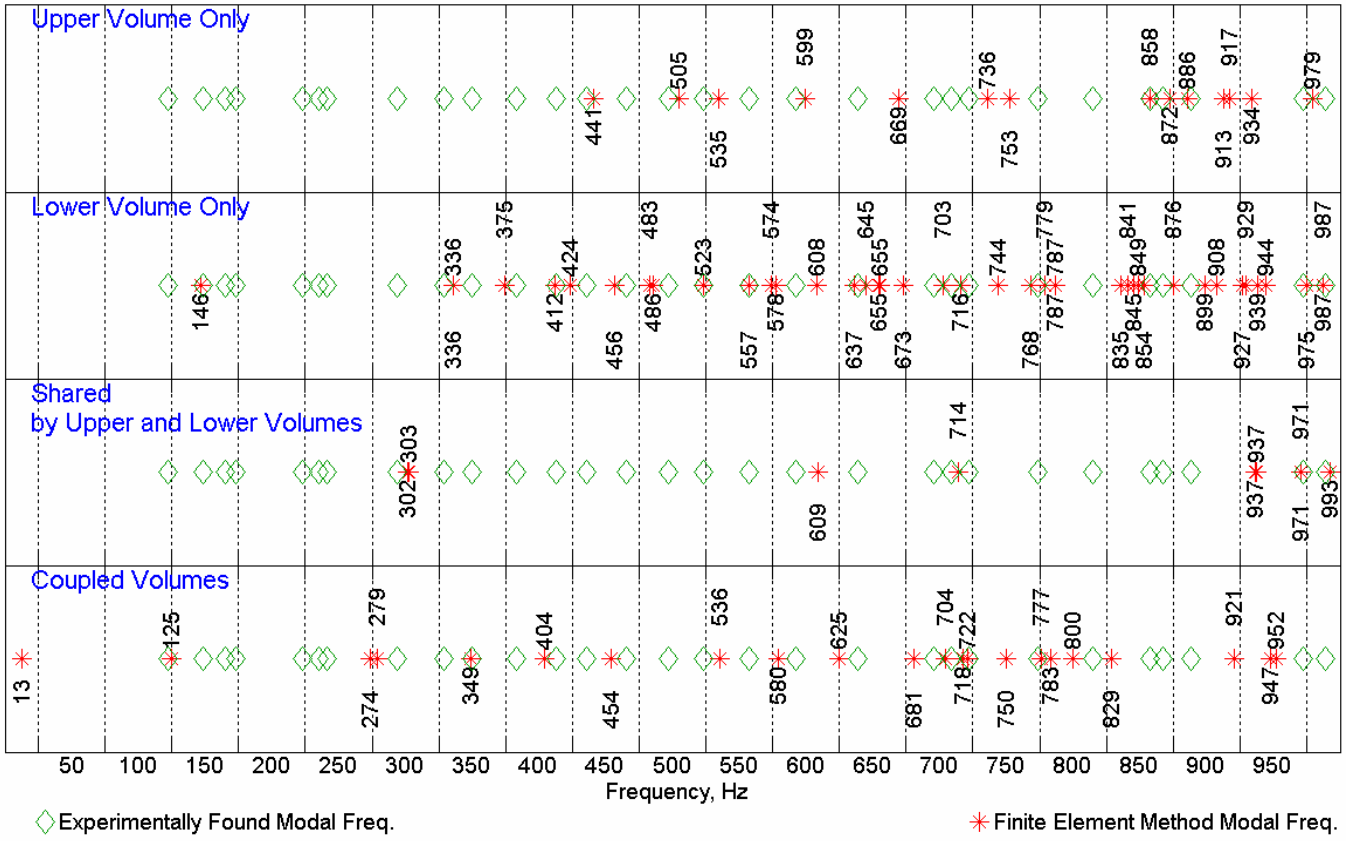

Figure 4.54 Experimentally Found Modal Frequencies with those of FEM Frequencies

CHAPTER 5

NOISE PATH ANALYSIS

5.1 Introduction

In the previous Chapter, an extensive analysis of an enclosure with acoustically, structurally coupled internal cavities is conducted via analytical and experimental tools related to physical phenomenon, which underlie its vibro-acoustical behavior. In this Chapter, some experimental methodologies for noise transmission path identification are investigated valid for cases where an enclosure is excited by a multi source distribution in an external environment with some receivers.

Figure 5.1 depicts such an enclosure excited by some noise sources of air-borne and structure borne type and receivers at the surrounding environment. The corresponding noise paths are characterized by the dominant media of noise propagation. However, for a noise control problem related to human annoyance due to perception by ear, eventually all transmission paths assume an air-borne characteristic. A transfer path connects a possible source mechanism to a

receiving point where response of the system is required

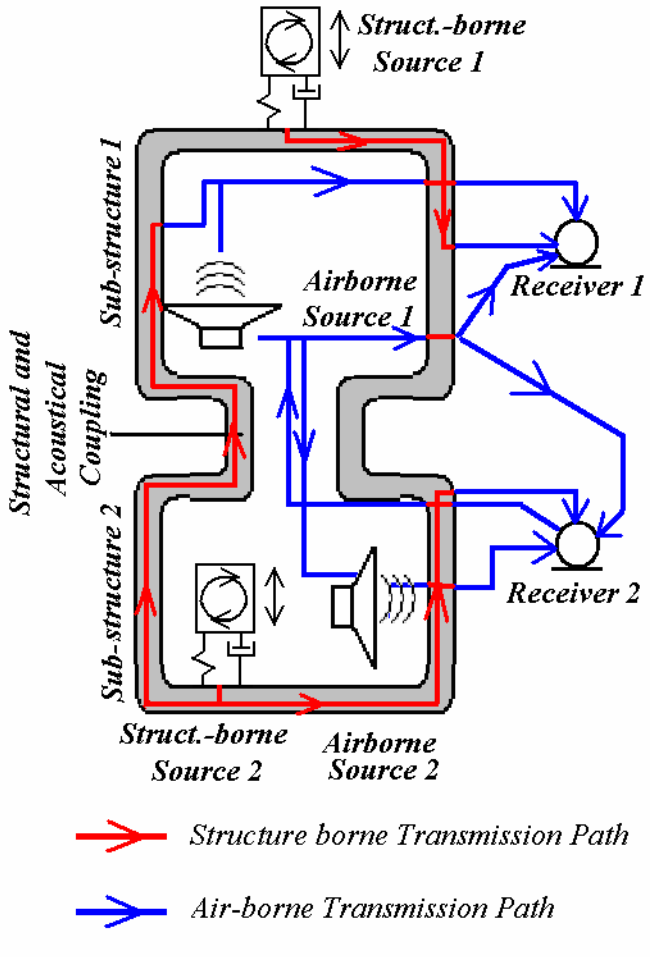

Figure 5.1 Enclosure with Multi Source Multi Receiver

Hence, for a single source, single receiver system, in other words, a single input, single output system, the source, path and receiver problem can be formulated as;

$$Y(f) = H(f) \cdot X(f) \qquad (5.1)$$

where, with f denoting frequency, $Y(f)$ is the output, $X(f)$ is the input and $H(f)$ is the Transfer Function or Frequency Response Function which is

nothing but the mathematical representation of the required noise transmission path mechanism. In case there are many sources, the system becomes a multi input, single output system and Equation 5.1 can be revised with summation over the sources as;

$$Y(f) = \sum_{i=1}^{N} H_i(f) \cdot X_i(f) \qquad (5.2)$$

Note that, this is possible if and only if, the principle of superposition holds, hence, the system is linear. Essentially, a transmission path analysis is, the estimation of transfer functions $H_i(f)$ as formulated in Equation 5.2.

In this chapter, this estimation is carried out by means of two methods. The first methodology exploits the correlation analysis techniques, where transfer functions are obtained via experimentally obtained correlation spectra in between excitation sources as inputs, and receivers as outputs. The second formulation is the direct measurement of this transfer functions by some means of artificial excitation. In most of the cases, this type of excitation is difficult, if not impossible, as the system must be disassembled for a direct measurement to be conducted. A remedy for this is to use the principle of reciprocity, valid for linear time invariant parameter systems, which sometimes offer a useful relationship that transforms a difficult input-output relation into a physically more manageable one.

In this study, these two methodologies are applied to the enclosure

structure presented in the previous chapters as a case study. The excitation mechanisms are considered in accordance with the requirements when the enclosure is operating in certain functional requirements, without any loss of generality. For some certain form of vibro-acoustically reciprocal measurements, an omni directional volume source is an urgent requirement as a transducer. In direct transfer path measurements, an omni-directional volume source is used which is designed, constructed and certified during the study, as well.

The transfer functions representing the transmission paths are compared with each other. Finally, they are interpreted physically by means of the extensive analysis presented in Chapter 4, for possible design modifications that may lessen the annoyance of human receivers, which is the ultimate aim of this study.

5.2 Correlation and Spectral Analysis Applied to Noise Path Identification

5.2.1 Theory

A multi input, multi output system can be considered as the superposition of the collection of multi input, single output (MISO) systems. [40,41]. Therefore, the theory can be simplified without any loss of generality to the analysis of a MISO system. In this case, consider the system defined by Equation 5.3 in frequency domain as;.

$$Y(f)=\sum_{i=1}^{N} H_i(f)X_i(f)+N(f) \qquad (5.3)$$

where f is frequency, $Y(f)$ and $X(f)$ are the output and input vectors, respectively, $H(f)$ is the matrix of corresponding transfer functions between the input-output pairs. Finally $N(f)$ is the noise vector, added to system at the output. Note that noise at the input can be handled by increasing the order of the input vector and this additional term is the only difference between Equation 5.2 and Equation 5.3, where the latter models a real measurement environment.

For the estimation of individual transfer functions, both sides of the Equation 5.3 is correlated by the complex conjugate of $X(f)$ as;

$$X_j^*(f)Y(f)=\sum_{i=1}^{N} H_i(f)X_j^* X_i(f)+X_j^* N(f) \qquad (5.4)$$

Equation 5.4 can be expressed in terms of related spectral density functions when the expected values of the terms are considered as;

$$G_{Z_i Z_j}(f)=\frac{lim}{T\to\infty}\frac{2}{T}E(Z_j^*(f)Z_i(f)) \qquad (5.5)$$

where $G_{Z_i Z_j}(f)$ is one sided auto spectral for $i=j$, or cross spectral for $i\neq j$, density function for $Z_{i,j}$, and $E()$ is the expected value operator taken over a sufficiently large period of time, T. The resulting expression after these operations is as follows;

$$G_{jy}(f)=\sum_{i=1}^{N} H_i(f)G_{ji}(f)+G_{jn}(f) \qquad (5.6)$$

Equation 5.6 simply states that the transfers functions, H_i's can be obtained from a solution of *N* number of linear equations, where the experimentally determined spectral correlation functions form the coefficient matrices. Note that, when noise component is completely uncorrelated with either one of the sources, $G_{jn}(f)$ term disappears.

On the other hand, if the conjugate of Equation 5.3 is taken as;

$$Y^*(f)=\sum_{i=1}^{N} H_i^*(f)X_i^*(f)+N^*(f) \tag{5.7}$$

and multiplied by the Equation 5.3 side by side as;

$$Y^*(f)Y(f)=\left[\sum_{i=1}^{N} H_i^*(f)X_i^*(f)+N^*(f)\right]\left[\sum_{j=1}^{N} H_i(f)X_i(f)+N(f)\right] \tag{5.8}$$

then, one obtains the following expression;

$$=\sum_{i=1}^{N}\sum_{j=1}^{N} H_i^*(f)H_j(f)X_i^*(f)X_j(f)+N^*(f)N(f)+$$

$$\sum_{i=1}^{N} H_i^*(f)X_i^*(f)N(f)+\sum_{j=1}^{N} H_j(f)N^*(f)X_j(f) \tag{5.9}$$

If expected values of both sides are taken, the expressions in terms of correlation functions can be obtained as;

$$G_{yy}(f)=\sum_{i=1}^{N}\sum_{j=1}^{N} H_i^*(f)H_J(f)G_{ij}(f)+G_{nn}(f)+$$

$$\sum_{i=1}^{N} H_i^*(f)G_{in}(f)+\sum_{j=1}^{N} H_j(f)G_{nj}(f) \tag{5.10}$$

Equation 5.10 defines the fundamental equation that can be exploited for a transfer path analysis formulation as conducted in this research. Notice that, if noise component is uncorrelated with any one of the inputs, this equation further

simplifies to;

$$G_{yy}(f)=\sum_{i=1}^{N}\sum_{j=1}^{N}H_i^*(f)H_j(f)G_{ij}(f)+G_{nn}(f) \tag{5.11}$$

Therefore, once individual transfer functions are obtained, auto-spectrum of the output signal can be constructed from these functions and the cross-correlation functions between the sources.

It is worth examining the special MISO case for two-input, one-output system. In this case open form of Equation 5.6 can be read as;

$$G_{1y}(f)=H_1(f)G_{11}(f)+H_2(f)G_{12}(f) \tag{5.12}$$

$$G_{2y}(f)=H_1(f)G_{21}(f)+H_2(f)G_{22}(f) \tag{5.13}$$

Hence solving for the transfer functions H's one obtains;

$$H_1(f)=G_{1y}(f)\left[1-\frac{G_{12}(f)G_{2y}(f)}{G_{22}(f)G_{1y}(f)}\right]\Big/G_{22}(f)\left[1-g_{12}^2(f)\right] \tag{5.14}$$

$$H_2(f)=G_{2y}(f)\left[1-\frac{G_{21}(f)G_{1y}(f)}{G_{11}(f)G_{2y}(f)}\right]\Big/G_{22}(f)\left[1-g_{12}^2(f)\right] \tag{5.15}$$

where,

$$g_{12}^2(f)=\frac{\left|G_{21}^2(f)\right|}{G_{11}(f)G_{22}(f)} \tag{5.16}$$

is the ordinary coherence function. For $g_{12}^{2}(f) \approx 1$, which corresponds to fully correlated noise sources, the solutions for the transfer functions become indeterminate.

5.2.2 Experimental Set-up

A set of experiments is designed for the analysis under operational conditions. Here, operational means, excitation of the system by physical sources under normal operating conditions. The response of the system is measured as microphone responses at some specified points. These specified points are chosen as seven microphone positions, located on a hypothetical, prismatic, enclosing surface. The enclosure is placed in front of a reflecting wall, and the surrounding environment is a semi-anechoic room, with a reflecting floor and absorptive surfaces, with a design cut-off frequency of 125Hz. Hence, the set-up fulfills all the requirements of sound power measurement of home appliances in accordance with the EN60704. Figure 5.2 presents the details of these locations.

The enclosure is considered under the excitation of by five input noise sources, namely, three of structure borne origin and two air-borne origin. The structure borne sources are modeled as mobility type sources, where excitation is specified in terms of vibration velocities, whereas the air-borne sources are considered to be of pressure fluctuations origin. Therefore, accelerometers, after integration in the frequency domain are used for structure borne, and microphones are used for air-borne sources as input reference pick-ups. Table 5.1 summarizes

these configurations.

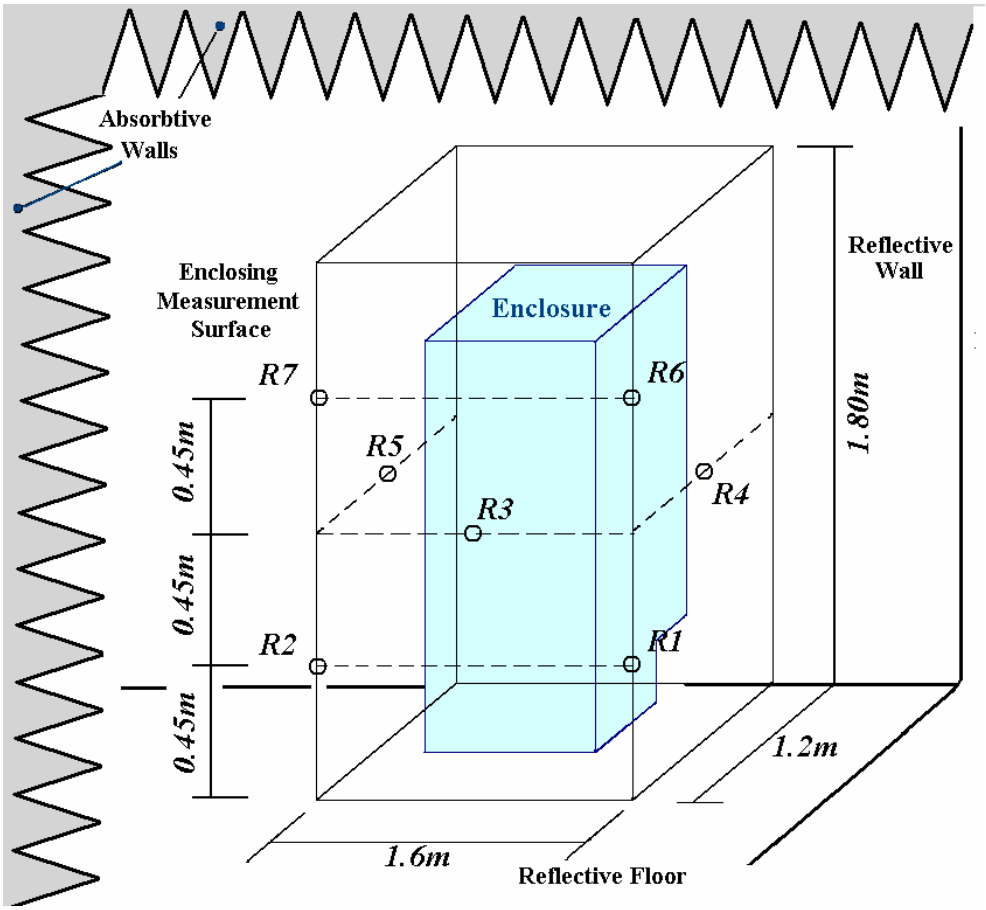

Figure 5.2 Locations of the Receiving Points

Table 5.1 Description of the Noise Sources

Source #	Pick-up	Source Type	Physical Signal	Unit	Reference for dB	Correlated Sources
S1	Accelerometer	Strucuture borne	Vibration Velocity	m/s	5.00E-08	S2
S2	Microphone	Air-borne	Sound Pressure	Pa	2.00E-05	S1
S3	Accelerometer	Strucuture borne	Vibration Velocity	m/s	5.00E-08	S4
S4	Microphone	Air-borne	Sound Pressure	Pa	2.00E-05	S3
S5	Accelerometer	Strucuture borne	Vibration Velocity	m/s	5.00E-08	*

The correct choice of reference pick-up is related to the characteristics of physical sources. In this case, there are three noise generation mechanisms. The first one is an axial fan located inside the enclosure cavity, mounted resiliently on the internal structure. The excitation is due to the structural vibrations of the fan electric motor, on the one hand, and due to flow of air, pressurized by the fan propeller mechanisms, on the other hand. Motor excitations can be handled as velocity sources successfully in the literature. The air flow noise due at low blade passing frequencies are, on the other hand, related to the dipole like, oscillating forces on the blades due to pressure fluctuations [43]. Hence, a pressure transducer is quite suitable for these kinds of sources.

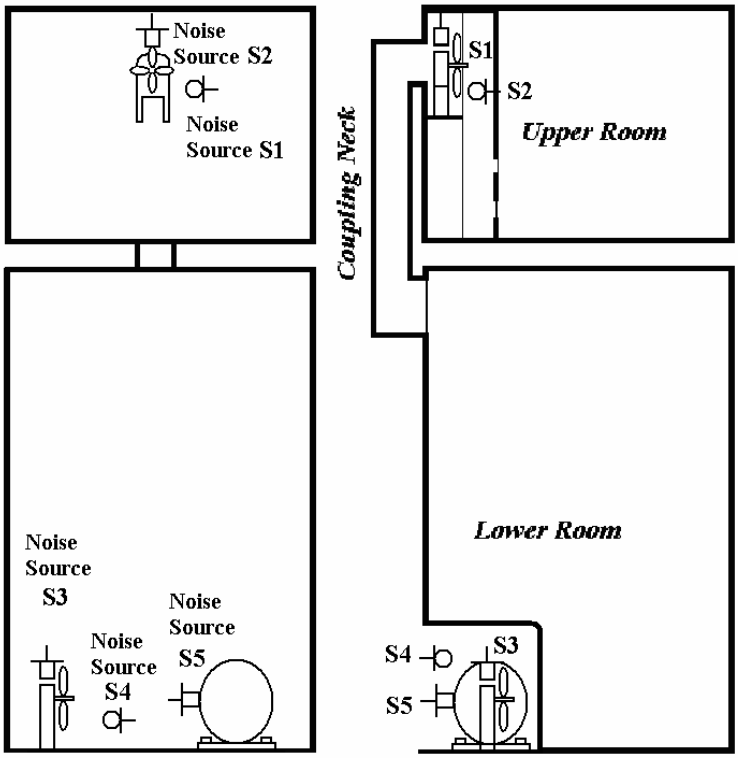

Figure 5.3 Location of the Sources on Enclosure Structure

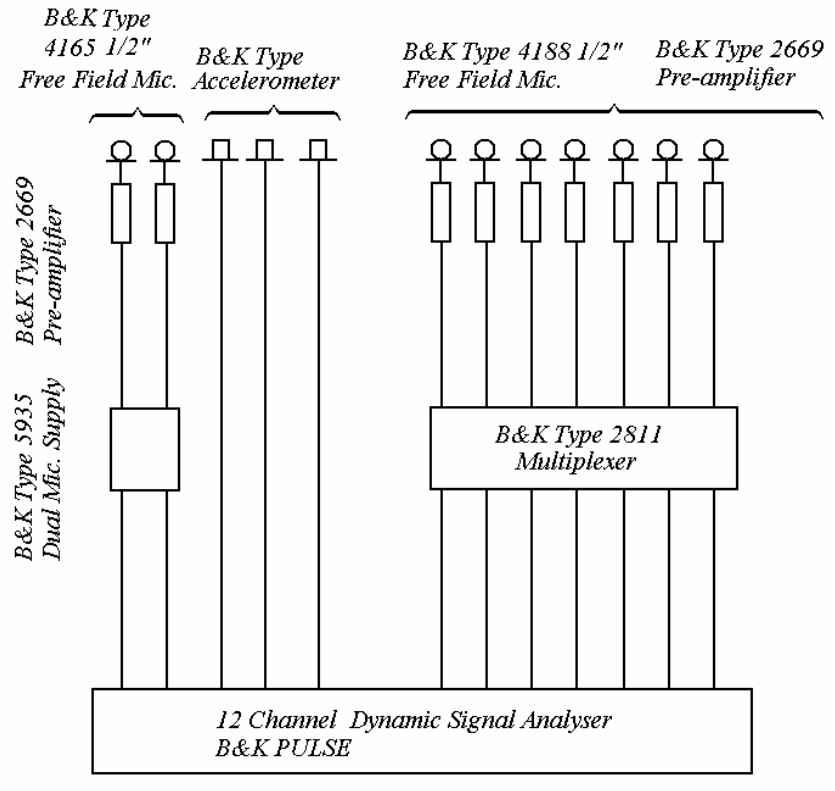

Figure 5.4 Measurement Equipment for MISO Analysis under Operational Conditions

The other physical source is almost similar to the first one, only slightly different hydrodynamic working conditions. The remaining physical source is a thick vibrating shell (hermetic compressor), which can be modeled with enough reliability by considering the velocity of the shell structure. However, as the physical insight clearly points out, the four of the excitations are correlated to each other in pairs of two. This fact is also indicated in the Table 5.1. Source locations on the enclosure used for the case study are shown in Figure 5.3. Note that, Sources S1 and S2 are located inside the cabinet without any direct air-borne transmission path, where as, S3, S4 and S5 are located in an external cavity, which has a direct path of air-borne origin. The signal flow chart and the

equipment for measurements are given in Figure 5.4.

A twelve-channel signal analysis unit is used for the measurement of required auto and cross-spectral density functions. A narrow band (FFT) analysis with frequency resolution of 2Hz is used for a frequency range of 0-3200Hz, although the post-processing of the data is conducted up to 2000Hz for the investigation of source behavior, and up to 1000Hz for transfer path analysis. Linear averaging with 100 spectra is used without overlapping, which corresponds to a total data record length of 50 seconds.

The physical sources of the case study can be mechanically switched off, without perturbing the function of the other remaining physical sources. Even if this can be a possibility for many practical cases, as a major drawback, it is not possible to estimate the individual contributions of different noise source or path mechanism when they are physically related to the same source. In this case study, two of the physical sources have effective air-borne and structural borne characteristics, and the simple acoustical shrouding applied in this study can not be used to predict their contribution. Never the less, the so-called acoustical shrouding methodology can be used in this analysis, at least, as a qualifier of the Multi Input, Multi Output (MISO) formulation.

5.2.3 Results

The combination of sources in the acoustical shrouding analysis is given in Table 5.2. Although suppression of any source reduces the system order, MISO

solutions are still carried out for an order N=5, and the signals from the non-operating components are considered as noise at the input.

Figure 5.5 to 5.11 show the responses for the acoustical shrouding cases in accordance to the order given in Table 5.2. The frequency range is extended to 2000 Hz in order have some insight of for the requirements of the problem. The plots give the responses for seven microphone positions. In all of the cases, it can be observed that the responses are different depending on the microphone locations. Hence, different noise transmission paths are effective.

Table 5.2 Source Combinations in Acoustical Shrouding

Physical Source #	*Related Excitations*
PS 1	**S1, S2**
PS 2	**S3, S4**
PS 3	**S5**

Combinations of Acoustical Shrouding		
CASE #	*Source #*	*Physical Source(s) On*
CASE 1	**S1 S2**	**PS 1**
CASE 2	**S3 S4**	**PS 2**
CASE 3	**S5**	**PS 3**
CASE 4	**S1 S2 S3 S4**	**PS 1 PS 2**
CASE 5	**S1 S2 S5**	**PS 1 PS 3**
CASE 6	**S3 S4 S5**	**PS 2 PS 3**
CASE 7	**S1 S2 S3 S4 S5**	**PS 1 PS 2 PS 3 (ALL)**

As mentioned before the pick-ups for source signals are operating at all conditions. Figure 5.12 to 5.16 depict the input spectra plotted for individual sources with respect to the Cases of acoustical Shrouding given in Table 5.2.

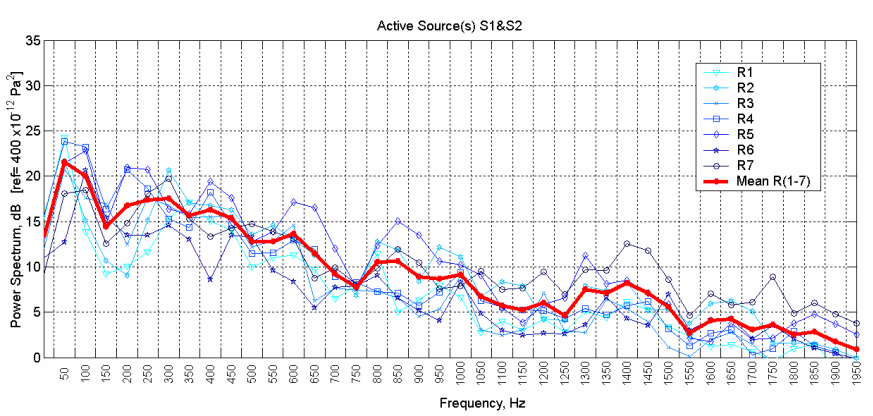

Figure 5.5 Responses for CASE1

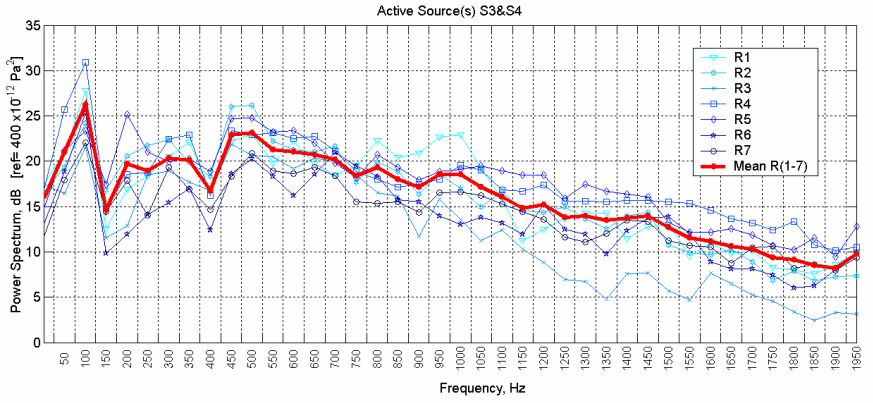

Figure 5.6 Responses for CASE2

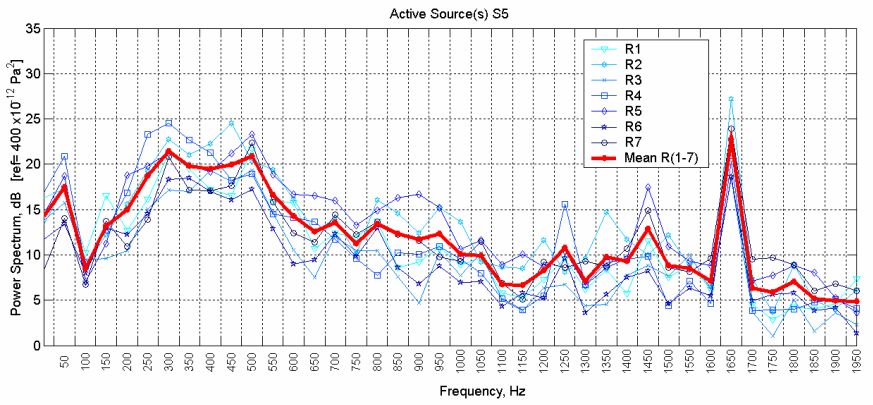

Figure 5.7 Responses for CASE3

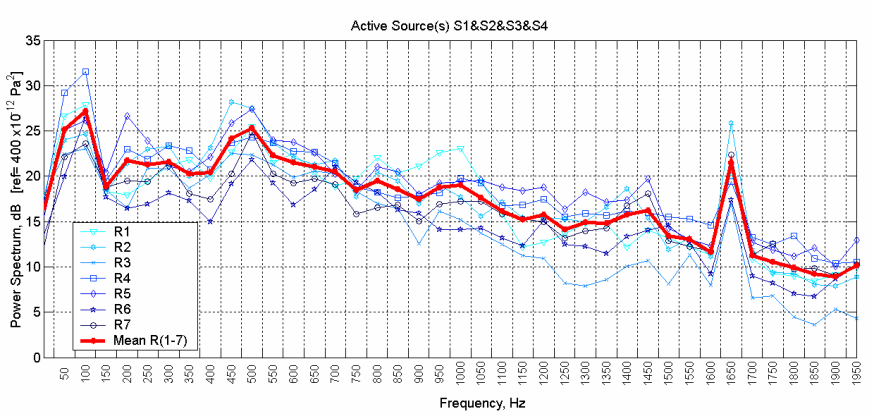

Figure 5.8 Responses for CASE4

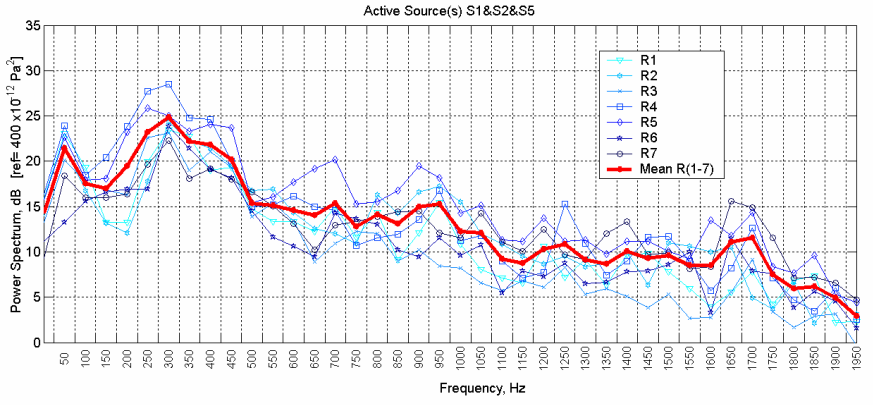

Figure 5.9 Responses for CASE5

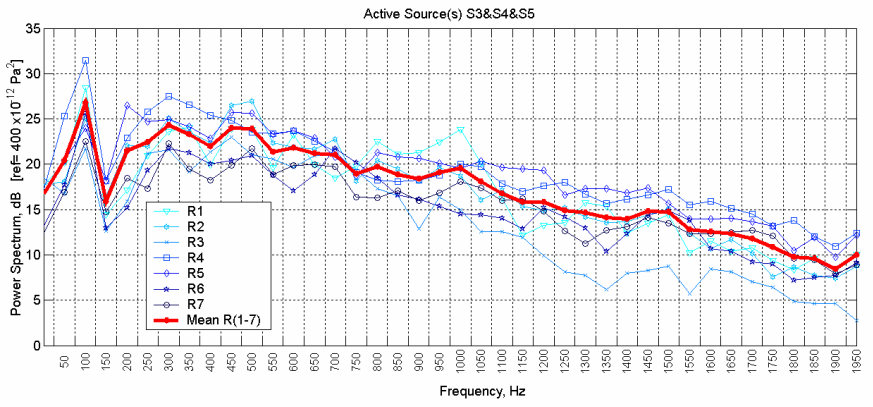

Figure 5.10 Responses for CASE6

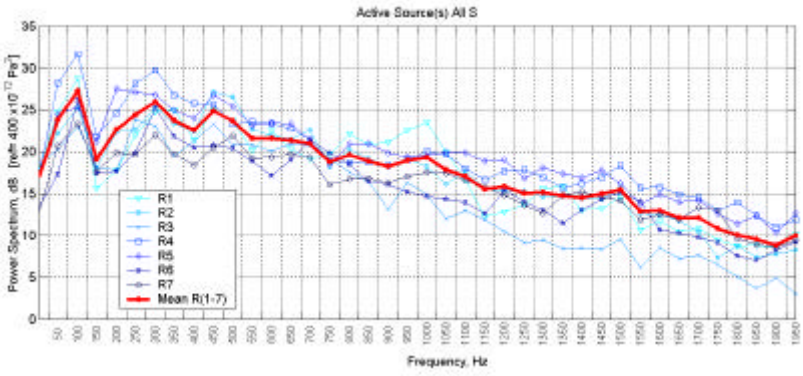

Figure 5.11 Responses for CASE7

The most important aspect these plots are revealing is that, the pick-ups, which are used to model the air-borne sources, namely, S2 and S4, are contaminated by the structure borne source. For Source 2 in Figure 5.13, at CASE 3 and CASE 6 where S1 and S2 are off, microphone at S2 has a spectrum around 200Hz to 400Hz very close to the values in case these forces are operating. For Source 4 in Figure 5.15, at CASE 3 and CASE 4 this time, the similar behavior is observable, although with a lower value of contamination. This is quite an expected behavior for an acoustically, structurally coupled system, and the very reason of conducting the MISO type correlation analysis techniques.

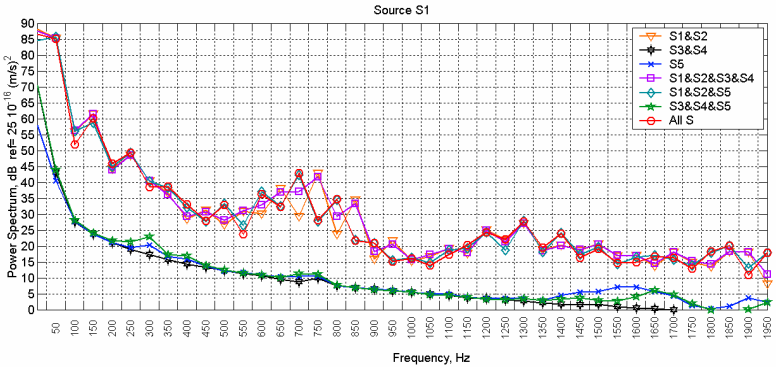

Figure 5.12 Input Spectra for Source 1 at CASES of Table 5.2

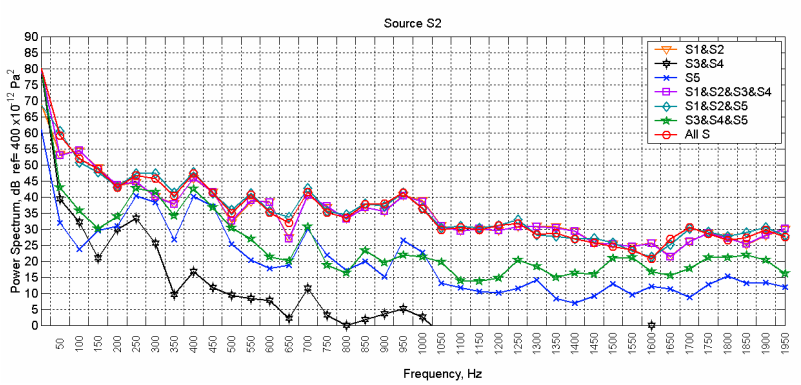

Figure 5.13 Input Spectra for Source 2 at CASES of Table 5.2

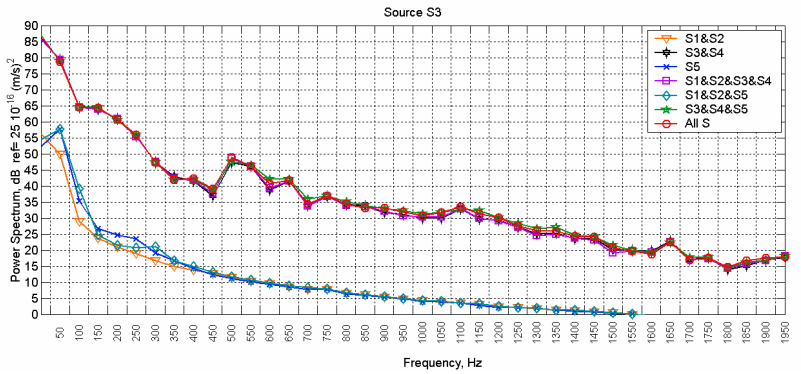

Figure 5.14 Input Spectra for Source 3 at CASES of Table 5.2

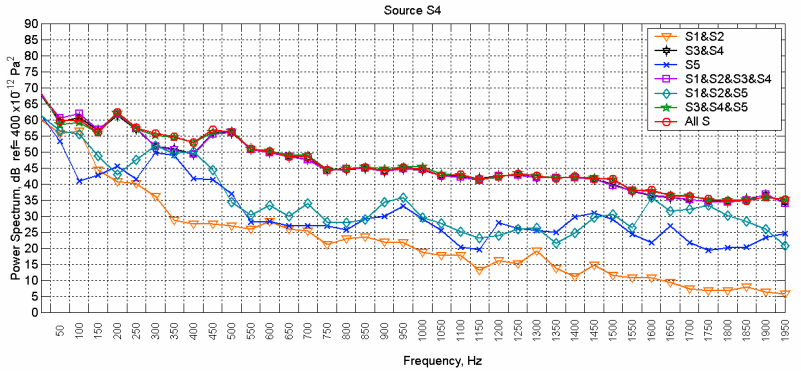

Figure 5.15 Input Spectra for Source 4 at CASES of Table 5.2

Figure 5.17 and Figure 5.18 summarize the response and excitation characteristics of the system with all the sources on as CASE 7 of Table 5.2 in the

former, and with the mean value of all response points under different cases of excitation.

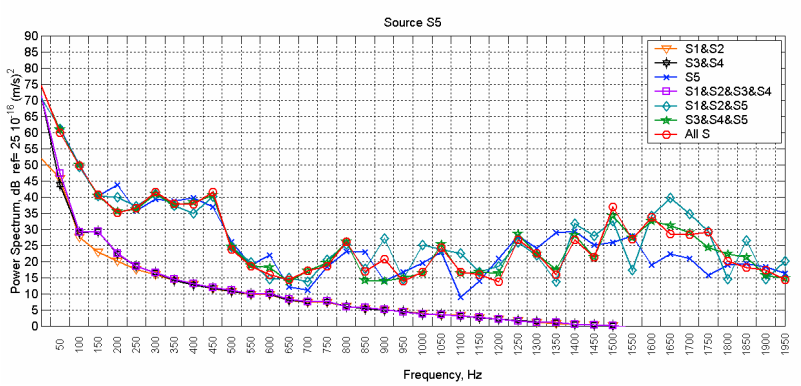

Figure 5.16 Input Spectra for Source 5 at CASES of Table 5.2

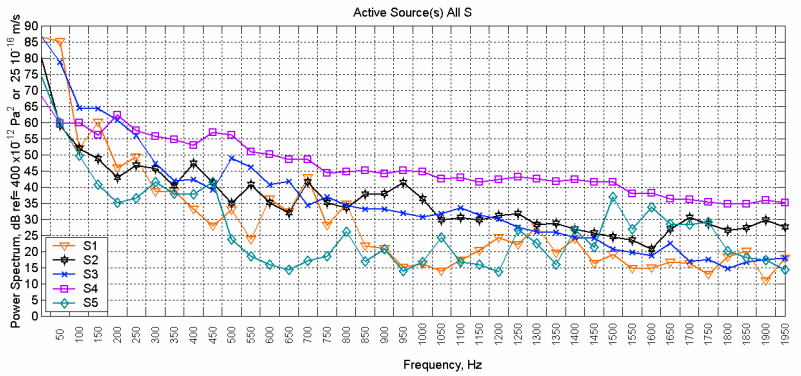

Figure 5.17 Input Spectra for All Sources at CASE 7 of Table 5.2

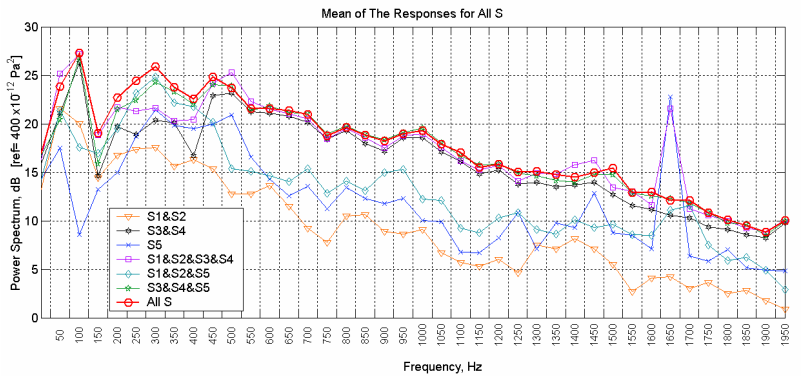

Figure 5.18 Mean Spectra of Responses for all CASES of Table 5.2

Figures 5.19 to 5.25 present the Transfer Functions obtained from the MISO solutions as the result of the analysis conducted in this section. Each figure is dedicated to one receiver point only. The transfer functions for the individual sources are plotted on different axes. For each source, four different CASES, where the related sources are on, are used for the estimations. The frequency range is 0-1000Hz again, and the bandwidth of the spectra is increased to 10Hz after a smoothening operation. Note that, this is the accuracy of the modal analysis in the previous chapter as well.

The results clearly shows that, almost all of the Insertion Loss Dip frequencies and coupled cavity resonance frequencies are observable in these transfer functions. Especially, for air-borne type noise sources, the coupled cavities resonance assume a very important role (150Hz, 350Hz, 500Hz).

For the structure borne type sources of S1 and S3, transfer functions have a clearly identifiable peak at a region 80Hz-100Hz. At these frequencies are Insertion Loss has dip frequencies, and the coupled cavities with rigid walls have no resonance. Hence, these frequencies are related to the acoustical-structural coupling of the internal air volume of the cavity and the enclosing structure.

Another result that fits very well to the predicted behavior is the transfer function related to the air-borne noise at S4 and receiver point at R2. There is a direct air-borne noise path, a so-called acoustic short cut, between these two locations (Figure5.3 and Figure 5.4), hence the contribution due to a transfer path over the enclosure is negligible as compared to this one. As a result, the transfer

function assumes none of the cavity resonance or Insertion Loss dip frequencies (Figure 5.20). Using the same argumentation, the transfer function between the same source point (S4) and receiver point R4 must assume some of the these resonance frequencies. This is the case, as can be observed at Figure 5.21. 80Hz IL dip frequency, 150 Hz coupled cavity resonance frequencies are clearly observable.

Another remark can be given related to the 125Hz where coupled cavity resonance and IL dip frequencies coincide. A resonance at this can be clearly observed between all the receiver points (R1-R7) and the structure borne sound sources (S1, S3, S5). Therefore, these kind of coincident frequencies are very effective when the structure of the enclosure is excited mechanically. The cavity resonance is due to the coupling of large air volumes of internal rooms, and this volume is specified in accordance with the function of the machinery, in this case amount of cold volume to be supplied. Therefore it is difficult alter this kind of bulk volume related frequencies and care must be given to isolate the excitation mechanisms, rather than a retrofitting of the enclosure

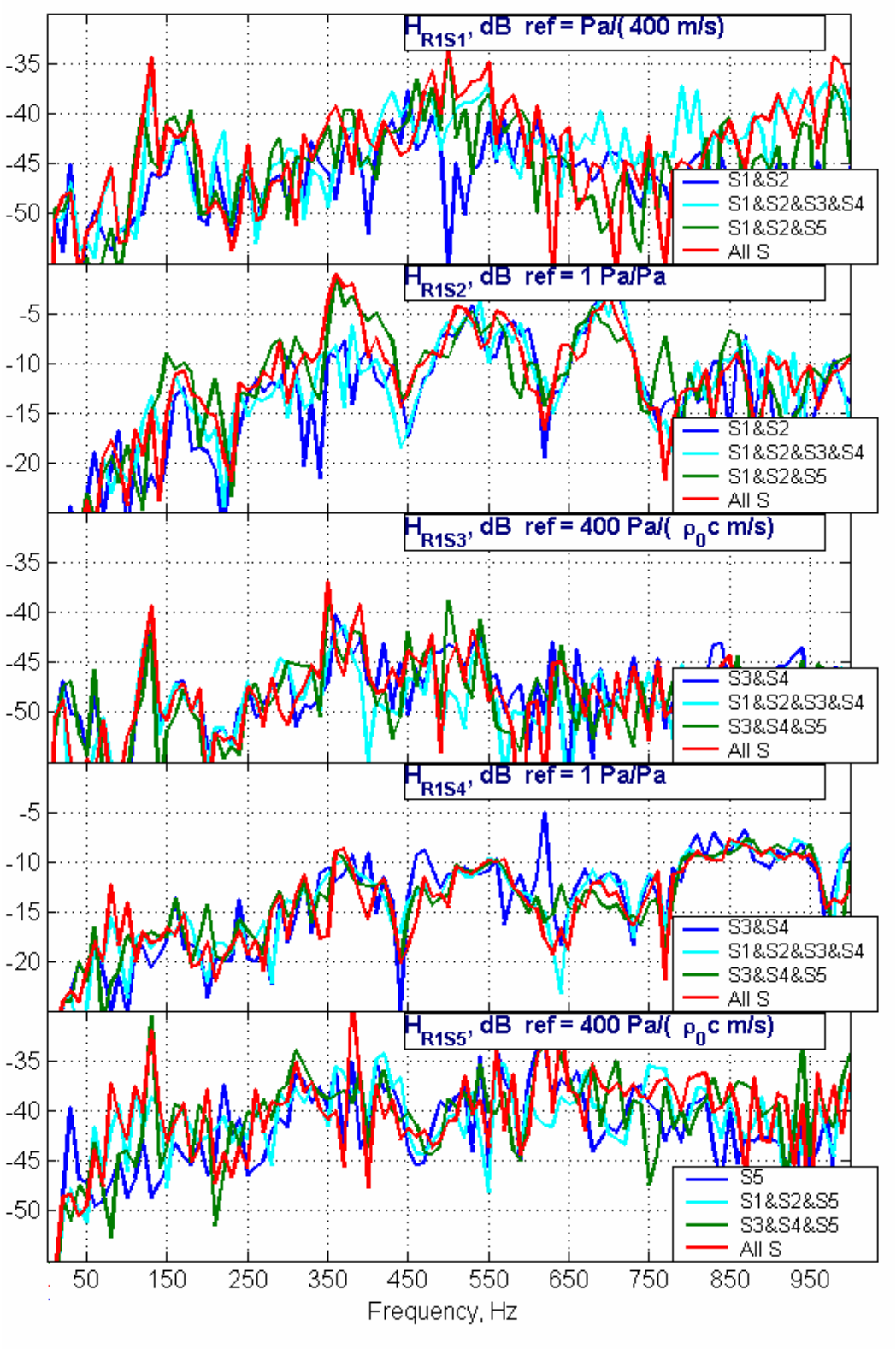

Figure 5.19 Transfer Functions from MISO Solutions For Receiver 1

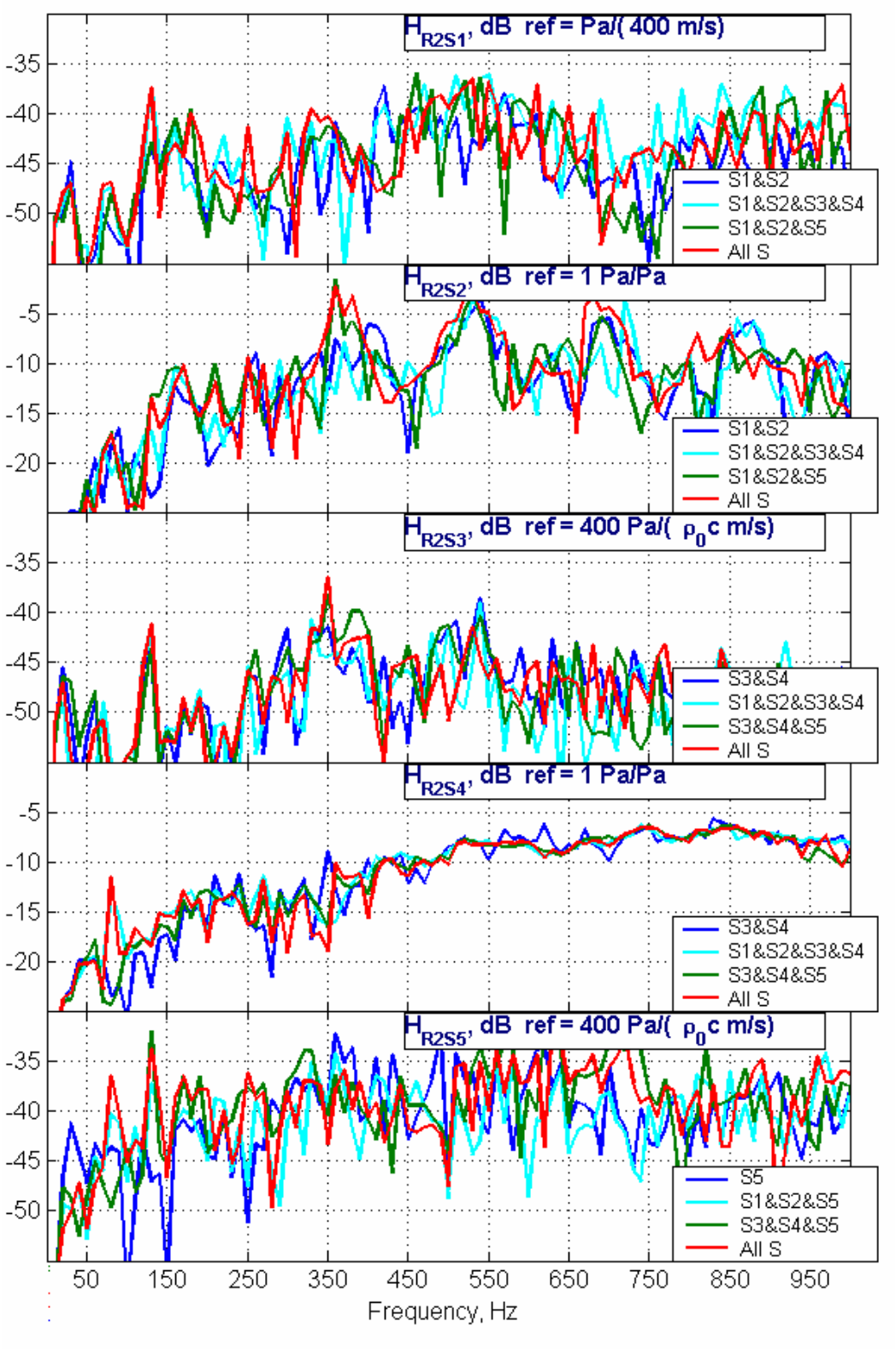

Figure 5.20 Transfer Functions from MISO Solutions For Receiver 2

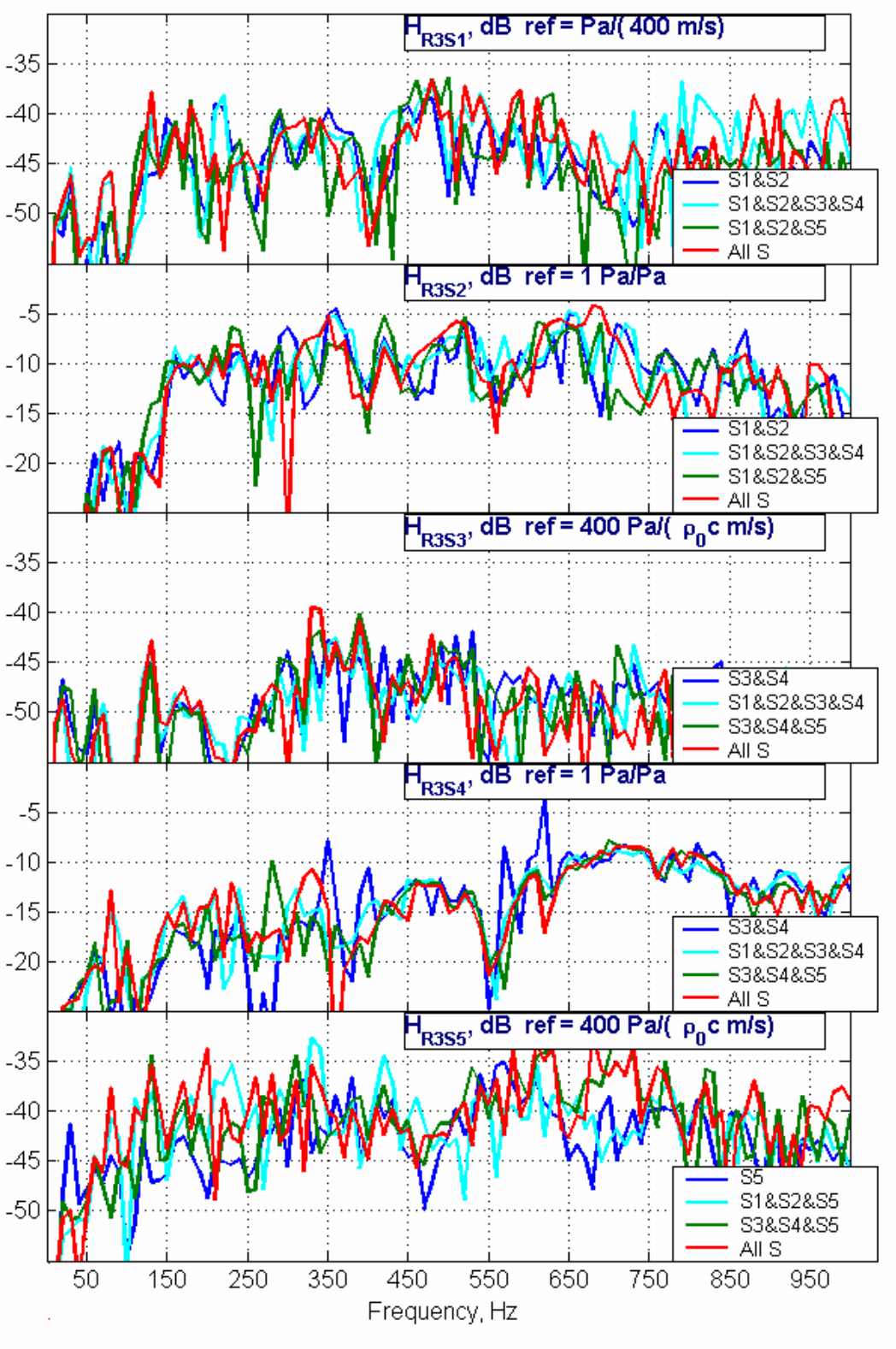

Figure 5.21 Transfer Functions from MISO Solutions For Receiver 3

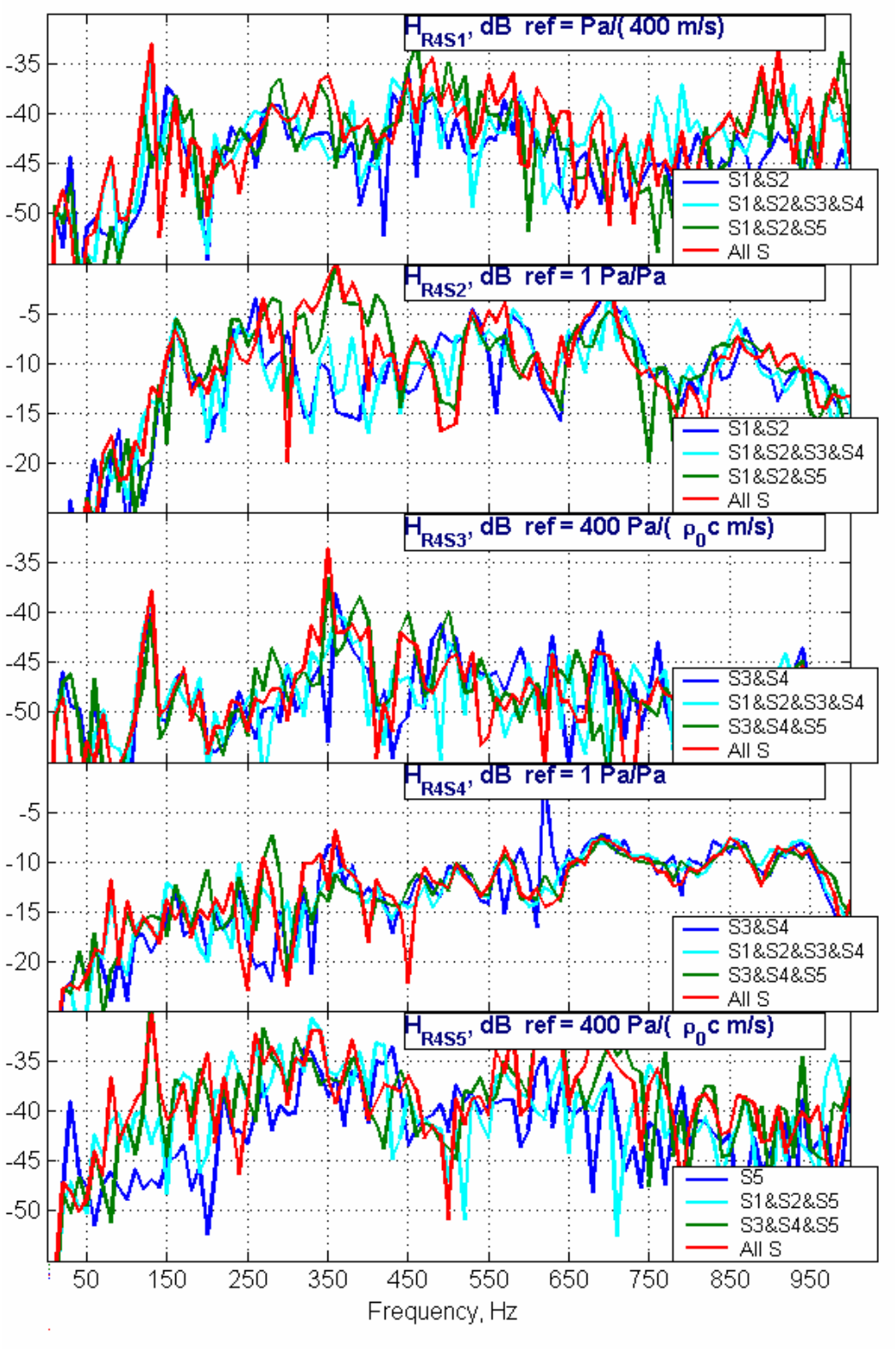

Figure 5.22 Transfer Functions from MISO Solutions For Receiver 4

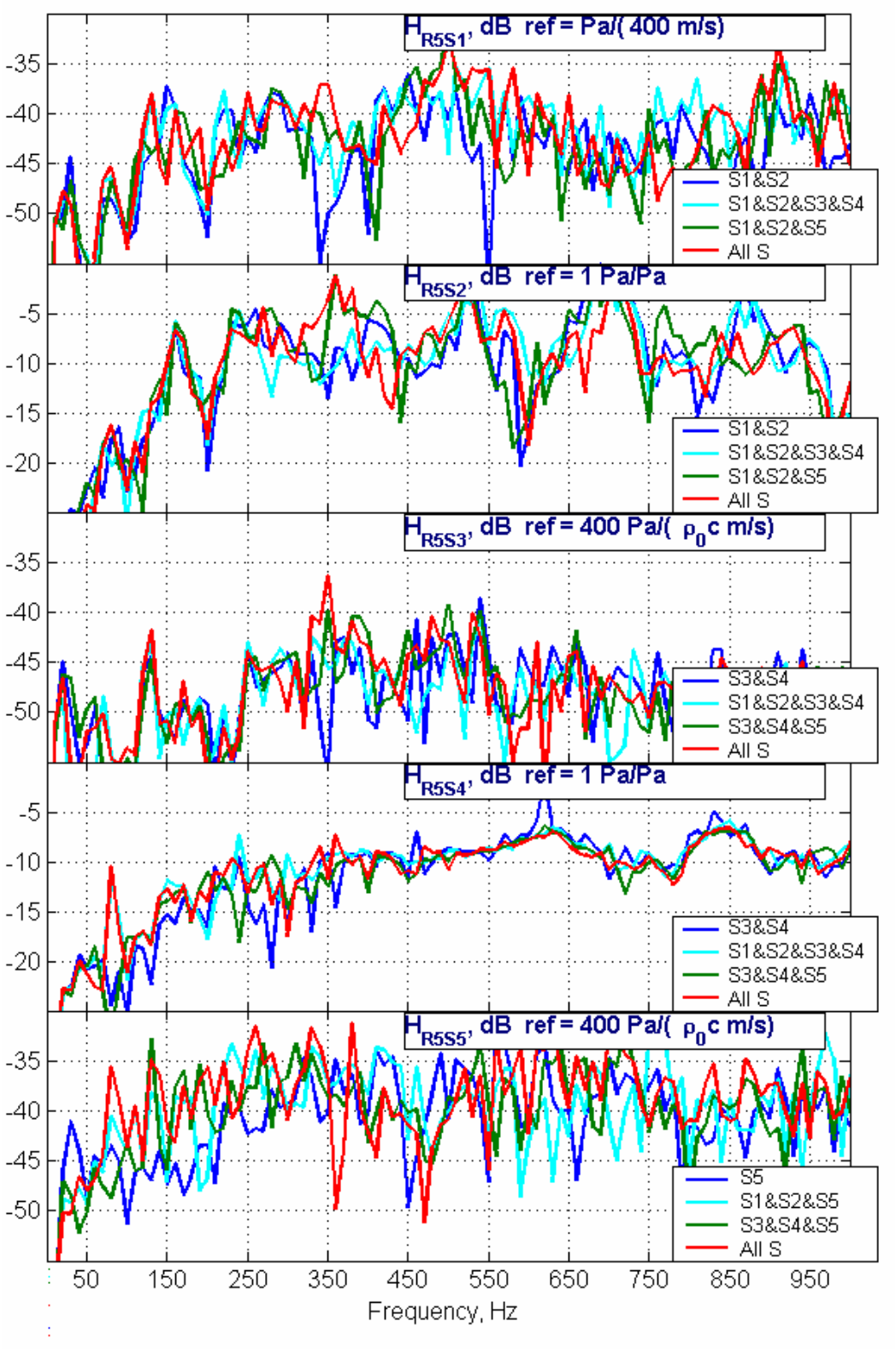

Figure 5.23 Transfer Functions from MISO Solutions For Receiver 5

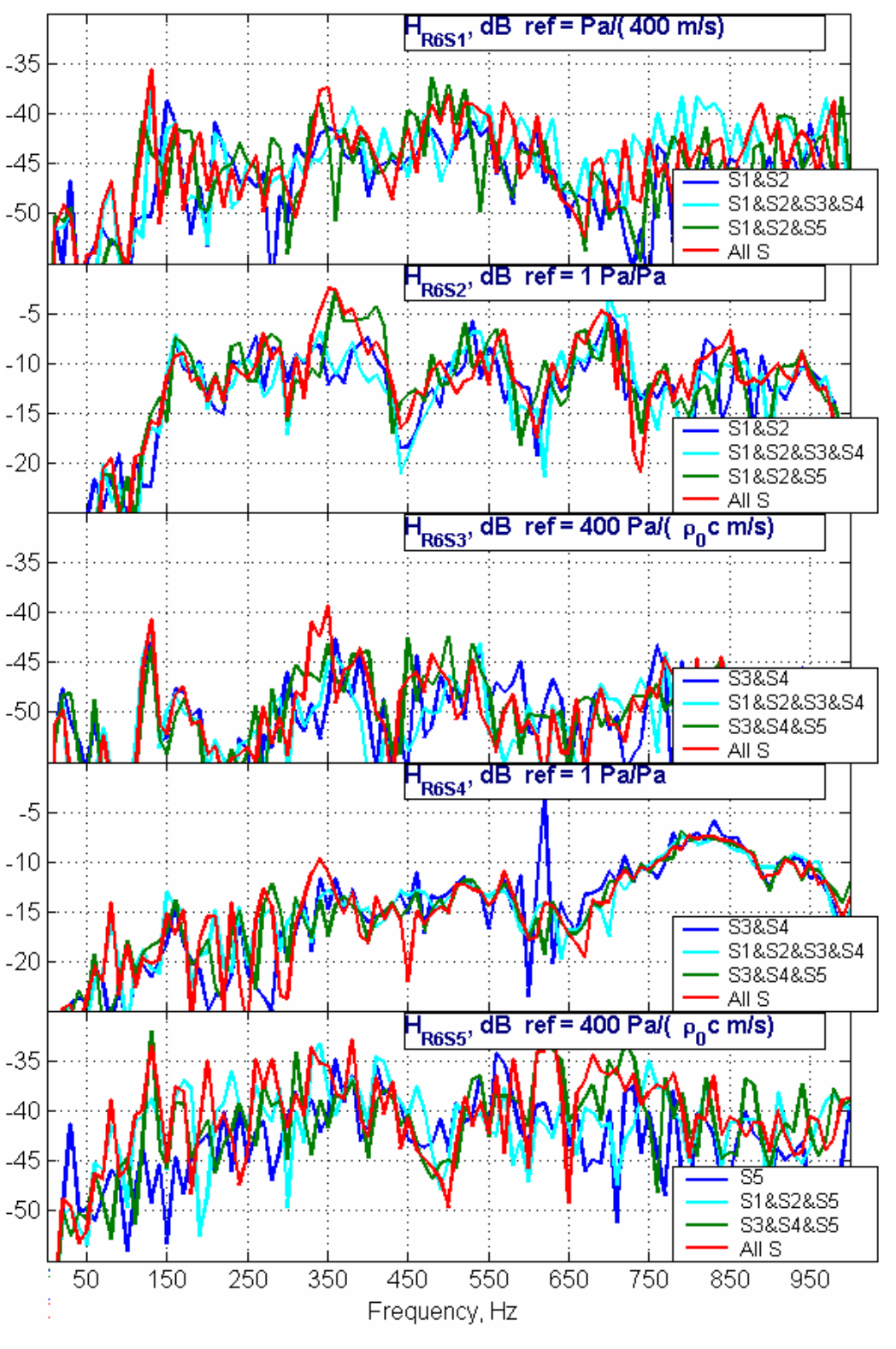

Figure 5.24 Transfer Functions from MISO Solutions For Receiver 6

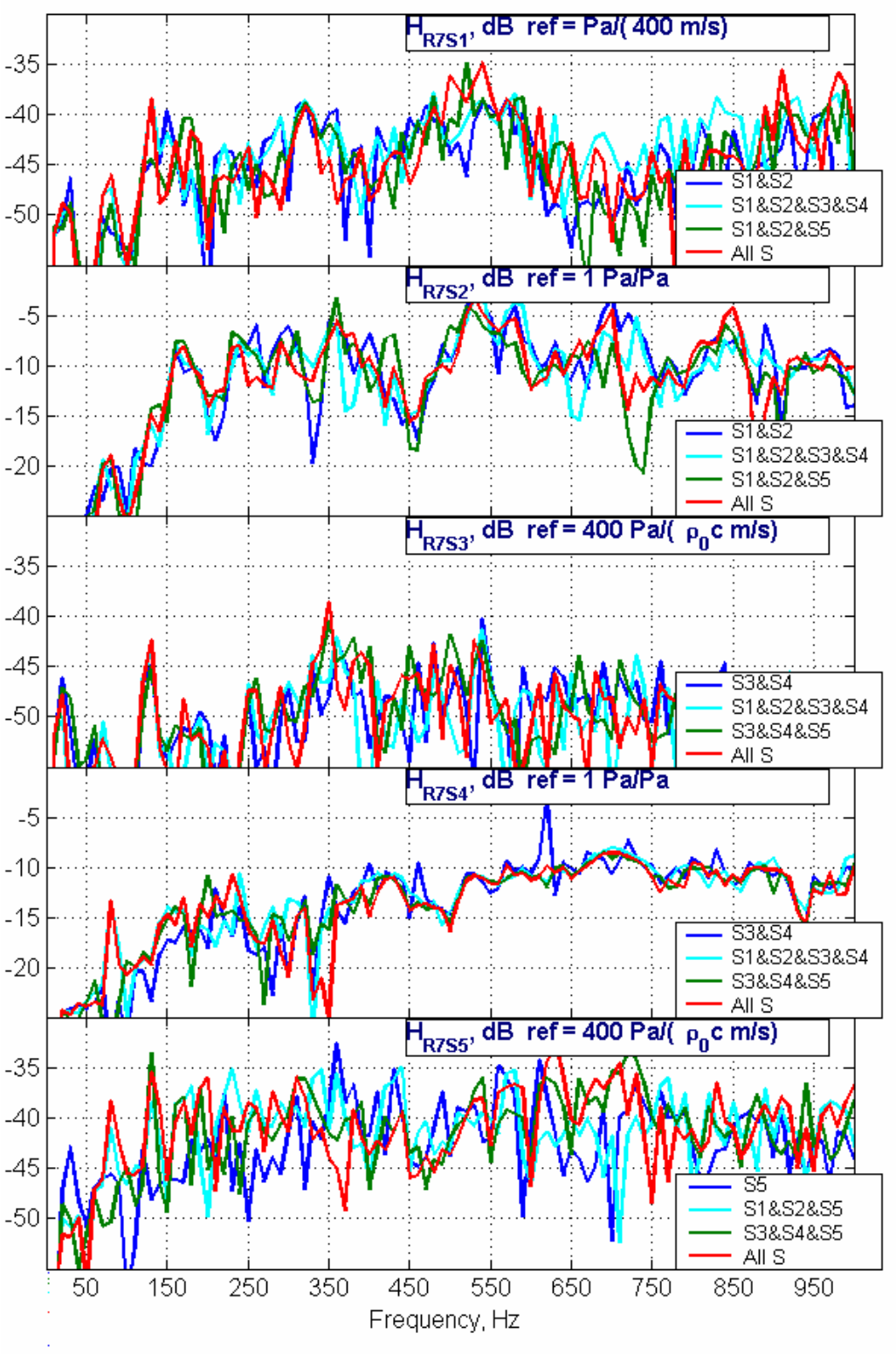

Figure 5.25 Transfer Functions from MISO Solutions For Receiver 7

5.3 Direct Transfer Function Measurements

5.3.1 Theory

The alternative for the MISO analysis of the precious section is the direct measurement of transfer functions by some means of artificial excitation. In most of the cases, this type of excitation is difficult, if not impossible, as the system must be disassembled for a direct measurement to be conducted. A remedy for this is to use the principle of reciprocity, valid for linear time invariant parameter systems, which sometimes offer a useful relationship that transforms a difficult input-output relation into a physically more manageable one.

Some typical cases of reciprocity that may be applied to vibro-acoustical measurements of interest are depicted schematically in Figure 5.26. The upper case is related to reciprocal replacement of a volume source and vibration velocity pick-up, whereas, the lower case is the fundamental case for vibro-acoustical reciprocity as it relates variables of mechanical vibrations, namely, mechanic force F, and velocity u, to variables of acoustics, namely, acoustic pressure p, and volume velocity, U.

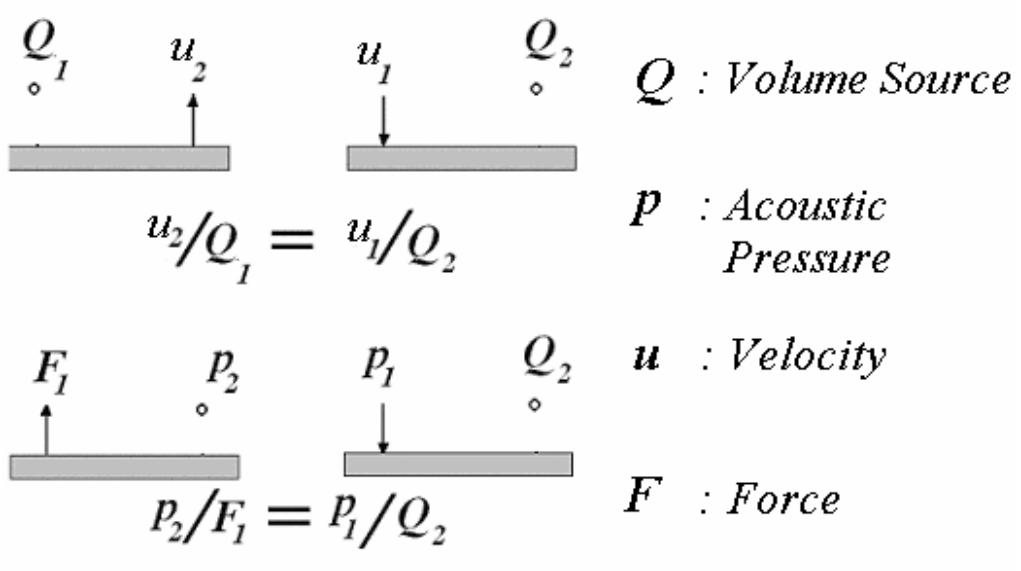

Figure 5.26 Some Reciprocal Relations for Vibro-acoustical Measurements

The application of reciprocity principle is possible with reciprocal transducers of similar type of directivity. The microphones used in this study are omni directional, condenser type microphones with linear system characteristic below 10 kHz. A reciprocal transducer is, then, an omni directional volume flow source that must be linear at the frequency range of interest, which is 0-1000 Hz for this study.

The common practice for the construction of an omni-directional array of sources is the usage of ideal polyhedrons. Among them, dodecahedron is the most suitable one with twelve faces out of regular pentagons. Loudspeakers of similar characteristics are mounted on each separate surface with parallel electrical connections to ensure equal phase behavior of the membranes.

Some constructional details of the omni directional volume source is given in Figure 5.27 and Figure 5.28 shows the source after the construction. The

cabinet is made out of 12mm thick plywood, the loudspeakers are 12cm in diameter and the diameter of the enclosing sphere is 18cm. In the calibration process, the linearity and the directivity of the volume source is checked. For the linearity check, the source is driven by a band-limited white noise (0-6000Hz), and the output of the system as sound power is measured.

Figure 5.27 Constructional Details of the Omni-directional Source

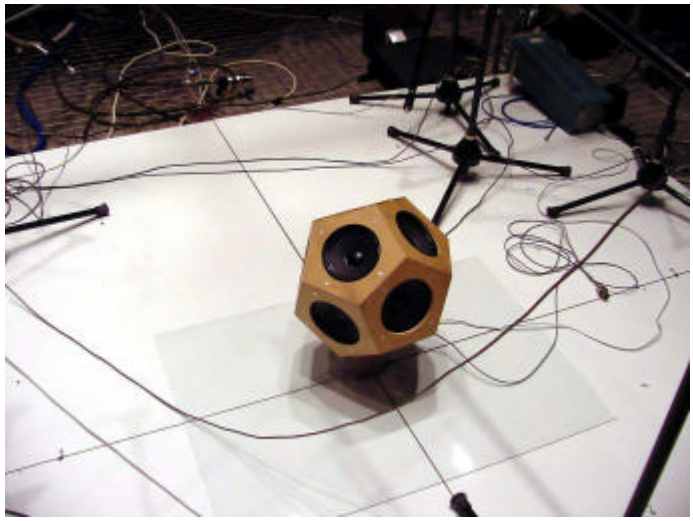

Figure 5.28 Omni-directional Source as Finished

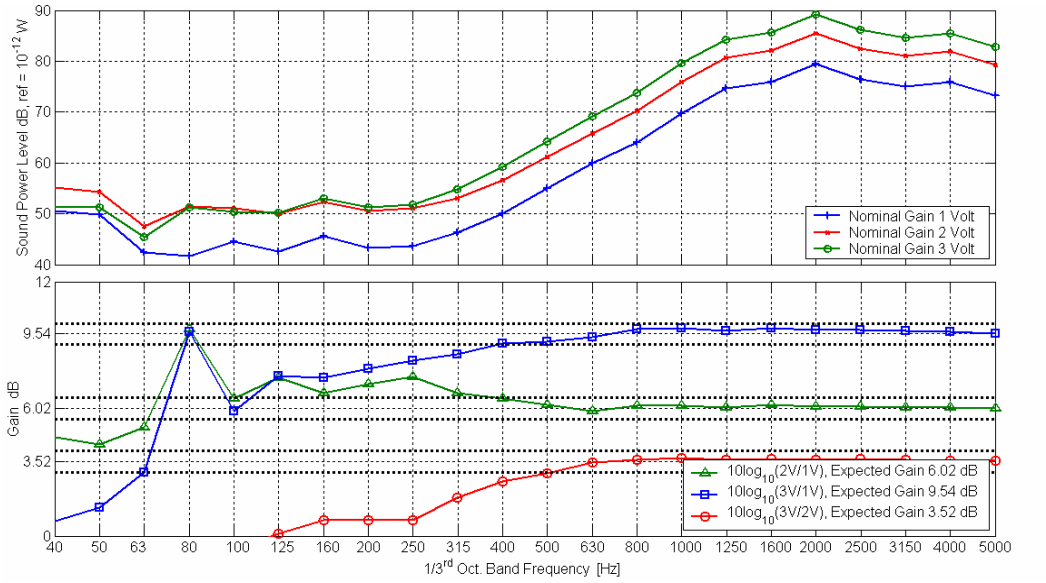

Figure 5.29 Linearity Check for the Omni-directional Source

Three different input levels, namely, 1V, 2V and 3V peak to peak, are applied to the source via an audio amplifier. Resulting sound power levels in 1/3 Octave Band frequency resolution are presented in Figure 5.29. The theoretically expected and measured level differences in dB's are presented at the lower portion of the graph. The ±1 dB bands of error clearly indicate that the linearity of the source is very reasonable at the frequency bands higher than 500Hz, and reasonably well at 250 – 400 Hz bands. However, below the 200 Hz band the linearity is highly distorted. Several factors that may cause this deviancy; enclosure characteristics of the source cavity, diaphragm resonance of the speakers are some of them to be named.

The directivity of the source is checked in a fully anechoic room by means of intensity measurements done at a radius of 1.5 m from the center of the source, which corresponds to the acoustical far field of the source. An enclosing hemi-

spherical surface with 15 degrees of arc segments in θ and φ directions, total 289 segments, is covered by an intensity probe as shown in Figure 5.30.

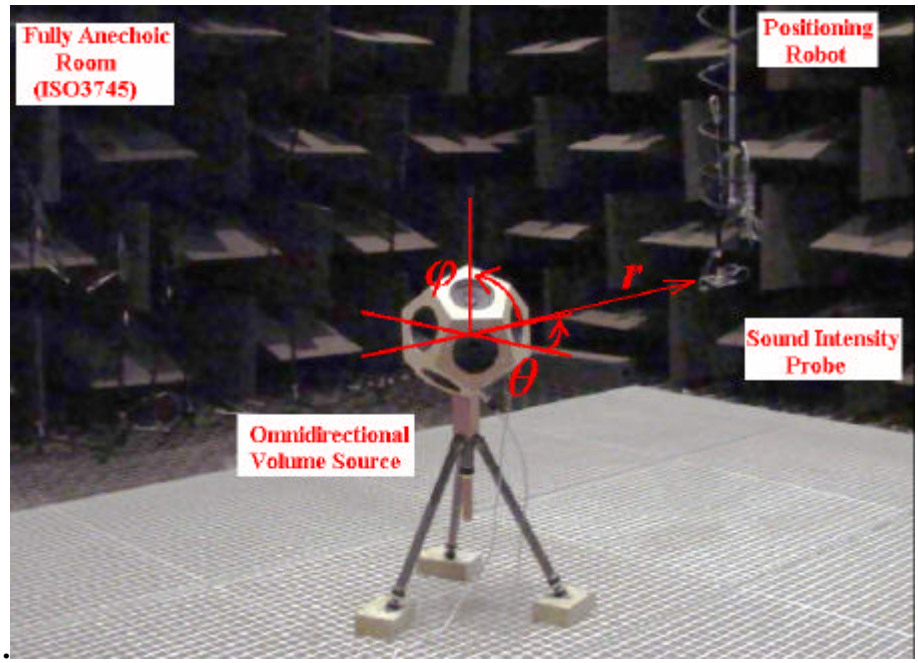

Figure 5.30 Set-up for Directivity Index Measurements

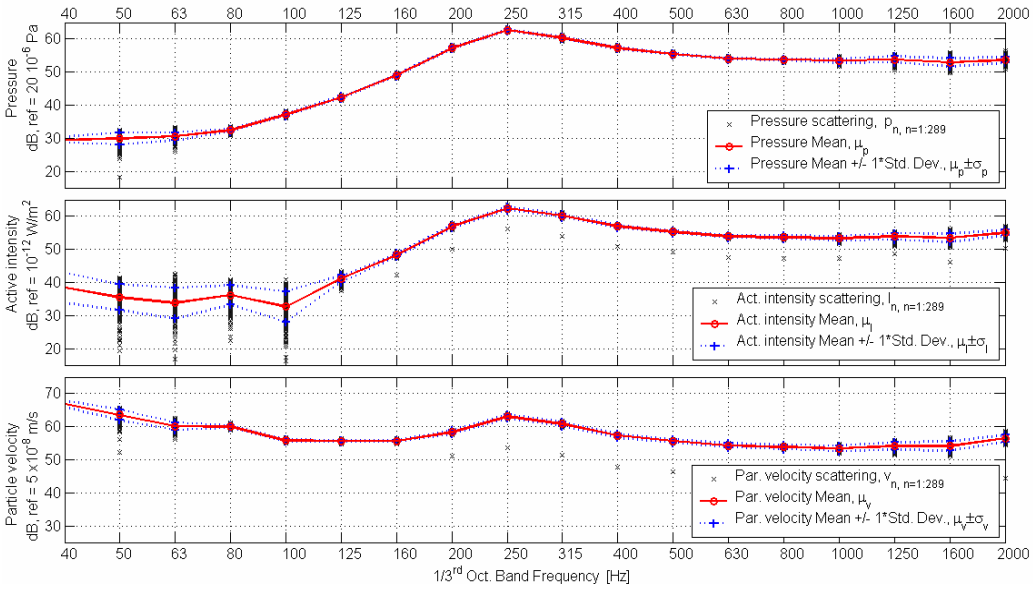

Figure 5.31 Directivity Check for Omni-directional Source

The results for 2V peak to peak, band limited white noise input are given in Figure 5.31. For the parameters checked at the far field, namely, sound pressure, particle velocity and active intensity, the source exhibits excellent directivity characteristics at a frequency range of 250 Hz to 1000 Hz. Outside of this range, the source has still reasonable directivity characteristics, and can be used as an omni-directional transducer by using the calibration charts obtained.

5.3.2 Experimental Set-up

For a reciprocal measurement with an omni-directional source, velocity levels at all possible directions must be measured at the receiving end, which is possible only with a three-dimensional, vector transducer. The problem is solved by using a lightweight, three-dimensional accelerometer. Although, the signals used for source descriptions are still in use, an additional three-dimensional signal is added for the every point of interest to obtain, additional transfer function for path analysis. The location of the enclosure in the measurement environment and the selected path points on the enclosure structure are shown in Figure 5.32 and Figure 5.33, respectively.

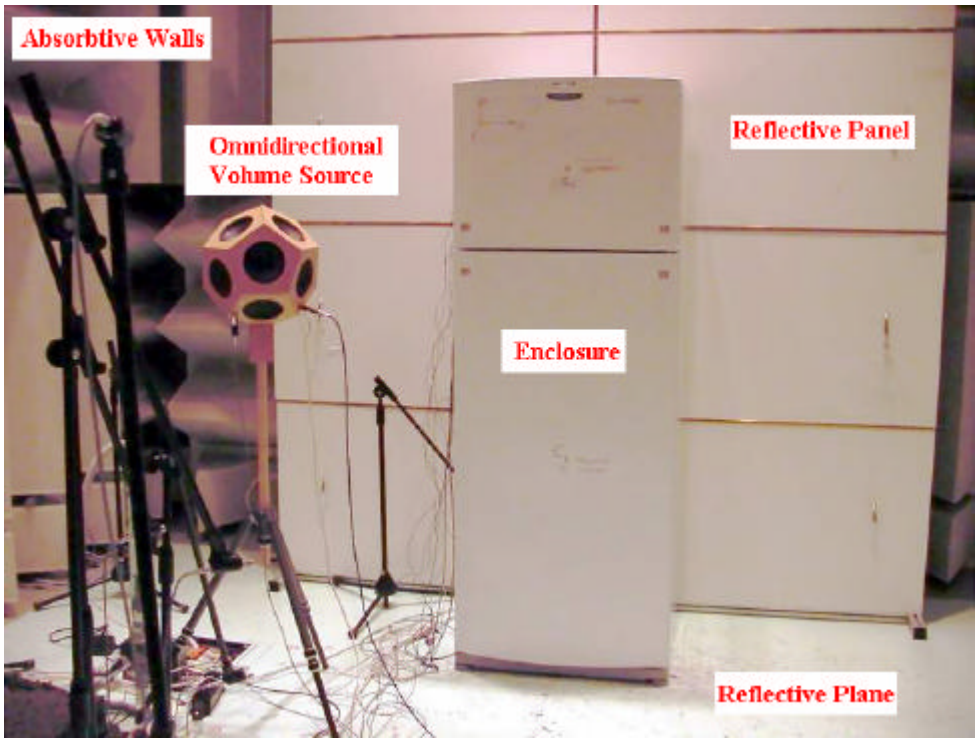

Figure 5.32 Location of the Enclosure in the Measurement Environment

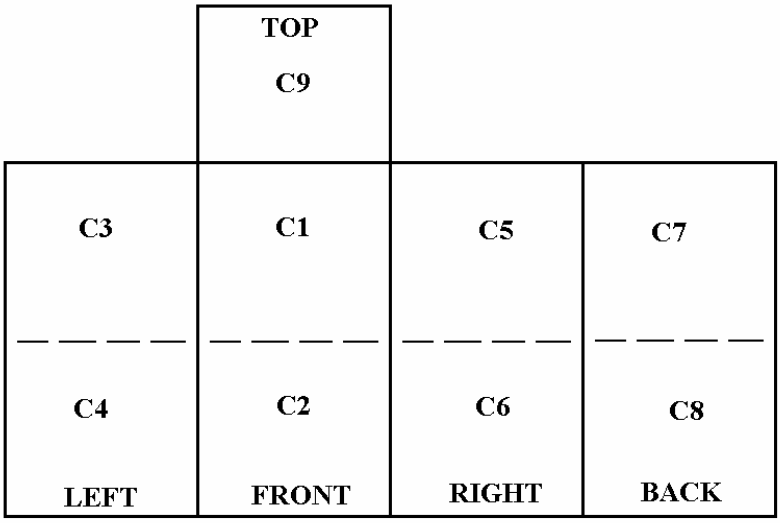

Figure 5.33 Points on the Enclosure Structure used for Path Analysis

At the first step, the three dimensional accelerometer is placed at one of the specified points, then the omni-directional sound source is moved over the points of the seven measurement points. After the end of three source locations,

nine path joint locations are traveled. These path points are chosen on each side of the refrigerator cabinet at the mid points of upper and lower portions. In addition to these eight points (2x4), the ninth point is chosen at the top of the refrigerator.

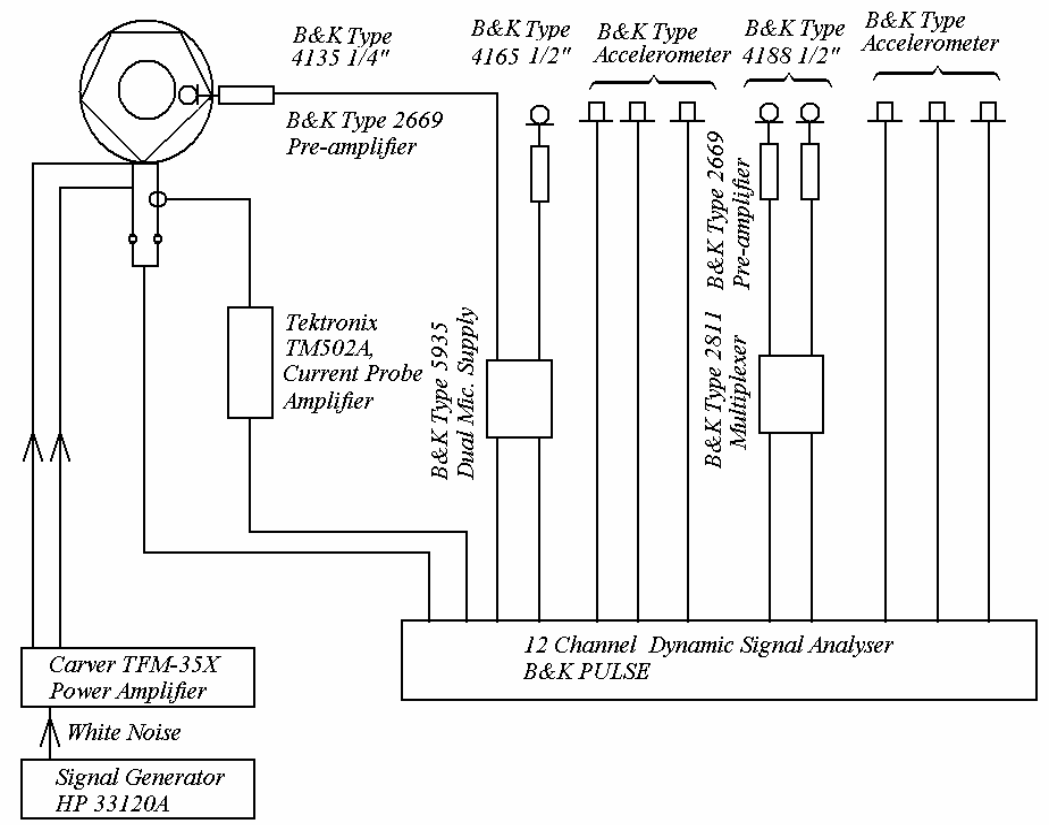

Figure 5.34 Equipment for Direct Transfer Function Measurements

Figure 5.34 depicts the equipment used for measurements. The most important part of these reciprocal measurements is the selection of the correct input signal for the omni-directional source. The source output is characterized by input voltage and input current. Magnitude of the volume source output is calibrated from the sound power level measurements. The phase relationship of these variables is discussed in the previous Chapter.

In addition to these signals, cavity pressure which is proportional to the volume velocity, far field pressure level measured at a point 2 meters away from the source on the opposite side of the structure, that is in both acoustical and hydrodynamic far field are measured. The far field pressure field on the undisturbed side of the environment must be proportional to the volume velocity again. Hence, these two signals are used as additional identifiers for the quality of the measurements and the performance of the volume source.

5.3.3 Results

Comparisons of the measured transfer functions for different input signals are given in Figure5.35 to Figure 5.37. The receiving points are averaged and three typical source-path locations are chosen for the analysis. The current and the voltage as input signals are in very good agreement, in magnitude. The general characteristics of the transfer functions for all signal inputs are in good agreement with each other. The acoustical input signals are damped heavily, and consequently, possible resonance frequencies are overlapped with each other. Hence, the resolution is poor in frequency domain.

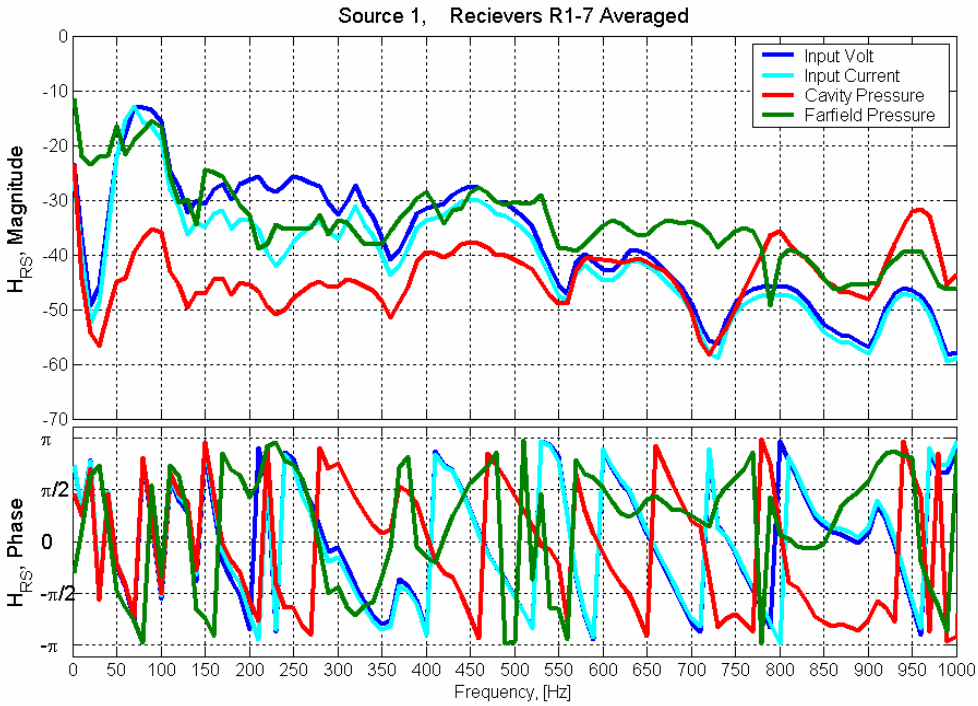

Figure 5.35 Comparison of Input Signals for Transfer Functions at Source 1

Magnitudes of the far field transfer functions, on the other hand, are highly distorted due to the possible reflections at the measurement room. This input signal may be most useful for open field measurements of machinery under in-situ conditions. Cavity pressure as an input signal is not qualified for these kinds of measurements with poor magnitude ands phase characteristics. Never the less, in case there are simple ways for monitoring and calibrating the output signal for electrical input values, it can be safely used for systems with distinct resonance frequency. The analysis in this study is carried for electrical current as input signal, calibrated for magnitude via sound power measurements as explained before.

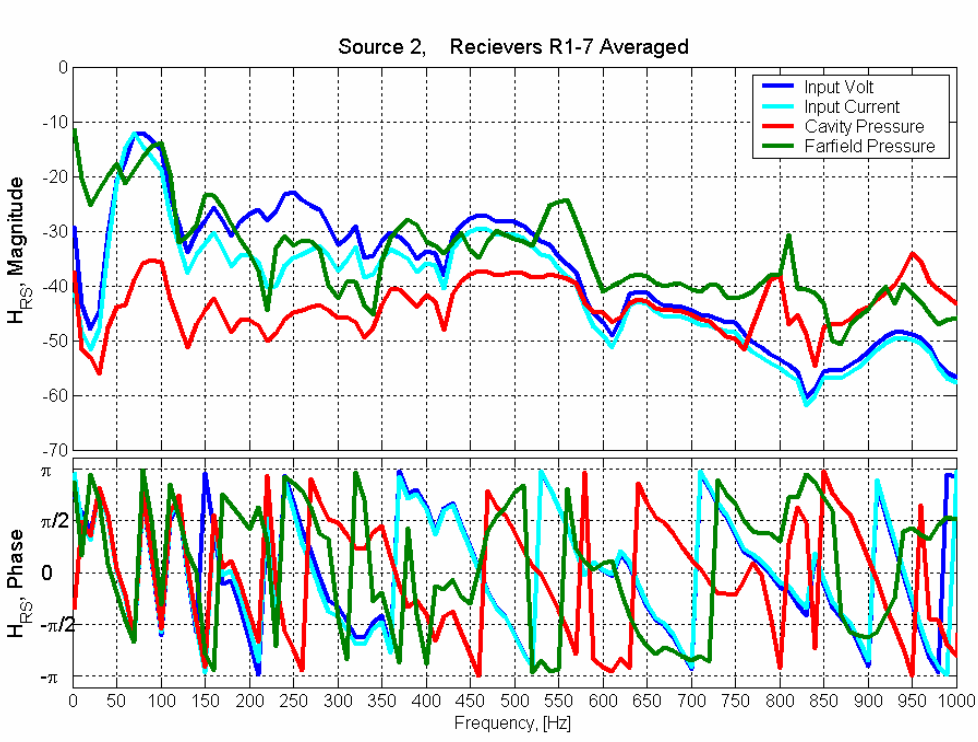

Figure 5.36 Comparison of Input Signals for Transfer Functions at Source 2

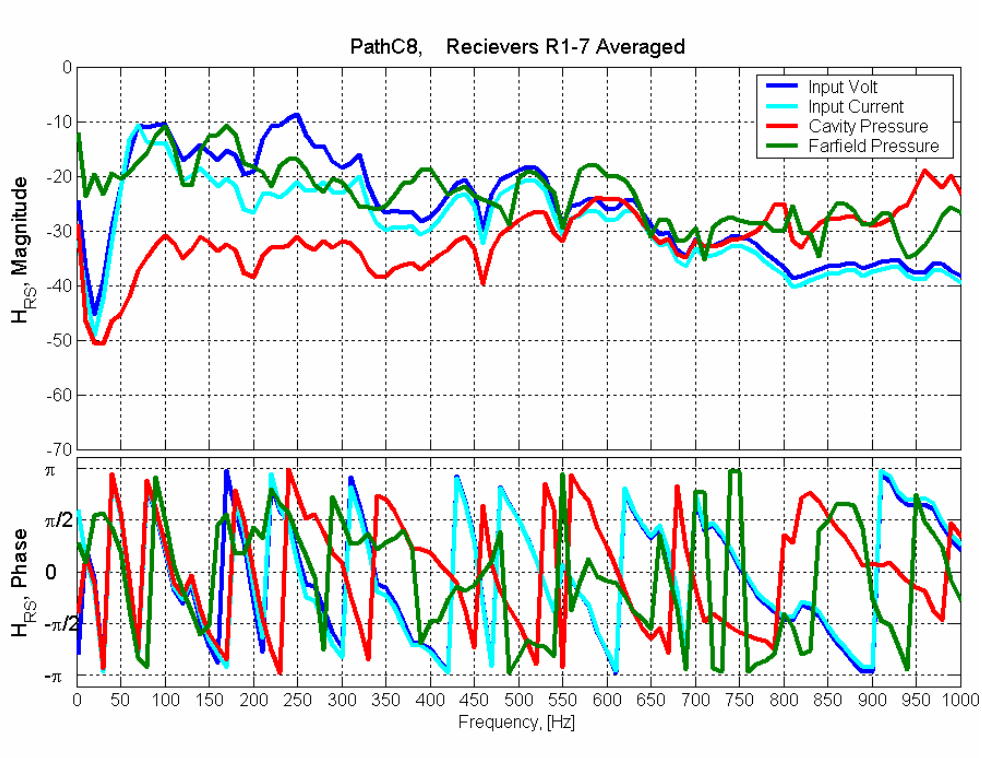

Figure 5.37 Comparison of Input Signals for Transfer Functions at Path C8

The related transfer functions for all the source and path points are presented in Figure 5.38 for the mean of all receiving points. The effect of the enclosure can be observed very clearly from the figure as all the transfer functions related to the external boundary of the enclosure assume higher values than those of source points which are located internally within the structure. Two of the path points, namely, PathC7 and PathC8 have the highest values in magnitude, which is expected from the results of vector sound intensity mappings.

The plots of this sort can be used as the ranking of transfer paths, which is one of the aims of this kind of analysis. Note also that the transfer functions averaged all over the Path points are related to the radiation efficiency of the enclosure, whereas, the average of the paths related to the inside points are related

directly to the Insertion Loss of the enclosure.

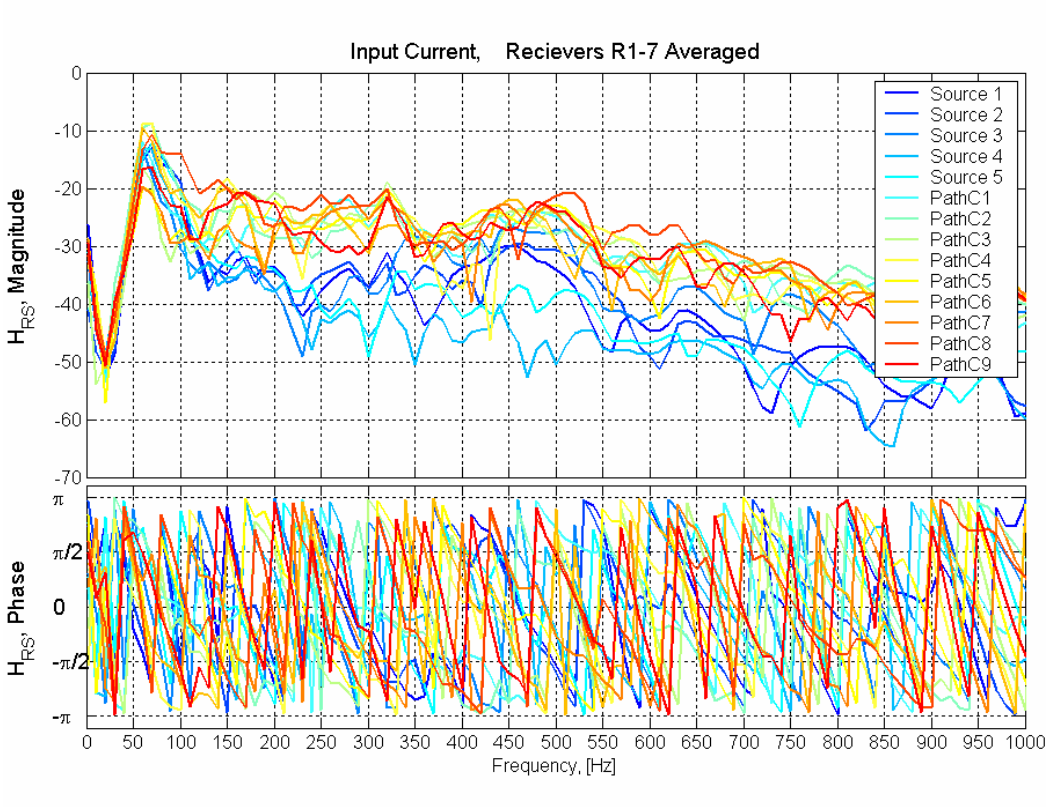

Figure 5.38 Comparison of Mean of Transfer Functions for All Locations

Transfer functions obtained from Multi Input, Signal Output (MISO) solutions are compared with the directly measured ones in Figure 5.39 and Figure 5.40 for two distinct locations related to a structure borne and an air-borne source paths, with S3 and S4, respectively. It should be mentioned that the physical quantities related to these transfer functions are not similar. The direct measurement transfer functions have a unit of $1/m^2$ and the MISO solution has a unit of Ns/m^3 for structure borne, and unity (Pa/Pa) for air-borne type sources. Hence, the resonance characteristics are under comparison, but not the quantitatively described magnitudes.

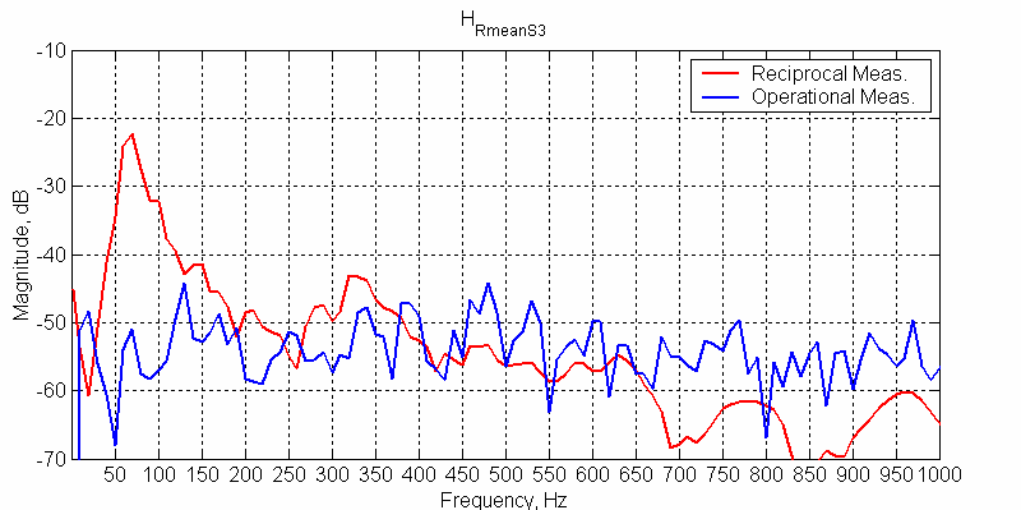

Figure 5.39 Comparison of Transfer Functions Obtained from MISO and Direct Measurements, Receiver Averaged, Source3

Insertion Loss dips at 75 Hz and 90 Hz observed in the related section of Chapter 4 can be clearly observed at both of the transfer functions. The coupled modal frequency at 350 Hz is also such a frequency. Apart from these kinds of frequencies where distinct Insertion Loss and cavity resonance are not present, the direct transfer functions are too damped compared to the MISO solutions. One basic reason of this is the improper signal to noise ratios involved in the measurements. The structure of the enclosure is too damped and stiff to be excited reciprocally by a volume source transducer. Hence, too high levels of input signals compared to the very low levels of output signals increases the dynamic range requirement higher than the values supplied by the available signal analyzers, which are 96 dB at most. Hence, the levels corresponding to the resonance frequencies can be resolved, but the remaining frequencies with lower levels are missed.

One remedy for this drawback is the conduct of measurements in narrow

bands and in bandwidths properly adjusted in accordance with the expected levels of resonance. This is a very tedious experimental procedure, and can only be conducted after a rough analysis as presented in this study.

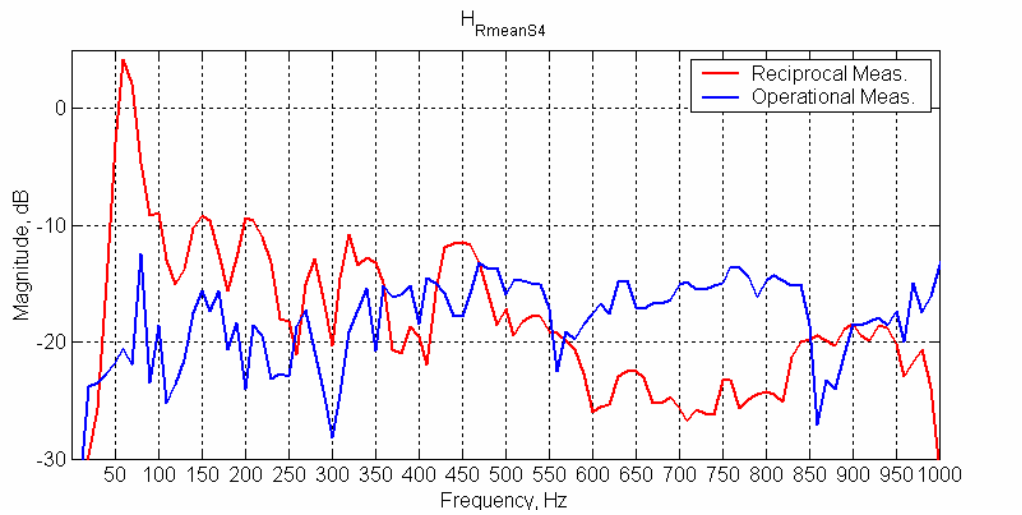

Figure 5.40 Comparison of Transfer Functions for the Mean of All Receiving Points at All Locations, Receiver Averaged, Source4

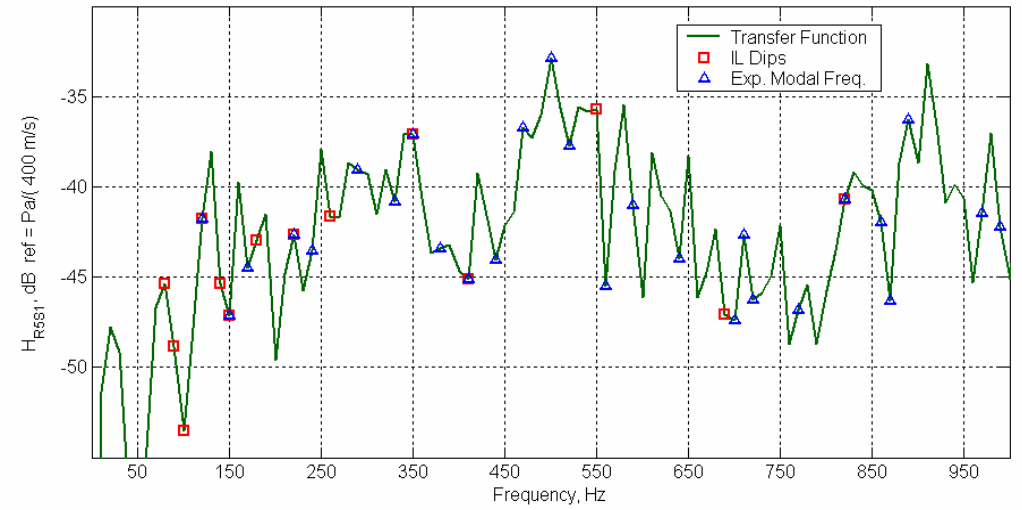

Figure 5.41 Comparison of Transfer Function between Source 1 and Receiving Point 5 and Experimentally Determined Modal and IL Frequencies

Finally, noise transfer paths obtained from MIMO analysis are compared with the IL dip frequencies and cavity resonance frequencies as obtained in Chapter 4, for all the source combinations with a receiving point at microphone number 5. Figure 5.41 presents this comparison for Source 1, which characterizes a structure borne type source. The effect of cavity resonance can be clearly observed at 500 Hz by assuming the largest gain of the noise transfer function. This behavior can be explained by considering that this resonance frequency is related to the upper section of the enclosure and Source 1 is located in this part.

On the other hand, similar comparison for Source 2, as depicted in Figure 5.42, reveals a distinct peak around 540 Hz and a broad band maximum at 700-720 Hz range exist, where all these frequency bands are related to the coupled acoustical resonance of the enclosure. Source 2 is an airborne type noise source and this kind of behavior is quite expectable at these coupling frequencies.

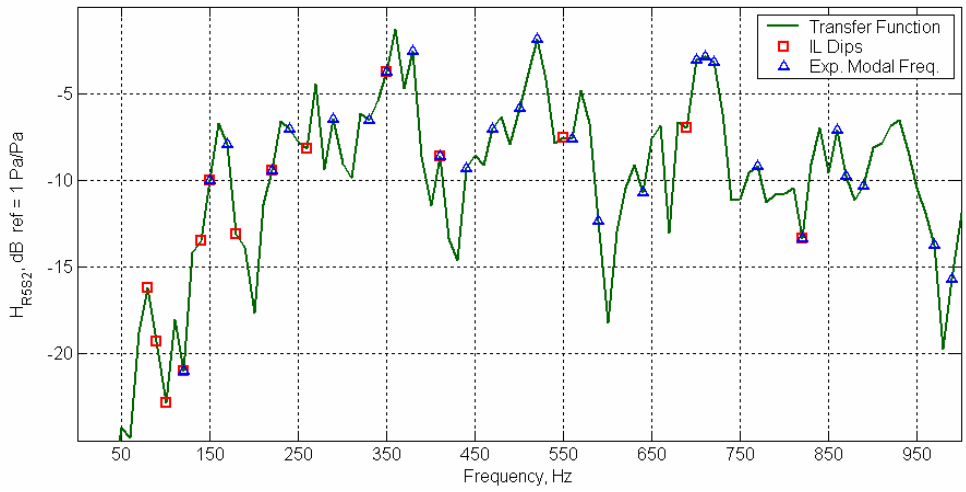

Figure 5.42 Comparison of Transfer Function between Source 2 and Receiving Point 5 and Experimentally Determined Modal and IL Frequencies

The maximum of the noise transfer function for Source 3, which is a structure borne type source, is observed at 350 Hz as shown in Figure 5.43. This is also an unexpected result from the findings of Chapter 4 due to the fact that, at this frequency value one of the coupled cavity resonance and IL dip frequencies are coincident. Hence, for this enclosure, isolation of the structure borne sources at this location is of prime importance for noise control purposes.

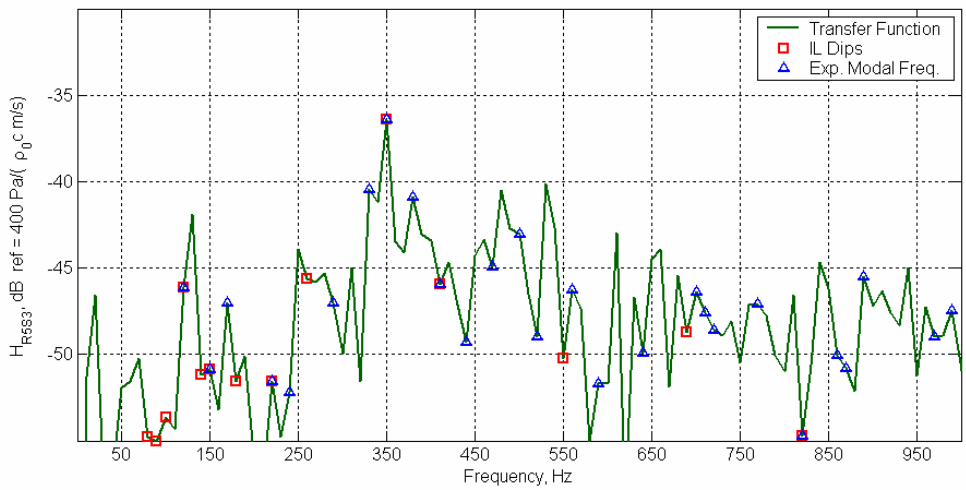

Figure 5.43 Comparison of Transfer Function between Source 3 and Receiving Point 5 and Experimentally Determined Modal and IL Frequencies

The case of Source 4 as shown in Figure 5.44 can be explained by considering the fact that there is a direct air-borne transmission path between an air –borne type source and the receiving point, hence, gain of the transfer function is flat and its level governed by the length of this path. However, at 80 Hz, an isolated peak can be observed which coincides with an IL dip frequency. Therefore, the enclosure is still effective on this path and improvement on the transmitted noise level is possible by means of possible retro-fittings applied to

the enclosure structure.

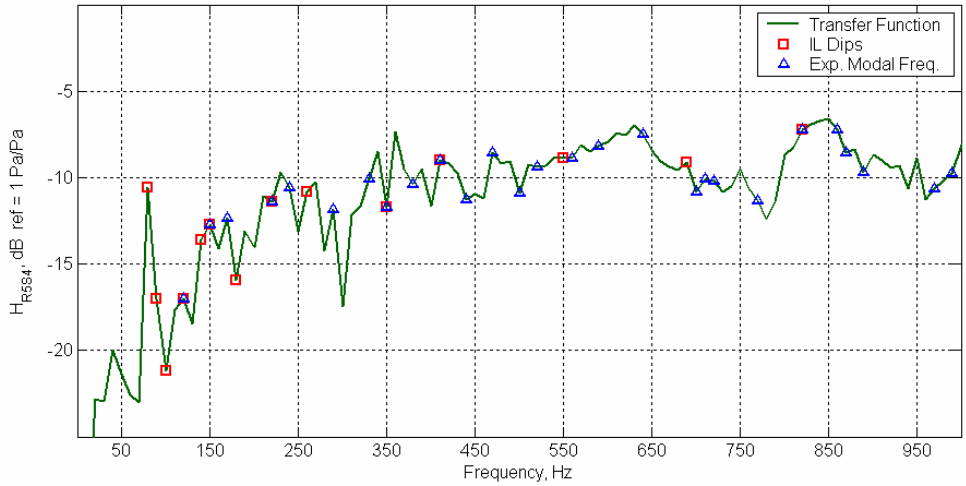

Figure 5.44 Comparison of Transfer Function between Source 4 and Receiving Point 5 and Experimentally Determined Modal and IL Frequencies

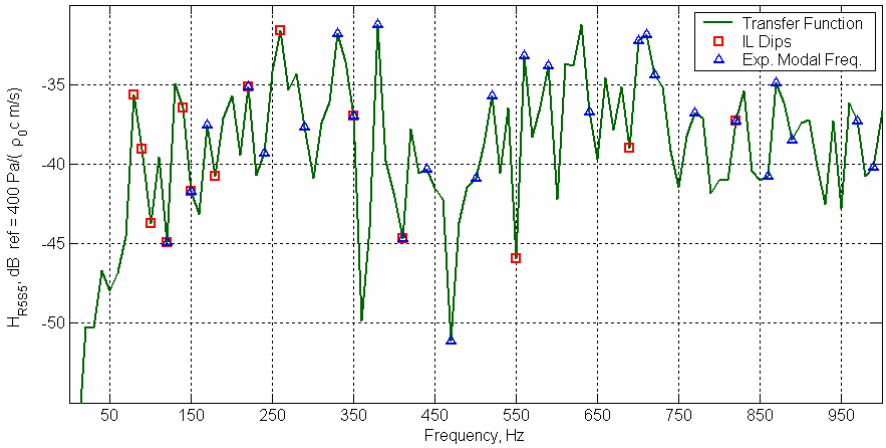

Figure 5.45 Comparison of Transfer Function between Source 5 and Receiving Point 5 and Experimentally Determined Modal and IL Frequencies

The case of Source 5 as shown in Figure 5.45, is different from the previous noise transmission due to a strong structural coupling to the enclosure body. Hence, the structural resonance frequencies, as identified IL dip frequencies at 80 Hz, 220 Hz and 260 Hz are effective on the noise transfer function.

Moreover, at cavity resonance frequencies 340 Hz and 380 Hz, which are also related to the coupled acoustical behavior of the cavity, the noise transfer functions again assume maxima. It can be concluded that for this transfer path, both of the acoustical and structural coupling of the mechanisms are effective.

CHAPTER 6

SUMMARY OF RESULTS AND CONCLUSIONS

6.1 Summary of Results

In this research, a methodology has been developed for the identification of noise transmission paths of structurally and acoustically coupled structures. Experimental methodologies are integrated into a coherent structure of measurements that can be applied to enclosure structures of practical importance operating at frequency ranges below 1000 Hz. There is no limitation on the geometry of the structures if an environmental background with low noise levels, are used during the measurements.

The results of most significance and which can be extended to similar type of structures are briefly summarized below. These points when applied to an existing enclosure as a retrofitting practice would help reducing the annoyance level of the machine, which is the goal of these kinds of studies.

1. The lowest resonance frequency of the enclosure is at 13Hz, which is obtained form finite element analysis and predicted from the lumped

parameter model as resonator type behavior where the lower compartment acts like an acoustical compliance and the coupling neck acts like an acoustical inertance. However, this frequency is well below the audio frequency band (16-20 Hz at lower bound), therefore, can be omitted for noise control purposes. Nevertheless, it is clear that a slight increase in the inertance of the coupling neck, or a decrease in the compliance of the lower compartment, can easily shift this frequency up to the audible region. This can be possible by lowering the volume of the lower compartments at one hand, and increasing the length or decreasing the effective cross-sectional area of the coupling neck on the other hand.

2. Another frequency that deserves attention is 125Hz, identified very clearly in finite element analysis, which is predicted with a slightly lower value as the tubular resonance frequency (organ pipe tone) of the coupling neck. This frequency is very precisely identified by the experimental modal analysis, as well. On the other hand, this frequency of resonance assumes its crucial importance due to the IL curve as a dip frequency. In other words, the IL dip at 122Hz is due to the cavity resonance of the enclosure, due to the isolated coupling neck resonance. Alterations of this volume without destroying its primary function as part of machinery can shift this frequency to a desired value.

3. The resonance of the cavity due to the modal behavior of the lower compartment at 145Hz is identified experimentally, as well. Although, the IL curve has no distinct dip frequencies at this frequency, the dip

frequencies at 137Hz and 154Hz suggest some structural coupling mechanism that can be related to this resonance behavior.

4. At 345 Hz, the enclosure has again an IL dip. At 349Hz, the finite element analysis identifies a coupled mode, and the corresponding mode shape clearly indicates the effect of coupling neck. The experimental modal analysis identifies this frequency as modal resonance frequency at 350Hz with ±5Hz accuracy.

5. Similarly, at modal resonance frequencies 404Hz, 412Hz, 680Hz and 815Hz, IL dip frequencies can easily be identified with the cavity resonance of the enclosure.

6. However, a complete description of the performance of an enclosure can be estimated when it is excited by means of a source distribution, as close as possible to its operating conditions. Moreover, the resulting noise transmission paths may assume some practical importance if they are related to some receiving points where optimization, or as in many cases minimization of noise is required.

7. The current and the voltage as input signals are in very good agreement, in magnitude. The general characteristics of the transfer functions for all signal inputs are in agreement with each other. The acoustical input signals are damped heavily, consequently, possible resonance frequencies are overlapped with each other. Hence, the resolution is poor in frequency domain. The analysis in this study is carried for electrical current as input

signal, calibrated for magnitude via sound power measurements as explained before.

8. Magnitudes of the far field transfer functions, on the other hand, are highly distorted due to the possible reflections at the measurement room. This input signal may be most useful for open field measurements of machinery under in-situ conditions. Cavity pressure as an input signal is not qualified for these kinds of measurements with poor magnitude ands phase characteristics. Never the less, in case there are simple ways for monitoring and calibrating the output signal for electrical input values, it can be safely used for systems with distinct resonance frequency.

9. The effect of the enclosure are observed very clearly as all the transfer functions related to the external boundary of the enclosure assume higher values than those of source points which are located at some internal points of the structure. Two of the path points, namely, PathC7 and PathC8 have the highest value in magnitude, which is expected from the results of vector sound intensity mappings. These type of information can be used for the ranking of transfer paths, which is one of the aims of this kind of analysis. Moreover, the transfer functions averaged all over the path points are related to the radiation efficiency of the enclosure, whereas, the average of the paths related to the inside points are related directly to the Insertion Loss of the enclosure.

10. Transfer functions obtained from (MIMO) solutions are compared with the

directly measured ones. In this study, only the resonance characteristics are compared, but not the quantitatively described magnitudes.

11. Insertion Loss dips at 75 Hz and 90 Hz observed in the related section of Chapter 4 can be clearly observed at both of the transfer functions. The coupled modal frequency at 350 Hz is also such a frequency. Apart from these kinds of frequencies where distinct Insertion Loss and cavity resonance are not present, the direct transfer functions are too damped compared to the MISO solutions. In addition to this drawback, signal to noise ratios are too low for direct measurements.

12. These kinds of drawbacks can be handled by using narrow bands measurements with properly adjusted bandwidths in accordance with the expected levels of resonance, whereas, a rough analysis as presented in this study gives the necessary preliminary information.

6.2 Conclusions

Acoustical response of acoustically and structurally coupled enclosed volumes has been investigated in this study. A novel experimental acoustical modal analysis technique has been developed for this purpose, which helps to verify and qualify solutions obtained from Finite Element Method applications. The primary contribution of this study to the field of experimental acoustical modal analysis has been the development of acoustical exciter that can work for small cavities with irregular geometries. Use of electro-acoustical reciprocity for

input signal definition is another novelty of this application.

The transmission of sound through the structure, on the other hand, is investigated by means of near field sound intensity mapping techniques where excitation of the acoustical cavities have been accomplished by means of practical volume sources developed.

In this study, the experimental and numerical modal analysis techniques are combined with near field sound intensity techniques have been successfully combined for the investigation of acoustical-structural coupling of enclosures which have applications in almost all of the machinery structures. This study, as a hybrid methodology using modal decomposition and energy flow methods, is a unique contribution to noise transmission path identification technologies.

Excitation due to an arbitrary distribution of noise sources has also been investigated as a multi input, multi output system problem, where the obtained transfer functions between inputs and outputs have been used to qualify the mechanisms of propagation, transmission and radiation of sound by enclosures. The methodology has been confirmed by direct measurements exploiting the principle of vibro-acoustical reciprocity. The calibration and input signal definitions of the omni-directional volume source constructed for this purpose is another contribution of this study, where the findings can be used in various applications on transfer path analysis.

For the structure under investigation, which is a domestic type refrigerator, possible transmission paths have been identified in accordance with the design

engineering requirements aimed to reduce the noise level of machinery. However, application of these methodologies to this present structure is a unique contribution to the noise abetment studies on domestic type electrical home appliances.

The methodologies developed in this study constitute a combined research tool for noise path identification, which is novel, unique and versatile for a broad field of noise control engineering applications.

REFERENCES

1. Beranek, L. L., I. L. Ver (editors), Noise and Vibration Control Engineering, John Wiley & Sons, New York, 1992.

2. Pierce, A. D., Acoustics, Acoustical Society of America, New York, 1991.

3. Cremer, L., M. Heckl, Structure-Borne Sound, 2nd edition, Springer-Verlag, New York, 1987.

4. Fahy, F., Sound and Structural Vibration, Academic Press Limited, London, 1998.

5. Sas, P., Advanced Techniques in Applied and Numerical Acoustics, Proceedings ISAAC7, Leuven, 1996.

6. Beranek, L. L., Acoustics, Acoustical Society of America, New York, 1984.

7. Singh, R., M. Schary, 1978, Journal of The Acoustical Society of America 64(4), 995-1003, Acoustic impedance measurement using sine sweep excitation and known volume velocity technique.

8. Kung, C. H., R. Singh, 1985, Journal of The Acoustical Society of America 77(2), 731-738, Experimental modal analysis technique for three-dimensional acoustics cavities.

9. Nieter, JN. J., R. Singh, 1982 Journal of The Acoustical Society of America 72(2), 319-326. Acoustic Modal Analysis Technique

10. Byrne, K. P., 1985, Journal of The Acoustical Society of America 77(2), 739-746, The use of acoustic pressure measurements to determine the

particle motions associated with the low order acoustic modes in enclosures.

11. Salava, T, 1974, J. Audio Eng. Soc., 22(3), 146-153. Sources of constant volume velocity and their use for acoustic measurements.

12. Anthony, D. K., S. J. Elliott, 1991, J. Audio Eng. Soc., 39(5), 355-366. A comparison of three methods of measuring the volume velocity of an acoustic source.

13. Lee, J.S., J.-G. Ih, 1995, Journal of Sound and Vibration, 182(4), 505-522. On the method for estimating the volume velocity of an acoustic source in a chamber.

14. Kim, Bong-Ki, Jeong-Guon Ih, 1993 Journal of The Acoustical Society of America 100(6), 2726-2731. In-situ estimation of an acoustic source in an enclosure and prediction of interior noise by using the principle of vibro-acoustic reciprocity.

15. Fahy, F. J., Sound Intensity, Elsevier Applied Science, London, 1989

16. Mann, J. A. III, J. Tichy, A. J. Romano, 1987, Journal of The Acoustical Society of America 82(1), 17-30, Instantaneous and time-averaged energy transfer in acoustical fields.

17. Li, J. F., J. C. Pascal, 1998, Journal of The Acoustical Society of America 103(2), 962-972, Energy fields of partially coherent sources.

18. Bolton, J. S., N.-M. Shiau, Y. J. Kang, 1996, Journal of Sound and Vibration, 191(3), 317-347. Sound transmission through multi-panel structures lined with elastic porous materials.

19. Moorhouse, .T, B.M.Gibbs, 1993, Journal of Sound and Vibration, 167(2), 223-237. Prediction of the structure-borne noise emission of machines: development of a methodology.

20. Moorhouse, A.T., B.M.Gibbs, 1995, Journal of Sound and Vibration, 180(1), 143-161. Measurement of structure-borne sound emission from resiliently mounted machines in situ.

21. Moorhouse, A.T., B.M.Gibbs, 1995, Journal of Sound and Vibration, 186(5), 781-803. Structure-borne sound power emission from resiliently mounted fans: case studies and diagnosis.

22. Mondot, J.M., B. Petersson, 1987, Journal of Sound and Vibration, 114(3), 507-518. Characterization of structure-borne sound sources: the source descriptor and the coupling function.

23. Petersson, B.A.T., B.M.Gibbs, 1993, Journal of Sound and Vibration, 168(1), 157-176. Use of the source descriptor concept in studies of multi-point and multi-directional vibrational sources.

24. Fulford, R.A., B.M. Gibbs, 1999, Journal of Sound and Vibration, 225(2), 239-282. Structure-borne sound power and source characterization in multi-point-connected systems. Part 3: Force ratio estimates.

25. Fulford, R.A., B.M. Gibbs, 1999, Journal of Sound and Vibration, 225(2), 239-282. Structure-borne sound power and source characterization in multi-point-connected systems. Part 2: About mobility functions and free velocities.

26. Jansenns, M.H.A., M.K. Termeer, C.A.F. de Jong, 1996, ISMA Proceedings. Comparison of the use of two methods for characterizing structure-borne sound sources.

27. Janssens, M.H.A., J.W. Verheij, D. J. Thompson, 1999, Journal of Sound and Vibration, 226(2), 305-328. The use of an equivalent forces method for the experimental quantification of structural sound transmission in ships.

28. Bettella, M., M. F. Harrison, R. S. Sharp, 2002, Journal of Sound and

Vibration, 255(3), 531-547. Investigation of automotive creep groan noise with a distributed-source excitation technique.

29. de Beer, F.G., J.W. Verheij, 2000, Journal of Sound and Vibration, 231(3), 639-652. Experimental determination of pass-by noise contributions from the bogies and superstructure of a freight wagon.

30. Rayleigh, J.W.S., The Theory of Sound Vol I&II, 2nd edition, Dover Publications, New York, 1945.

31. Verheij,, J. W., 1997, International Journal of Acoustics and Vibration, 2(3), 103-112. Inverse and reciprocity methods for machinery noise source characterization and sound path quantification. Part 2: Transmission paths.

32. Ver, Istvan L.,Robert W. Oliphant, 1996, Sound and Vibration, 1996(3), 14-17, Acoustic reciprocity for source-path-receiver analysis.

33. Mason, J.M., F.J. Fahy, 1989, Noise Control Engineering, 34(2), 43-52. Development of a reciprocity technique for the prediction of propeller noise transmission through aircraft fuselages.

34. MacMartin, D. G., G. L. Basso, F. W. Slingerland, 1995, Journal of Sound and Vibration, 187(3), 467-483. Aircraft fuselage noise transmission measurements using a reciprocity technique.

35. Zheng, Junhua, Frank J. Fahy, David Anderton, 1994, Applied Acoustics 42, 333-346. Application of a Vibro-acoustic reciprocity technique to the prediction of sound radiated by a motored IC engine.

36. Stratman, J. A., 1991, Audio Eng. Soc. Preprint, 3112(A-5). Computer-aided application of acoustic transfer function measurement in automotive audio system design.

37. Beguet, B., J.L. Chauray, 1992, Internoise92 Proceedings. Identification of transmission path in interior acoustical problems.

38. Gilbert, P., Nis Bjorn Moller, Yun S. Ryu, 2000, ISMA Proceedings. PULSE™ Modal test Consultant using MATLAB™ a dedicated tool for Noise Path analysis.

39. Li, W., P., A. D. Ball, A. Y. T. Leung, 2000, ISMA Proceedings. The identification of diesel engine sources.

40. Bendat, J. S., Allan G. Piersol, Engineering Applications of Correlation and Spectral Analysis, 2nd edition, Wiley-Interscience, New York, 1993.

41. Bendat, J. S., Allan G. Piersol, Random Data \ Analysis and Measurement Procedures, 2nd edition, Wiley-Inter-science, New York, 1986.

42. Ewins, D. J., Modal Testing: Theory and Practice, Research Studies Press, New York, 1984.

43. Harris, C. M., Handbook of Acoustical Measurements and Noise Control, Acoustical Society of America, 3rd edition, New York, 1998.

BIBLIOGRAPHY

1. Cook, Richard K., 1996 Journal of The Acoustical Society of America 99(1), 24-29. Lord Rayleigh and reciprocity in physics.

2. Dickens, J.D., C. J. Norwood, 2001, Journal of Sound and Vibration, 244(4), 685-696. Universal method to measure dynamic performance of vibration isolators under static load.

3. Easwaran, V., V. H. Gupta, M. L. Munjal, 1993, Journal of Sound and Vibration, 161(3), 515-525. Relationship between the impedance matrix and the transfer matrix with specific reference to symmetrical, reciprocal and conservative systems.

4. Kim, S., R. Singh, 2001, Journal of Sound and Vibration, 245(5), 877-913. Multi-dimensional characterization of vibration isolators over a wide range of frequencies.

5. Mencik, J.-M., Y. Champoux, A. Berry, 2001, Journal of Sound and Vibration, 254(4), 669-684. Development of a blocked pressure criterion for application of the principle of acoustic reciprocity.

6. Merhaut, J., 1982, J. Audio Eng. Soc., 30(12), 882-888. Low-frequency measurement of loudspeakers by the reciprocity method.

7. Nolte, B., L. Gaul, 1996, Mechanical Systems and Signal Processing, 10(3), 351-364. Sound Energy Flow in the Acoustic Near Field of a

8. Rust, Alfred, Ingo Edlinger, 2002, Sound and Vibration, 2002(2), 14-18. Active path tracking for vehicle noise source identification.

9. Salava, T., 1988, J. Audio Eng. Soc., 36(10), 763-775. Acoustic load and transfer functions in rooms at low frequencies.

10. Tanaka, N. S. D. Snyder, C. Hansen, 1996, Journal of The Acoustical Society of America 99(2), 942-953. Vorticity Characteristics of the Vibrational Intensity Field in an Actively Controlled Thin Plate

11. Tohyama, M., T. Koike, Fundamentals of Acoustic Signal Processing, Academic Press, San Diego, 1998.

12. Tolonen, T., 2000, Audio Eng. Soc. Preprint, 5174. Object-based sound source modeling for the musical signals

13. Wapenaar, C. P. A., 1996 Journal of The Acoustical Society of America 100(6), 3508-3518. Reciprocity theorems for two way and one way wave vectors: A comparison.

14. Wu, J.H., H.L. Chen, 2002, Journal of Sound and Vibration, 249(3), 417-427. A method to predict acoustic radiation from an enclosed multi-cavity structure.

15. Wyckaert, K. F. Augusztinovicz, P. Sas, 1996, Journal of The Acoustical Society of America 100(5), 3172-3181. Vibro-Acoustical Modal Analysis: Reciprocity, model symmetry, and modal validity

16. Yap, S. H, B. M. Gibbs, 1999, Journal of Sound and Vibration, 222(1), 85-98. Structure-borne sound transmission from machines in buildings, Part 1: Indirect measurement of force at the machine-receiver interface of a single and multi-point connected system by a reciprocal method

17. Yap, S. H., B. M. Gibbs, 1999, Journal of Sound and Vibration, 222(1), 99-113. Structure-borne sound transmission from machines in buildings, Part 2: Indirect measurement of force and moment at the machine-receiver interface of a single and multi-point connected system by a reciprocal method

18. Zhe, J., 2000, Journal of The Acoustical Society of America 107(2), 725-730. Intensity Streamlines and Vorticity Streamlines in Three-dimensional

Sound Fields

19. Ziemba, M. 2001, Audio Eng. Soc. Preprint, 5287. Test signals for the objective and subjective evaluation of automotive audio systems.

BIOGRAPHY

A Hakan Serafettinoglu was born August 29, 1963, in Bursa, Turkey. He graduated from Ankara Fen Lisesi, Ankara, Turkey and enrolled at Middle East Tecnical University in the fall of 1981.

He received the Bachelor of Science degree in Mechanical Engineering at Middle East Technical University in 1985. He completed a thesis on a topic related to noise control engineering in 1987 and received the Master of Science degree. He spent the following two years as a Research Assitant and PhD student at Northwestern University and completed the required graduate courses.

Since 1992, he has been employed as a Senior Research Engineer by the Research and Technology Development Center of Arçelik A.S., a leading home appliance company in Turkey. He worked at the planning and establishment of the Vibration and Acoustics Laboratory of the Department. He is currently acting as a senior engineer in the same center.